# Throughput Characterizations of Wireless Networks via Stochastic Geometry and Random Graph Theory

A Thesis

Submitted to the Faculty

of

Drexel University

by

Jeffrey William Wildman II

in partial fulfillment of the

requirements for the degree

of

Doctor of Philosophy

June 2015

# Dedications

*To my wife, Becky.*

# Acknowledgments

I wish to express my sincere gratitude to my advisor, Dr. Steven Weber, whom I first met when he interviewed me for an undergraduate research position during my freshman year at Drexel. For over a decade since that fortuitous interview, Dr. Weber has been a major source of encouragement during both the ups and downs that are invariably part of graduate research, often lending a willing ear for matters both professional and personal. I have learned a great deal from him while working on many interesting research projects during this time and it has been a truly enjoyable and rewarding experience.

Many thanks go to the members of my dissertation committee, Dr. Kapil Dandekar, Dr. Harish Sethu, Dr. Ali Shokoufandeh, and Dr. John MacLaren Walsh for not only their words of wisdom and constructive criticism, but also for the many courses I have had the pleasure of taking from each of them. I would be remiss if I did not acknowledge and thank both Dr. Matti Latva-aho and Dr. Pedro H. J. Nardelli for making the Center for Wireless Communications (CWC) such a welcoming, warm, and productive environment during my collaborative research visit with them at the University of Oulu, Finland. To Dr. Moshe Kam I would like to express my appreciation for his positive influence and direction during particularly formative years of my bachelor's and master's degrees. For their help on numerous occasions, often on short notice, I am grateful to the administration and staff within the Electrical and Computer Engineering Department, including Kathy Bryant, Tanita Chapelle, Sean Clark, Chad Morris, and Phyllis Watson.

Thanks to my friends and labmates in the Modeling and Analysis of Networks Laboratory (MANL), Data Fusion Lab (DFL), and elsewhere at Drexel for the countless interesting discussions and shared camaraderie – I am a richer individual for it. A special thanks in particular to a frequent partner in crime, Dr. Bradford Boyle, with whom I've shared many enlightening whiteboard sessions and whose oft-solicited advice and feedback has always proved genuine and insightful. I am without a doubt also indebted to my family for creating a caring and supportive environment

over the years; it has been instrumental in getting me where I am today. Finally, most of all, I want to thank my wonderful wife, Becky, whose love, patience, and support has been unequaled and unwavering throughout this journey.

# Table of Contents

# List of Tables

# List of Figures

# Abstract

Throughput Characterizations of Wireless Networks via Stochastic Geometry and Random Graph Theory
Jeffrey William Wildman II
Steven Patrick Weber, Ph.D.

The shared medium of wireless communication networks presents many technical challenges that offer a rich modeling and design space across both physical and scheduling protocol layers. This dissertation is organized into tasks that characterize the throughput performance in such networks, with a secondary focus on the interference models employed therein.

We examine the throughput ratio of greedy maximal scheduling (GMS) in wireless communication networks modeled as random graphs. A throughput ratio is a single-parameter characterization of the largest achievable fraction of the network capacity region. The throughput ratio of GMS is generally very difficult to obtain; however, it may be evaluated or bounded based on specific topology structures. We analyze the GMS throughput ratio in previously unexplored random graph families under the assumption of primary interference. Critical edge densities are shown to yield bounds on the range and expected GMS throughput ratio as the network grows large.

We next focus on the increasing interest in the use of directional antennas to improve throughput in wireless networks. We propose a model for capturing the effects of antenna misdirection on coverage and throughput in large-scale directional networks within a stochastic geometry framework. We provide explicit expressions for communication outage as a function of network density and antenna beamwidth for idealized sector antenna patterns. These expressions are then employed in optimizations to maximize the spatial density of successful transmissions under ideal sector antennas. We supplement our analytical findings with numerical trends across more realistic antenna patterns.

Finally, we characterize trade-offs between the protocol and physical interference models, each used in the prior tasks. A transmission is successful under the protocol model if the receiver is free of any single, significant interferer, while physical model feasibility accounts for multiple interference sources. The protocol model, parameterized by a guard zone radius, naturally forms a decision

rule for estimating physical model feasibility. We combine binary hypothesis testing with stochastic geometry and characterize the guard zone achieving minimum protocol model prediction error. We conclude with guidelines for identifying environmental parameter regimes for which the protocol model is well suited as a proxy for the physical model.

# Chapter 1: Introduction

The shared medium of wireless communication networks presents many technical challenges that offer a rich modeling and design space across the physical and medium access control layers of the protocol stack. Many network design objectives center on end user experience as well as overall network utility; very often these objectives may be characterized in terms of throughput, or how quickly data may be transmitted between various parties in the network. Accordingly, the high level goals of this dissertation are to increase our understanding of the throughput performance and limitations of existing wireless communications techniques, as well as to characterize how our modeling assumptions influence the predicted throughput performance of such systems. This thesis is organized into three tasks that are primarily concerned with characterizing and maximizing throughput performance in such networks, with a secondary focus on the interference models employed therein. These tasks are investigated using random graph theory and stochastic geometry as a core set of analytical tools.

In Ch. 2[1], we study the throughput ratio of a low-complexity, greedy scheduling technique in wireless communications networks. Throughput ratios, when available, provide a single-parameter means of expressing the achievable capacity region (and thus optimality) of a given scheduling algorithm on a given network topology. Scheduling protocols with a larger provable throughput ratio guarantee a higher degree of stability and robustness to the varied traffic loads that are inherent to wireless networks. For one such algorithm, greedy maximal scheduling (GMS), a host of research literature has characterized its throughput ratio via an alternative, but equivalent, definition called the Local Pooling (LoP) factor. While the LoP factor of an arbitrary network topology is generally very difficult to obtain, it may be evaluated or bounded based on specific topology structures.

Within the field of random graph theory, it is common to use *threshold functions* to investi-

[1]The work in Ch. 2 has been accepted for publication as: J. Wildman and S. Weber, "On characterizing the local pooling factor of greedy maximal scheduling in random graphs," *IEEE/ACM Trans. Netw., (accepted: May 2015)*, arXiv: 1409.0932.

gate graph properties of interest through their sensitivity to the density of edges in the network. When established, a threshold function provides the limiting likelihood of satisfying a specific graph property (*e.g.*, connectivity) across various choices of specific graph construction parameters as the network grows large. These parameters effectively control the density of edges in the network; in Erdős-Rényi (ER) graphs, the parameter is the probability with which edges are added between each pair of nodes in the network, while in random geometric (RG) graphs, the equivalent parameter is the maximum distance under which each pair of nodes is connected by an edge. We posit that the randomized structure of wireless networks will be prohibitive to the throughput optimality of GMS. In this chapter, we explore this hypothesis by employing threshold functions to characterize the sensitivity of the GMS throughput ratio to the density of edges in large networks modeled as ER and RG graphs under the primary interference model. For sufficiently dense, large random graphs, we find that the throughput ratio is bounded between 1/2 and 2/3 and conclude that GMS is sub-optimal with high probability in this regime. However, in the opposite regime of sparse random graphs, we demonstrate that GMS optimality, if permitted, must necessarily come at the cost of network connectivity.

In Ch. 3[2], we focus on maximization of spatial throughput in large wireless networks employing directional antennas subject to orientation error. Spatial throughput is the spatial density of concurrent, successful transmissions in a wireless network whose transmitter and receiver locations are typically modeled as point processes. In this setting, the trade-off between the increase in spatial intensity of active transmissions and the resulting decrease in transmission success rate can be addressed and analyzed via stochastic geometry. Quality of service requirements in the form of outage constraints are also typically built into the maximization of spatial throughput; this results in the well-known throughput metric called transmission capacity. Both spatial throughput and transmission capacity may be improved by the deployment of directional antennas, which focus transmitted energy towards intended recipients and reduce interference in directions away from the

[2]The work in Ch. 3 is the result of a collaborative research visit with Dr. Matti Latva-aho and Dr. Pedro H. J. Nardelli at the Center for Wireless Communications (CWC), University of Oulu, Finland. This work has been published as: J. Wildman, P. H. J. Nardelli, M. Latva-aho, and S. Weber, "On the joint impact of beamwidth and orientation error on throughput in directional wireless Poisson networks," *IEEE Trans. Wireless Commun.*, vol. 13, no. 12, pp. 7072–7085, Jun. 2014. DOI: 10.1109/TWC.2014.2331055.

recipient. Related research in this area has characterized notions of spatial throughput in large scale wireless networks employing directional antennas, but all surveyed works assume perfect pointing or beamforming between transmitters and receivers. As a consequence of an orientation error-free model, these works analytically demonstrate unbounded throughput gains as antenna directionality is narrowed.

In large scale, highly directional networks, we expect the effects of antenna misalignment and/or beamsteering error to have a significant role in determining network coverage and throughput. We propose that the maximization of spatial throughput over a configurable antenna beamwidth will require a careful tradeoff between reducing interference with antenna beamwidths that are not so narrow that transmitters and receivers are also likely to miss each other. In this chapter, we define a stochastic geometry based model that captures the effects of beam misdirection on coverage and throughput in such networks. We are able to use this framework to provide explicit expressions for communication outage as a function of network density and antenna beamwidth for idealized sector antenna patterns. We then explore the optimization of both spatial throughput and transmission capacity, where we confirm the existence of a throughput-optimal beamwidth that appropriately navigates the above tradeoffs, and supplement our findings with matching numerical trends across more realistic antenna patterns.

In Ch. 4[3], we turn our attention to interference models, which form a key component in the simulation and design of large scale wireless networks. Several models have seen extensive use over the past several decades, including the *physical* and *protocol* interference models. Under the physical interference model, successful reception requires the receiver's signal-to-interference-plus-noise (SINR) ratio, computed from all interference sources, to fall above a given threshold. In contrast, the protocol interference model places constraints on the max power observed at the receiver from any one source of interference. Usage of the protocol model is typically parameterized by a guard zone distance around each receiver; when the guard zone contains any source of interference, the transmission is declared as being in outage. For network operating environments of interest,

[3]Portions of the work in Ch. 4 have been presented in poster form at the 2015 Simons Conference on Networks and Stochastic Geometry held at The University of Texas at Austin.

specific settings for the guard distance have been shown to produce protocol model outage rates that closely approximate those of the physical model. Of note in this area is a guard zone set to exclude *dominant* interferers, those who individually violate SINR constraints.

While a guard zone may be chosen to match the outage rate (and thus, spatial throughput) predicted by networks employing the physical interference model, it is not immediately clear if such a guard zone also yields a high degree of correlation between the subsets of transmissions that are predicted successful by both models. We hypothesize that the protocol model configured to use a dominant interferer guard zone can achieve both objectives for most regimes of interest. In this chapter, we note that the usage of the protocol model in networks modeled as points processes fits nicely within the framework of binary hypothesis testing. We treat the protocol interference model, parameterized by a guard zone distance, as a decision rule to evaluate/predict physical model success of a typical transmission; given the simple observation of the distance from the receiver to the closest interferer, the protocol model must decide between success/outage under the physical model. Under this framework, we employ Bayes estimation and stochastic geometry to characterize the optimal guard zone that minimizes the prediction error rate associated with the protocol model decision rule. We find that the efficacy of the optimal protocol model decision rule is tightly coupled with the overall quality (outage) of the physical model channel. In regimes of low physical model outage, we demonstrate that a guard zone radius based on dominant interference incurs little additional error over the optimal guard zone and correlates well with physical model feasibility, in support of our hypothesis. This framework is then extended to the case of directional networks, where we are able to draw similar conclusions.

In Ch. 5, we summarize our findings and discuss their implications for future research.

# Chapter 2: On Characterizing the Throughput Ratio of Greedy Maximal Scheduling in Random Graphs

## 2.1 Introduction

The *stability region* (or capacity region) of a queueing network is often defined as the set of exogenous traffic arrival rates for which a stabilizing scheduling policy exists. A scheduling policy is *optimal* if it stabilizes the network for the entire stability region. In [1], Tassiulas and Ephremides proved the optimality of the Maximum Weight Scheduling (MWS) policy, which prioritizes backlogged queues in the network. However, for arbitrary communication networks and interference models, employing MWS incurs large computation and communication costs. Under the assumption of graph-based networks with primary interference, the MWS policy simplifies to that of the Maximum Weighted Matching (MWM) problem, for which there are polynomial-time algorithms.

Greedy and heuristic scheduling can help reduce these operating costs further, usually at the expense of optimality. The relative performance of these policies is often defined by their largest achievable fraction $\gamma$ of the stability region, called a *throughput ratio*. For example, Sarkar and Kar [2] provide a $O(\Delta \log \Delta \log n)$-time (where $\Delta$ is the max degree of the network) scheduling policy that attains at least $2/3$ of the stability region for tree graphs under primary interference. Lin and Shroff [3] prove that a maximal scheduling policy on arbitrary graphs can do no worse than $1/2$ of the stability region under primary interference. Maximal matching policies can be implemented to run in $O\big(\log^2 n\big)$-time [4]. Lin and Rasool [5] propose a constant, $O(1)$-time algorithm that asymptotically achieves at least $1/3$ of the stability region under primary interference. This naturally leads to the question of whether or not greedy scheduling techniques may in fact be optimal ($\gamma = 1$).

### 2.1.1 Related Work

Sufficient conditions for the optimality of Greedy Maximal Scheduling (GMS) employed on a network graph $G(V, E)$ were produced by Dimakis and Walrand [6] and called Local Pooling (LoP). The GMS algorithm (called Longest Queue First, LQF [6]) consists of an iterated selection of links in order of

decreasing queue lengths, subject to pair-wise interference constraints. Computing whether or not an arbitrary graph $G$ satisfies LoP consists of solving an exponential number of linear programs (LPs), one for each subset of links in $G$. Trees are an example of one class of graphs proved to satisfy LoP. While LoP is necessary and sufficient under deterministic traffic processes, a full characterization of the graphs for which GMS is optimal under random arrivals is unknown.

The work by Birand *et al.* [7] produced a simpler characterization of all LoP-satisfying graphs under primary interference using forbidden subgraphs on the graph topology. Even more remarkably, they provide an $O(n)$-time algorithm for computing whether or not a graph $G$ satisfies LoP. Concerning general interference models, the class of *co-strongly perfect* interference graphs are shown to satisfy LoP conditions. The definition of co-strongly perfect graphs is equated with the LoP conditions of Dimakis and Walrand [6]. Additionally, both Joo *et al.* [8] and Zussman *et al.* [9] prove that GMS is optimal on tree graphs for $k$-hop interference models.

For graphs that do not satisfy local pooling, Joo *et al.* [10, 8] provide a generalization of LoP, called $\sigma$-LoP. The LoP factor of a graph, $\sigma$, is formulated from the original LPs of Dimakis and Walrand [6]. Joo *et al.* [8] show that the LoP factor is in fact equivalent to GMS's throughput ratio $\sigma = \gamma$. Li *et al.* [11] generalize LoP further to that of $\Sigma$-LoP, which includes a per-link LoP factor $\sigma_l$ that scales each dimension of $\Lambda$ independently and recovers a superset of the provable GMS stability region under the single parameter LoP factor.

As mentioned, checking LoP conditions can be computationally prohibitive, particularly under arbitrary interference models. Therefore, algorithms to easily estimate or bound $\sigma$ and $\sigma_l$ are of interest and immediate use in studying GMS stability. Joo *et al.* [8] provide a lower bound on $\sigma$ by the inverse of the largest interference degree of a nested sequence of increasing subsets of links in $G$, and provide an algorithm for computing the bound. Li *et al.* [11] refine this algorithm to provide individual per-link bounds on $\sigma_l$. Under the primary interference model, Joo *et al.* [10] show that $\Delta/(2\Delta - 1)$ is a lower bound for $\sigma$. Leconte *et al.* [12], Li *et al.* [11], and Birand *et al.* [7] note that a lower bound for $\sigma$ is derived from the ratio of the min- to max-cardinality maximal schedules.

Joo *et al.* [8] define the worst-case LoP over a class of graphs, and in particular find bounds on the

worst-case $\sigma$ for geometric-unit-disk graphs with a $k$-distance interference model. Birand *et al.* [7] list particular topologies that admit arbitrarily low $\sigma$, and provide upper and lower bounds on $\sigma$ for several classes of interference graphs. The body of work by Brzezinski *et al.* [13, 9, 14] brings some attention to multi-hop (routing) definitions for LoP. Brzezinski *et al.* [14] investigate scheduling on arbitrary graphs by decomposing, or pre-partitioning, the graph topology into multiple 'orthogonal' trees and then applying known LoP results about GMS optimality on trees. Both Joo *et al.* [10] and Kang *et al.* [15] also treat the case of multi-hop traffic and LoP conditions.

### 2.1.2 Motivation & Contributions

Much of the work reviewed above focuses on the issue of identifying the performance of GMS via the LoP factor for a given graph or select classes of graphs. However, aside from the worst-case LoP analysis in geometric-unit-disk graphs by Joo *et al.* [8] we are not aware of any work on establishing statistics and trends on the LoP factor $\sigma$ in networks modeled as random graphs. We note that the topology and structure of random graphs families, such as Erdős-Rényi (ER) and random geometric (RG) graphs, are tightly coupled with the density of edges present in the graph. This chapter seeks to fill this void by rigorously establishing relationships between network edge densities and the resulting LoP factor in networks modeled as random graphs. When viewed within the context of Joo *et al.* [8], statistics on the LoP factor $\sigma$ are equivalent to statistics on GMS's throughput ratio $\gamma$, the relative size of GMS's stability (or capacity) region. We then place LoP within a larger context of commonly studied properties in both random graph families by comparison with the likelihood of connectivity properties.

This chapter and contributions are organized as follows. In §2.2, we introduce our network model and provides essential definitions of threshold functions and the graph properties of interest. In §2.3, we examine ER graphs due to their analytical tractability and gain insight into the behavior of the LoP factor relative to the chosen edge probability function. We establish a regular threshold function based on the forbidden subgraph characterization of LoP [7] that dictates the likelihood that a graph satisfies LoP $\sigma = 1$ conditions (Thm. 2.2) and carry this analysis into bounds on the expected LoP factor (Thm. 2.3). In §2.4, we extend our analysis to the case of RG graphs due to their natural

connection to wireless network models. While the spatial dependence between edges in RG graphs complicates analysis, we are able to establish an upper bound for LoP threshold function (Prop. 2.4 and Cor. 2.4) as well as similar bounds on the expected LoP factor (Thm. 2.5). In both ER and RG sections, the LoP threshold functions are shown to produce a mutual exclusion between LoP and notions of connectedness (giant components and traditional connectivity) as the size of the network grows, for a large class of edge probability/radius functions (Thm. 2.4 and Cor. 2.3 for ER graphs; Thm. 2.6 and Cor. 2.5 for RG graphs). ). In §2.5, we comment on aspects of our numerical results, particularly on algorithm implementation to detect necessary or sufficient conditions for LoP in *i.i.d.* realizations of ER and RG graphs. In §2.6, we compare the analytical mutual exclusion of LoP and giant components with that of numerical results for finite network sizes and find that convergence to this exclusion between properties is rather quick as the network grows in size. In §2.7, we conclude our work and touch upon ideas for future investigation. Finally, for clarity, long proofs are presented in App. A.

## 2.2 Model & Definitions

Let $\mathcal{G}_n$ be the set of all $2^{\binom{n}{2}}$ simple graphs on $n$ nodes. A common variant of an Erdős-Rényi (ER) graph is constructed from $n$ nodes where undirected edges between pairs of nodes are added using *i.i.d.* Bernoulli trials with *edge probability* $p \in [0,1]$. For each choice of $p$, let $\mathcal{G}_{n,p}$ denote the finite probability space formed over $\mathcal{G}_n$.

We will also consider a common variant of a random geometric (RG) graph, in which $n$ node positions are modeled by a Binomial Point Process (BPP) within a unit square $[-1/2, 1/2]^2 \subset \mathbb{R}^2$. Undirected edges between pairs of nodes are added iff the Euclidean distance between the two nodes is less than a given, fixed distance $r \in [0, \infty)$. For each choice of $r$, let $\mathcal{G}_{n,r}$ denote the finite probability space formed over $\mathcal{G}_n$. Note that the particular RG model we have chosen is equivalent to a Poisson Point Process (PPP) conditioned on having $n$ nodes within the unit square, producing an 'equivalent' intensity $\lambda = n$.

Interference in a graph $G_n \in \mathcal{G}_n$ is captured as a pairwise function between its edges. Specifically, we adopt the primary (one-hop) interference model, under which adjacent edges (sharing a common

node) interfere with one another. Under this assumption, we can employ the forbidden subgraph characterization of LoP conditions found in [7].

Let $\mathcal{P}$ refer to both *i)* a specific property or condition of a graph $G_n$, as well as *ii)* the subset of graphs of $\mathcal{G}_n$ for which the property holds, as described by Def. 2.1.

**Definition 2.1** (Graph Property [16])**.** *A* graph property $\mathcal{P}$ *is a subset of* $\mathcal{G}_n$ *that is closed under isomorphism* ($\sim_{\text{iso}}$)*:* i.e.*,* $G \in \mathcal{P}, H \in \mathcal{G}_n, G \sim_{\text{iso}} H \Rightarrow H \in \mathcal{P}$.

**Definition 2.2** (Monotone Graph Property [17])**.** *Graph property* $\mathcal{P}$ *is* monotone increasing *if* $G \in \mathcal{P}, H \supset G \Rightarrow H \in \mathcal{P}$. *Correspondingly, graph property* $\mathcal{P}$ *is* monotone decreasing *if* $G \in \mathcal{P}, H \subset G \Rightarrow H \in \mathcal{P}$.

Let $\mathbb{P}\{G_{n,p} \in \mathcal{P}\}$ denote the probability that a random graph $G_{n,p}$ generated according to $\mathcal{G}_{n,p}$ satisfies graph property $\mathcal{P}$. For a monotone (increasing or decreasing) graph property, $\mathcal{P}$, increasing the edge probability $p \in [0,1]$ will cause a corresponding transition of $\mathbb{P}\{G_{n,p} \in \mathcal{P}\}$ between 0 and 1. Similarly, $\mathbb{P}\{G_{n,r} \in \mathcal{P}\}$ (analogously defined using $G_{n,r}$ and $\mathcal{G}_{n,r}$) for a monotone graph property will also experience a transition as the edge distance $r \in [0,\infty)$ increases. In this case, it is of interest to study the behavior of the limiting probability $\lim_{n\to\infty} \mathbb{P}\big\{G_{n,p(n)} \in \mathcal{P}\big\}$ and $\lim_{n\to\infty} \mathbb{P}\big\{G_{n,r(n)} \in \mathcal{P}\big\}$ in response to the choice of $p(n)$ and $r(n)$, respectively. We will use $\mathbb{P}\{\mathcal{P}\}$ as a short form for $\mathbb{P}\big\{G_{n,p(n)} \in \mathcal{P}\big\}$ or $\mathbb{P}\big\{G_{n,r(n)} \in \mathcal{P}\big\}$ and use a general edge function $e(n)$ as a stand in for either $p(n)$ or $r(n)^2$. Note, thresholds of RG graphs on $\mathbb{R}^2$ are more easily expressed as the square of the edge distance $r(n)^2$ as opposed to $r(n)$. A threshold function $e^*(n)$ for graph property $\mathcal{P}$, when it exists, helps determine the limiting behavior of $\mathbb{P}\{\mathcal{P}\}$ for choices of edge function $e(n)$ relative to $e^*(n)$. As in [18], we use the phrase '$\mathcal{P}$ holds asymptotically almost surely (*a.a.s.*)' to mean $\lim_{n\to\infty} \mathbb{P}\{\mathcal{P}\} = 1$ and the phrase '$\mathcal{P}$ holds asymptotically almost never (*a.a.n.*)' to mean $\lim_{n\to\infty} \mathbb{P}\{\mathcal{P}\} = 0$. The asymptotic equivalence of two functions is denoted $f(n) \sim g(n)$, that is $\lim_{n\to\infty} f(n)/g(n) = 1$. We use the phrase 'asymptotically positive' to describe $f(n)$ if $\exists n_0 : f(n) > 0, \forall n > n_0$. Finally, let $\Phi(x)$ be the *c.d.f.* of a standard normal *r.v.*, and let $n^{\underline{k}} = n!/(n-k)!$ denote the falling factorial.

### 2.2.1 Threshold Functions

First, we restate threshold function definitions in [19] for a graph property $\mathcal{P}$ using edge function $e(n)$, threshold function $e^*(n)$, and the asymptotic notation of [20].

**Definition 2.3** (Threshold Function)**.** *$e^*(n)$ is a* threshold function *for monotonically increasing graph property $\mathcal{P}$ if:*

$$\lim_{n\to\infty} \mathbb{P}\{\mathcal{P}\} = \begin{cases} 0, & e(n) \in o(e^*(n)) \\ \\ 1, & e(n) \in \omega(e^*(n)) \end{cases}. \tag{2.1}$$

**Definition 2.4** (Regular Threshold Function)**.** *$e^*(n)$ can be called a* regular threshold function *if there exists a distribution function $F(x)$ for $0 < x < \infty$ such that at any of $F$'s points of continuity, $x$:*

$$e(n) \sim xe^*(n) \Rightarrow \lim_{n\to\infty} \mathbb{P}\{\mathcal{P}\} = F(x). \tag{2.2}$$

*$F(x)$ is known as the* threshold distribution function *for graph property $\mathcal{P}$.*

When satisfied, Def. 2.3 covers the limiting behavior of $\mathbb{P}\{\mathcal{P}\}$ for all $e(n)$ that lie an order of magnitude away from threshold $e^*(n)$. Conversely, any function $e(n) \in \Theta(e^*(n))$ is also a threshold function of graph property $\mathcal{P}$. Def. 2.3 has also been called a weak, or coarse, threshold function [21, 16, 18]. When Def. 2.4 applies, we can control the limiting value of $\mathbb{P}\{\mathcal{P}\}$ to the extent that $F(x)$ allows. This can be accomplished by choosing $e(n)$ to be a multiplicative factor $x$ of $e^*(n)$.

The two 'statements' of a threshold function:

$$e(n) \in o(e^*(n)) \Rightarrow \lim_{n\to\infty} \mathbb{P}\{\mathcal{P}\} = 0$$

$$e(n) \in \omega(e^*(n)) \Rightarrow \lim_{n\to\infty} \mathbb{P}\{\mathcal{P}\} = 1,$$

are commonly referred to as the 0-statement and the 1-statement, as they dictate when $\mathcal{P}$ holds with limiting probability 0 or 1. For a monotone decreasing property, the 0- and 1-statements are appropriately reversed.

### 2.2.2 Sharp Threshold Functions

Stronger variations of the weak threshold have been defined, called either sharp, strong, or very strong threshold functions [21, 22, 18]. We restate sharp threshold function definitions in [19] using $e(n)$, $e^*(n)$, and the asymptotic notation of [20].

**Definition 2.5** (Sharp Threshold Function)**.** *A $(e^*(n), \alpha(n))$ pair is a* sharp threshold function *for monotonically increasing graph property $\mathcal{P}$ if $\alpha(n) \in o(e^*(n))$, $\alpha(n)$ is asymptotically positive, and:*

$$\lim_{n\to\infty} \mathbb{P}\{\mathcal{P}\} = \begin{cases} 0, & e(n) \in e^*(n) - \omega(\alpha(n)) \\ \\ 1, & e(n) \in e^*(n) + \omega(\alpha(n)) \end{cases}. \tag{2.3}$$

When satisfied, Def. 2.5 covers the limiting behavior of $\mathbb{P}\{\mathcal{P}\}$ for all $e(n)$ that lie an additive factor (greater than order $\alpha(n)$) away from $e^*(n)$. Conversely, any function $e(n) \in e^*(n) + O(\alpha(n))$ is also a sharp threshold function of graph property $\mathcal{P}$. Also note: by itself, $e^*(n)$ is a regular threshold function, that is, $e^*(n)$ satisfies Def. 2.4 with 'degenerate' distribution function $F(x) = \mathbf{1}\{x > 1\}$ [19]. When presented alone (without $\alpha(n)$), $e^*(n)$ is still referred to as a sharp/strong threshold function [18], perhaps prompting [22] to propose the term 'very strong' to denote a $(e^*(n), \alpha(n))$ pair.

**Definition 2.6** (Regular Sharp Threshold Function)**.** *A sharp threshold function $(e^*(n), \alpha(n))$ is a* regular sharp threshold function *if there exists a distribution function $F(x)$ for $-\infty < x < \infty$ such that for any of $F$'s points of continuity, $x$:*

$$e(n) \sim e^*(n) + x\alpha(n) \Rightarrow \lim_{n\to\infty} \mathbb{P}\{\mathcal{P}\} = F(x). \tag{2.4}$$

*$F(x)$ is known as the* sharp-threshold distribution function *for graph property $\mathcal{P}$.*

When Def. 2.6 applies, we may control the limiting value of $\mathbb{P}\{\mathcal{P}\}$ to the extent that $F(x)$ allows by choosing $e(n)$ to be $e^*(n)$ plus a term asymptotically equivalent to $x\alpha(n)$.

**Table 2.1:** Graph Properties

| Symbol | Property |
|---|---|
| $\mathcal{P}_{\text{lop}}$ | satisfies LoP (Thm. 2.1) |
| $\mathcal{P}_{\text{edge}}$ | contains no more than $2n$ edges |
| $\mathcal{P}_{\text{lop}}^{\text{L}}$ | contains no cycles |
| $\mathcal{P}_{\text{lop}}^{\text{U}}$ | contains no cycles of lengths $\{k \geq 6, k \neq 7\}$ |
| $\mathcal{P}_{\text{conn}}$ | is connected |
| $\mathcal{P}_{\text{giant}}(\beta)$ | largest component has normalized size $\geq \beta, \beta \in (0,1)$ |
| $\mathcal{P}_{\text{giant}}$ | $\exists \beta > 0$: largest component has normalized size $\geq \beta$ |

### 2.2.3 Graph Properties

We are interested in several graph properties listed in Tab. 2.1. We first list results from Birand *et al.* [7] establishing *i)* a set of forbidden subgraphs that characterizes Local Pooling $\mathcal{P}_{\text{lop}}$ under primary interference constraints, and *ii)* a simple upper bound on the number of edges permitting Local Pooling, $\mathcal{P}_{\text{edge}}$. We then establish some useful properties and bounds of $\mathcal{P}_{\text{lop}}$, namely separate sufficient and necessary properties for Local Pooling, $\mathcal{P}_{\text{lop}}^{\text{L}}$ and $\mathcal{P}_{\text{lop}}^{\text{U}}$. Later, thresholds for these three properties $\mathcal{P}_{\text{edge}}$, $\mathcal{P}_{\text{lop}}^{\text{L}}$, and $\mathcal{P}_{\text{lop}}^{\text{U}}$ will be compared with thresholds for two connectivity properties, $\mathcal{P}_{\text{conn}}$ and $\mathcal{P}_{\text{giant}}$.

**Theorem 2.1** (Local Pooling $\mathcal{P}_{\text{lop}}$ [7, Thm. 3.1])**.** *A graph $G_n \in \mathcal{P}_{\text{lop}}$ if and only if it contains no subgraphs within the set $\mathcal{F} = \{C_k | k \geq 6, k \neq 7\} \cup \{D_k^{s,t} | k \geq 0; s,t \in \{5,7\}\}$, where $C_k$ is a cycle of length $k \geq 3$ and $D_k^{s,t}$ is a union of cycles of lengths $s$ and $t$ joined by a $k$-edge path (a 'dumbbell').*

**Lemma 2.1** ($\mathcal{P}_{\text{edge}}$ Necessary for $\mathcal{P}_{\text{lop}}$ [7, Lem. 3.6])**.** *$\mathcal{P}_{\text{edge}}$ is a necessary condition for graph property $\mathcal{P}_{\text{lop}}$.*

**Lemma 2.2** ($\mathcal{P}_{\text{lop}}$ Monotonicity)**.** *$\mathcal{P}_{\text{lop}}$ is a monotone decreasing property.*

*Proof.* See App. A.2. □

Since $\mathcal{P}_{\text{lop}}$ is a monotone property, we are assured of the existence of a threshold function (for both ER graphs [23, Thm. 1.24] and RG graphs [24, Thm. 1.1]). While we establish a regular threshold for $\mathcal{P}_{\text{lop}}$ in ER graphs (Thm. 2.2), we note that a threshold function for $\mathcal{P}_{\text{lop}}$ in RG graphs is not currently known to us. In the latter case, separate necessary and sufficient conditions bound the subset $\mathcal{P}_{\text{lop}}$ (Lem. 2.3) as well as the probability $\mathbb{P}\{\mathcal{P}_{\text{lop}}\}$ (Lem. 2.4). These bounds will hold regardless of the random graph model (ER or RG) employed, and are used later in our numerical results (§2.6).

**Lemma 2.3** (Separate Sufficient and Necessary Conditions for $\mathcal{P}_{\text{lop}}$)**.** *$\mathcal{P}^{\text{L}}_{\text{lop}}$ and $\mathcal{P}^{\text{U}}_{\text{lop}}$ are sufficient and necessary properties for $\mathcal{P}_{\text{lop}}$, respectively, producing nested subsets:*

$$\mathcal{P}^{\text{L}}_{\text{lop}} \subseteq \mathcal{P}_{\text{lop}} \subseteq \mathcal{P}^{\text{U}}_{\text{lop}}. \tag{2.5}$$

*Proof.* See App. A.3. □

**Lemma 2.4** (Probability Bounds for $\mathcal{P}_{\text{lop}}$)**.** *Under any choice of $p(n)$ ($r(n)$) used to generate ER (RG) graphs on $n$ nodes:*

$$\mathbb{P}\big\{\mathcal{P}^{\text{L}}_{\text{lop}}\big\} \leq \mathbb{P}\{\mathcal{P}_{\text{lop}}\} \leq \mathbb{P}\big\{\mathcal{P}^{\text{U}}_{\text{lop}}\big\}, \quad \forall n \in \mathbb{Z}^{+}. \tag{2.6}$$

*Proof.* See App. A.4. □

We will also look to establish statistics on the LoP factor, $\sigma \in [0, 1]$, for specific random graph families. In this regard, Lem. 2.5 and Lem. 2.6 will prove helpful.

**Lemma 2.5** ($\sigma$-LoP Bounds [3, 10])**.** *For an arbitrary graph $G$, its LoP factor $\sigma(G)$ adheres to the following bounds:*

$$\frac{1}{2} \leq \sigma(G) \leq \sigma(H), \quad \forall H \subseteq G. \tag{2.7}$$

*Proof.* The lower bound of 1/2 is immediate from [3]. The upper bound follows from [7, Def. 2.5], a reformulation of [10, Def. 6]. □

**Lemma 2.6** ($\sigma$-LoP of $C_{6k}$ [7])**.** $\sigma(C_{6k}) = 2/3, \forall k \in \mathbb{N}_+$.

*Proof.* Under primary interference, the interference graph of $G$ is its line graph. The line graph of any cycle $C_k$ is itself. The result follows immediately by a specialization of [7, Lem. 5.1] with $6k$ in place of $n$. □

## 2.3 ER Graphs

In this section, we examine several properties of interest for ER graphs. We first provide a regular sharp threshold function for $\mathcal{P}_{\text{edge}}$, a necessary property for $\mathcal{P}_{\text{lop}}$. We also find that a regular threshold and distribution function can be directly established for property $\mathcal{P}_{\text{lop}}$ by considering the presence of forbidden subgraphs in $\mathcal{F}$. We extend this argument to bound the support of the LoP factor $\sigma(G_{n,p(n)})$ as well as its expectation. Known threshold functions for connectivity and giant components are re-stated for comparison with that of $\mathcal{P}_{\text{lop}}$. We show that the threshold function for $\mathcal{P}_{\text{lop}}$ is incompatible with the known regular threshold function for $\mathcal{P}_{\text{giant}}(\beta)$ — that is, choosing $p(n)$ so that $\mathcal{P}_{\text{giant}}(\beta)$ holds *a.a.s.* implies that $\mathcal{P}_{\text{lop}}$ holds *a.a.n.*. It then follows that the stricter notion of connectivity is also incompatible with $\mathcal{P}_{\text{lop}}$.

### 2.3.1 Local Pooling

If we want to keep the expected number of edges in $G_{n,p(n)}$ to be exactly $2n$, we should set $p(n) = 4/(n-1)$. This naturally suggests a threshold function of $p^*(n) = 1/n$. This is indeed a threshold function for $\mathcal{P}_{\text{edge}}$ (as are $p^*(n) = 4/(n-1)$ and $p^*(n) = 4/n$). While not particularly novel, we include Prop. 2.1 as we have not come across a citation for the result.

**Proposition 2.1** (Regular Sharp Threshold for $\mathcal{P}_{\text{edge}}$ in $G_{n,p(n)}$)**.** *The pair* $(p^*(n) = 4/n, \alpha(n) = 2\sqrt{2n}/n^2)$ *is a regular sharp threshold function for graph property* $\mathcal{P}_{\text{edge}}$ *with distribution function* $F(x) = \Phi(-x)$ *(flipped Normal).*

*Proof.* See App. A.5. □

Note, the condition $\mathcal{P}_{\text{edge}}$ is not sufficient for $\mathcal{P}_{\text{lop}}$ and only provides an upper bound on a threshold function for $\mathcal{P}_{\text{lop}}$. We improve upon this by considering established thresholds for the

presence of individual forbidden subgraphs (such as cycles and dumbbells) in $G_{n,p(n)}$. Note, the threshold for the existence of edge-induced subgraphs in ER graphs is related to the maximum density of edges to vertices of the subgraph [18]. Cycles of a given length, being less 'dense', will tend to occur at a lower threshold $p(n) \sim 1/n$ than dumbbells. By focusing on just the set of forbidden cycles, we find that these individual thresholds combine to form a 'semi-sharp' regular threshold function for $\mathcal{P}_{\text{lop}}$, similar in form to the threshold for all cycles [19, Thm. 5b]. This is formalized by Thm. 2.2.

**Theorem 2.2** (Regular Threshold for $\mathcal{P}_{\text{lop}}$ in $G_{n,p(n)}$)**.** *$p^*(n) = 1/n$ is a regular threshold function for graph property $\mathcal{P}_{\text{lop}}$, with distribution function:*

$$F(x) = \begin{cases} \sqrt{1-x}\exp\left(\sum_{k\in\mathcal{K}} \frac{x^k}{2k}\right), & x < 1 \\ 0, & x \geq 1 \end{cases} \tag{2.8}$$

*where $\mathcal{K} = \{1, 2, 3, 4, 5, 7\}$.*

*Proof.* See App. A.6. □

Thm. 2.2 provides the limiting behavior of $\mathbb{P}\{\mathcal{P}_{\text{lop}}\}$ when $p(n)$ is chosen relative to $1/n$. In the case that $p(n)$ is asymptotically larger than $1/n$, we have that $\mathcal{P}_{\text{lop}}$ is satisfied *a.a.n.*. However, in order to guarantee that $\mathcal{P}_{\text{lop}}$ is satisfied *a.a.s.*, $p(n)$ must be chosen $o(1/n)$. Thus, we have established how to choose $p(n)$ in order to asymptotically satisfy $\mathcal{P}_{\text{lop}}$ with probability between 0 and 1. Correspondingly, Thm. 2.2 can be weakened to provide a threshold function for property $\mathcal{P}_{\text{lop}}$.

**Corollary 2.1** (Threshold Function for $\mathcal{P}_{\text{lop}}$ in $G_{n,p(n)}$)**.** *$p^*(n) = 1/n$ is a threshold function for $\mathcal{P}_{\text{lop}}$.*

*Proof.* See App. A.7. □

In dense networks above the threshold $p^*(n) = 1/n$, we find that the support for the LoP factor is bounded between 1/2 and 2/3:

**Proposition 2.2** ($\sigma$-LoP Bounds in $G_{n,p(n)}$)**.** *When $p(n) \sim c/n, c > 1$, the limiting behavior of the LoP factor $\sigma$ may be bounded as follows:*

$$\lim_{n\to\infty} \mathbb{P}\big\{1/2 \leq \sigma(G_{n,p(n)}) \leq 2/3\big\} = 1. \tag{2.9}$$

*Proof.* See App. A.8. □

**Theorem 2.3** ($\mathbb{E}[\sigma]$ Bounds in $G_{n,p(n)}$)**.** *Let $p(n) \sim c/n$. The limiting behavior of $\mathbb{E}\big[\sigma(G_{n,p(n)})\big]$ may be bounded by.*

$$\frac{1}{2}\left(1 + F_l(c)\right) \leq \lim_{n\to\infty} \mathbb{E}\big[\sigma(G_{n,p(n)})\big] \leq \frac{1}{3}\left(2 + F_u(c)\right) \tag{2.10}$$

*where:*

$$F_l(x) = \begin{cases} \sqrt{1-x}\exp\left(\sum_{k\in\mathcal{K}} \frac{x^k}{2k}\right), & x < 1 \\ 0, & x \geq 1 \end{cases}, \tag{2.11}$$

$$F_u(x) = \begin{cases} (1-x^6)^{1/12}, & x < 1 \\ 0, & x \geq 1 \end{cases} \tag{2.12}$$

*with $\mathcal{K} = \{1, 2, 3, 4, 5, 7\}$.*

*Proof.* See App. A.9. □

Note, when $p(n) \sim c/n$ and $c > 1$, bounds on the expected value of $\sigma(G)$ are a primarily a function of the restricted support provided by Prop. 2.2. A visualization of the bounds is provided in Fig. 2.2, which prove to be quite tight for $c < 1$.

### 2.3.2 Connectivity and Giant Components

Previously established results provide a sharp threshold function for connectivity in ER graphs:

**Lemma 2.7** (Regular Sharp Threshold for $\mathcal{P}_{\text{conn}}$ in $G_{n,p(n)}$ [25, 17])**.** *The pair $(p^*(n) = \log(n)/n, \alpha(n) = 1/n)$ is a regular sharp threshold function for graph property $\mathcal{P}_{\text{conn}}$ with distribution function $F(x) =$*

$\exp(-\exp(-x))$ *(Gumbel).*

We can also loosen our restriction that $G$ be connected and look at threshold functions for the formation of giant components in random graphs. A giant component exists if the largest connected components contains a positive fraction of the vertices of $G$ as $n \to \infty$. Janson *et al.* provide a relevant threshold function $p^*(n) = c(\beta)/n$ for the existence of a giant component with normalized size $\beta \in (0, 1)$ [18, Thm. 5.4]. We find that the same threshold function easily applies to the existence of a giant component of size at least $\beta$.

**Corollary 2.2** (Regular Threshold for $\mathcal{P}_{\text{giant}}(\beta)$ in $G_{n,p(n)}$ [18])**.** *Let $\beta^* \in (0, 1)$, then $p^*(n) = c(\beta^*)/n$ is a regular threshold function for graph property $\mathcal{P}_{\text{giant}}(\beta^*)$, with distribution function $F(x) = \mathbf{1}\{x > 1\}$, where:*

$$c(\beta) = \frac{1}{\beta} \ln\left(\frac{1}{1-\beta}\right). \tag{2.13}$$

*Proof.* See App. A.10. □

Given the facts that that *i)* $\mathcal{P}_{\text{lop}}$ and $\mathcal{P}_{\text{giant}}$ are monotone decreasing and increasing, resp., and *ii)* their respective threshold functions do not 'overlap' (recall that $c(\beta) > 1$), we present a statement of mutual exclusion between the two properties:

**Theorem 2.4** (Mutual Exclusion of $\mathcal{P}_{\text{lop}}$ and $\mathcal{P}_{\text{giant}}(\beta)$ in $G_{n,p(n)}$)**.** *In ER graphs with edge probability function $p(n)$ and desired giant component size $\beta \in (0, 1)$:*

$$\lim_{n\to\infty} \frac{p(n)}{1/n} \geq 0 \Rightarrow \lim_{n\to\infty} \mathbb{P}\{\mathcal{P}_{\text{lop}} \cap \mathcal{P}_{\text{giant}}(\beta)\} = 0. \tag{2.14}$$

*Proof.* See App. A.11. □

Note that the threshold for connectivity has a higher order than that of giant components ($\log(n)/n$ vs. $c(\beta)/n$), thus, we expect (and find) that properties $\mathcal{P}_{\text{lop}}$ and $\mathcal{P}_{\text{conn}}$ exhibit an identical mutual exclusion:

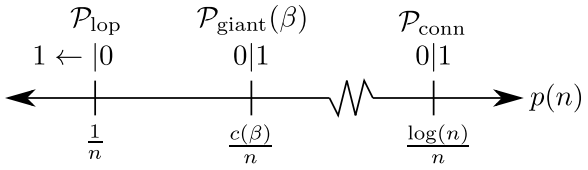


**Figure 2.1:** The limiting behavior of the graph properties in Tab. 2.1 along the design space of functions $p(n)$ chosen relative to established threshold functions for ER graphs. Listed from top to bottom are *i)* the graph properties, *ii)* their limiting probabilities relative to an established threshold function, *iii)* the established threshold function.

**Corollary 2.3** (Mutual Exclusion of $\mathcal{P}_{\text{lop}}$ and $\mathcal{P}_{\text{conn}}$ in $G_{n,p(n)}$)**.** *In ER graphs with edge probability function $p(n)$:*

$$\lim_{n\to\infty} \frac{p(n)}{1/n} \geq 0 \Rightarrow \lim_{n\to\infty} \mathbb{P}\{\mathcal{P}_{\text{lop}} \cap \mathcal{P}_{\text{conn}}\} = 0. \tag{2.15}$$

*Proof.* $\mathcal{P}_{\text{giant}}(\beta)$ is necessary for connectivity $\mathcal{P}_{\text{conn}}$, thus: $\mathbb{P}\{\mathcal{P}_{\text{lop}} \cap \mathcal{P}_{\text{conn}}\} \leq \mathbb{P}\{\mathcal{P}_{\text{lop}} \cap \mathcal{P}_{\text{giant}}(\beta)\}$. Mutual exclusion between $\mathcal{P}_{\text{lop}}$ and $\mathcal{P}_{\text{conn}}$ follows immediately from Thm. 2.4. □

We note that the set of $p(n)$ covered by Thm. 2.4 and Cor. 2.3 is a rather large class, covering all functions that can be placed into an asymptotic relationship with $1/n$. This includes $o(1/n)$ and $\omega(1/n)$, but leaves out certain functions that contain periodic components (*e.g.*, $(\sin(n) + 1)/n$). We note that these 'sinusoidal' functions may oscillate across the threshold $1/n$ for certain graph properties of interest and do not make sense to employ when attempting to satisfy monotone properties in ER graphs. We also note that a more elegant, larger characterization of the set of $p(n)$ that satisfy this mutual exclusion may exist (particularly for $\mathcal{P}_{\text{conn}}$, whose threshold lies at a higher order than that of $\mathcal{P}_{\text{lop}}$). Refer to Fig. 2.1 for a visual comparison of the limiting behavior of the properties in Tab. 2.1 in ER graphs.

## 2.4 RG Graphs

In this section, we examine several properties of interest for RG graphs. We first provide a regular sharp threshold function for $\mathcal{P}_{\text{edge}}$, a necessary property and threshold upper bound for $\mathcal{P}_{\text{lop}}$. We obtain a tighter threshold upper bound for $\mathcal{P}_{\text{lop}}$ by considering the presence of forbidden subgraphs in $\mathcal{F}$. This upper bound is sufficient to prove the threshold for $\mathcal{P}_{\text{lop}}$ is incompatible with known

regular threshold function $r^*(n)^2 = \log(n)/(\pi n)$ for $\mathcal{P}_{\text{conn}}$ — that is, choosing $r(n)^2$ so that $\mathcal{P}_{\text{lop}}$ holds *a.a.s.* implies that $\mathcal{P}_{\text{conn}}$ holds *a.a.n.*. Further, relaxing our desire for connectivity from $\mathcal{P}_{\text{conn}}$ to $\mathcal{P}_{\text{giant}}$ lowers the regular threshold function from $\log(n)/(\pi n)$ to $\lambda_c/n$ with $\lambda_c \in (0, \infty)$. However, we find that this is insufficient to prevent the incompatibility of $\mathcal{P}_{\text{lop}}$ with $\mathcal{P}_{\text{giant}}$.

### 2.4.1 Local Pooling

**Proposition 2.3** (Regular Sharp Threshold for $\mathcal{P}_{\text{edge}}$ in $G_{n,r(n)}$)**.** *The pair* $(r^*(n)^2 = 4/(\pi n), \alpha(n) = 2\sqrt{2n}/(\pi n^2))$ *is a regular sharp threshold function for graph property* $\mathcal{P}_{\text{edge}}$ *with sharp-threshold distribution function* $F(x) = \Phi(-x)$ *(flipped Normal).*

*Proof.* See App. A.12. □

**Remark 2.1.** *The leading term of the threshold in Prop. 2.3 was motivated by solving an expression for the expected number of edges in* $G_{n,r(n)}$ *for* $r(n)^2$*. The second term of the threshold is specifically chosen such that all multiplicative factors other than* $-x$ *cancel out from scaling* $(a)$ *and subsequent standardization* $(d)$ *in the proof.*

**Proposition 2.4** (Upper Bound for $\mathcal{P}_{\text{lop}}$ in $G_{n,r(n)}$)**.** *When* $r^*(n)^2 \sim c/n^{6/5}$*, an upper bound for LoP may be expressed:*

$$\limsup_{n\to\infty} \mathbb{P}\{\mathcal{P}_{\text{lop}}\} \leq \exp\left(\frac{-(\pi c/4)^5}{6!}\right) \tag{2.16}$$

*Proof.* See App. A.13. □

**Remark 2.2.** *Unlike the case of ER graphs where cycles of all orders began appearing at the same threshold* $p(n) \sim 1/n$*, the RG thresholds of forbidden subgraphs in* $\mathcal{F}$ *are more spread out (order* $k$ *vertex-induced subgraphs yielding an order* $k$ *edge-induced forbidden subgraph begin to appear at* $r(n)^2 \sim n^{-k/(k-1)}$*). For Prop. 2.4, we wished to find the tightest upper bound for* $\mathcal{P}_{\text{lop}}$ *that was amenable to asymptotic analysis. Thus, we first restricted our attention to the lowest order vertex-induced subgraphs (subgraphs of order* $6$*). Second, we noted that evaluating* $\mu_{\Gamma_6}$ *for all feasible, order* $6$ *graphs that contain the forbidden edge-induced* $C_6$ *appears to be neither analytically tractable nor*

*computationally viable, so we apply a second upper bound by focusing on a specific vertex-induced subgraph, the complete graph $K_6$, and derive an easy upper bound for $\mu_{K_6}$.*

The upper bound in Prop. 2.4 yields a 0-statement:

**Corollary 2.4** (0-statement for $\mathcal{P}_{\text{lop}}$ in $G_{n,r(n)}$)**.** *When $r(n)^2 \in \omega\big(1/n^{6/5}\big)$, $\lim_{n\to\infty} \mathbb{P}\{\mathcal{P}_{\text{lop}}\} = 0$.*

*Proof.* This follows immediately from Prop. 2.4. □

Due to fact that all forbidden subgraphs contain at least 6 or more vertices, it does not seem likely that a corresponding 1-statement would hold at a lower threshold than $r^*(n)^2 \sim 1/n^{6/5}$. Thus, we are led to make the following conjecture:

**Conjecture 2.1** (Threshold for $\mathcal{P}_{\text{lop}}$ in $G_{n,r(n)}$)**.** *$r^*(n)^2 = 1/n^{6/5}$ is a threshold function for graph property $\mathcal{P}_{\text{lop}}$.*

The difficulty in proving this conjecture lies in establishing a sufficient condition whose probability lower bounds $\mathbb{P}\{\mathcal{P}_{\text{lop}}\}$ while maintaining enough tractability to take its limit as $n \to \infty$. In terms of applying the same proof strategy as used for ER graphs, we note that the FKG inequality does not appear readily applicable. We note that none of the results presented in this chapter depends on this conjecture.

Similar to the case for ER graphs, the asymptotic support for the LoP factor for dense RG networks (above the threshold $r^*(n)^2 = 1/n^{6/5}$) also lies between 1/2 and 2/3:

**Proposition 2.5** ($\sigma$-LoP Bounds in $G_{n,r(n)}$)**.** *When $r(n)^2 \in \omega\big(1/n^{6/5}\big)$, the limiting behavior of the LoP factor $\sigma$ may be bounded as follows:*

$$\lim_{n\to\infty} \mathbb{P}\big\{1/2 \leq \sigma(G_{n,r(n)}) \leq 2/3\big\} = 1. \tag{2.17}$$

*Proof.* See proof in App. A.17. □

**Theorem 2.5** ($\mathbb{E}[\sigma]$ Bounds in $G_{n,r(n)}$)**.** *Let $r(n)^2 \sim c/n^{6/5}$. We may bound the limiting behavior*

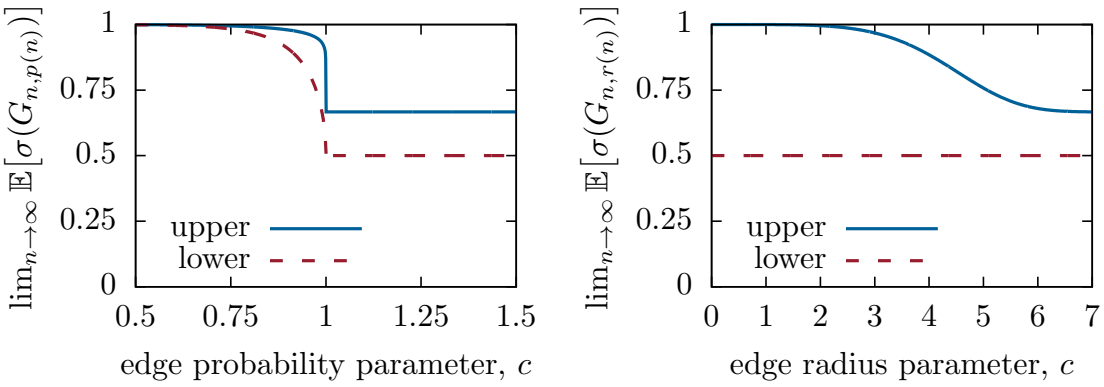


**Figure 2.2:** Limiting bounds ($n \to \infty$) on $\mathbb{E}[\sigma(G)]$ in ER graphs when $p(n) \sim c/n$ (**left**), and RG graphs when $r(n)^2 \sim c/n^{6/5}$ (**right**).

*of* $\mathbb{E}\left[\sigma(G_{n,r(n)})\right]$ *as a function of* $x$.

$$\frac{1}{2} \leq \lim_{n\to\infty} \mathbb{E}\left[\sigma(G_{n,r(n)})\right] \leq \frac{1}{3}\left(2 + \exp\left(-\frac{(\pi c/4)^5}{6!}\right)\right). \tag{2.18}$$

*Proof.* See proof in App. A.18. □

In Fig. 2.2, we present a visual comparison of the limiting behavior of $\mathbb{E}[\sigma]$ for both ER and RG graphs. These bounds are provided by Thm. 2.3 and Thm. 2.5, respectively. We note that the tighter bounds for ER graphs is afforded by the coinciding cycle subgraph thresholds at $p(n) \sim 1/n$.

### 2.4.2 Connectivity and Giant Components

Previously established results provide a regular sharp threshold function for connectivity and a regular threshold for giant components in RG graphs:

**Lemma 2.8** (Regular Sharp Threshold for $\mathcal{P}_{\text{conn}}$ in $G_{n,r(n)}$ [26])**.** *The pair* $(r^*(n)^2 = \log(n)/(\pi n), \alpha(n) = 1/(\pi n))$ *is a regular sharp threshold function for graph property* $\mathcal{P}_{\text{conn}}$ *with sharp-threshold distribution function* $F(x) = \mathrm{e}^{-\mathrm{e}^{-x}}$ *(Gumbel).*

**Lemma 2.9** (Regular Threshold for $\mathcal{P}_{\text{giant}}$ in $G_{n,r(n)}$ [26])**.** $r^*(n)^2 = \lambda_c/n$ *is a regular threshold function for graph property* $\mathcal{P}_{\text{giant}}$ *with threshold distribution function* $F(x) = \mathbf{1}\{x > 1\}$*, where* $\lambda_c \in (0, \infty)$ *is the critical percolation threshold.*

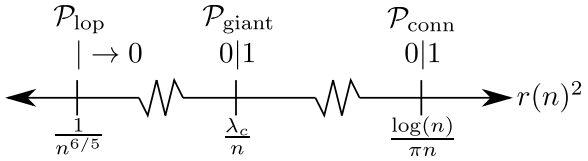


**Figure 2.3:** The limiting behavior of the graph properties in Tab. 2.1 along the design space of functions $r(n)^2$ chosen relative to established threshold functions for RG graphs. Listed from top to bottom are *i)* the graph properties, *ii)* their limiting probabilities relative to an established threshold function or 0-statement in the case of $\mathcal{P}_{\text{lop}}$, *iii)* the established threshold function.

Given the facts that that *i)* $\mathcal{P}_{\text{lop}}$ and $\mathcal{P}_{\text{giant}}$ are monotone decreasing and increasing properties respectively, and *ii)* their respective 0-statements 'overlap', we present a statement of mutual exclusion between the two properties:

**Theorem 2.6** (Mutual Exclusion of $\mathcal{P}_{\text{lop}}$ and $\mathcal{P}_{\text{giant}}$ in $G_{n,r(n)}$)**.** *In RG graphs with edge radius function $r(n)$:*

$$\lim_{n\to\infty} \frac{r(n)^2}{1/n} \geq 0 \Rightarrow \lim_{n\to\infty} \mathbb{P}\{\mathcal{P}_{\text{lop}} \cap \mathcal{P}_{\text{giant}}\} = 0. \tag{2.19}$$

*Proof.* See App. A.16. □

Again, in the case of RG graphs, the threshold for connectivity has a higher order than that of giant components ($\log(n)/(\pi n)$ vs. $\lambda_c/n$), thus, we expect (and find) that properties $\mathcal{P}_{\text{lop}}$ and $\mathcal{P}_{\text{conn}}$ exhibit an identical mutual exclusion:

**Corollary 2.5** (Mutual Exclusion of $\mathcal{P}_{\text{lop}}$ and $\mathcal{P}_{\text{conn}}$ in $G_{n,r(n)}$)**.** *In RG graphs with edge radius function $r(n)$:*

$$\lim_{n\to\infty} \frac{r(n)^2}{1/n} \geq 0 \Rightarrow \lim_{n\to\infty} \mathbb{P}\{\mathcal{P}_{\text{lop}} \cap \mathcal{P}_{\text{conn}}\} = 0. \tag{2.20}$$

*Proof.* $\mathcal{P}_{\text{giant}}$ is necessary for connectivity $\mathcal{P}_{\text{conn}}$, thus $\mathbb{P}\{\mathcal{P}_{\text{lop}} \cap \mathcal{P}_{\text{conn}}\} \leq \mathbb{P}\{\mathcal{P}_{\text{lop}} \cap \mathcal{P}_{\text{giant}}\}$. Mutual exclusion between $\mathcal{P}_{\text{lop}}$ and $\mathcal{P}_{\text{conn}}$ follows immediately from Thm. 2.6. □

In the case of RG graphs, we note that the threshold for $\mathcal{P}_{\text{lop}}$ must lie at a lower order than both that of $\mathcal{P}_{\text{giant}}$ and $\mathcal{P}_{\text{conn}}$, whereas in ER graphs, $\mathcal{P}_{\text{lop}}$ and $\mathcal{P}_{\text{giant}}$ were both located at $1/n$. Refer to Fig. 2.3 for a visual comparison of the limiting behavior of the properties in Tab. 2.1 in RG graphs.

## 2.5 Algorithms for Bounding $\mathcal{P}_{\text{lop}}$

Birand *et al.* [7] outline an $O(n)$-time exact algorithm checking whether or not a graph with $n$ vertices satisfies $\mathcal{P}_{\text{lop}}$ under primary interference constraints. At a high-level, the algorithm involves decomposition of the graph into bi-connected components and checking each component for certain characteristics; among these is a test for 'long' cycles (in order to exclude forbidden cycle lengths). Our analytical results suggest that the formation of cycles are the major factor prohibiting LoP in ER and RG random graphs, so we have implemented algorithms to check for necessary and sufficient conditions for LoP in random graphs ($\mathcal{P}^{\text{L}}_{\text{lop}}$ and $\mathcal{P}^{\text{U}}_{\text{lop}}$). Our simulations are performed in Matlab, where we make use of MatlabBGL [27] for graph decomposition into connected components and depth-first-search. These following algorithms and their supporting functions are listed in Listing 1 and are centered around the detection of long cycles.

HasCycleEq accepts an input graph $G$, a cycle-length $k$, and a maximum number of iterations $I$ and reports whether or not a cycle of length $k$ exists within $G$. HasCycleEq relies directly upon a randomized algorithm, denoted AYK, proposed by Alon *et al.* [28, Thm. 2.2], which iteratively generates random, acyclic, directed subgraphs of $G$ and tests for cycles via the subgraph's adjacency matrix. If no cycles of length $k$ are found after the $I$th iteration, we have HasCycleEq report that no length $k$ cycles exist in $G$, which may be a false negative. As a result, HasCycleEq is suitable for use in upper-bounding the probability of the non-existence of forbidden cycles, namely in PlopU.

HasCycleGeq accepts an input graph $G$, a minimum cycle-length $K$, and a maximum number of iterations $I$ and reports whether or not a cycle of length $K$ or greater exists within $G$. In general, the decision problem formulation (also known as the long-cycle problem) is NP-hard, but polynomial for fixed-parameter $k$. We make use of a result by Gabow and Nie [29, Thm. 4.1]; for $K > 3$, depth-first-search DFS may be used to detect the existence of cycles of length longer than $2K - 4$ by examining the back-edges discovered by DFS. Note, a DFS back-edge of length $K - 1$ implies the existence of a length $K$ cycle. Thus, if a 'long' back-edge is found by DFS, we may report that such a cycle exists (line 7). In the event that DFS fails to detect long backedges, a long simple cycle

(if it exists) will have length between $K$ and $2K-4$ [29, Thm. 4.1]. For each length $k$ within this range, we call the randomized algorithm in HasCycleEq, thus HasCycleGeq may also report false negatives. Alternately, when $K=3$, HasCycleGeq is an exact algorithm (lines 8-10 involving HasCycleEq are short-circuited) that checks for the existence of any cycle. This is accomplished by running DFS and examining the resulting tree for back-edges of length 2 or longer. In the event no such back-edges are found, we may conclude that graph $G$ is cycle-free.

Finally, we discuss PlopL and PlopU. PlopL checks for the existence of any cycles and calls HasCycleGeq directly. For the reasons discussed above, PlopL is an exact (not randomized) algorithm and suitable for lower bounding the probability of satisfying LoP conditions. PlopU checks for the existence of forbidden cycles. For forbidden cycles of length 6, we call HasCycleEq, while for fobidden cycles of length 8 or longer, we call HasCycleGeq. For this reason, the curves displayed for $\mathcal{P}_{\text{lop}}^{\text{U}}$ in later figures are an upper bound for $\mathcal{P}_{\text{lop}}^{\text{U}}$ (which can be improved by increasing the number of allowed iterations, $I$), but nevertheless yield valid upper bounds for $\mathcal{P}_{\text{lop}}$ and additionally demonstrate the mutual exclusivity between $\mathcal{P}_{\text{lop}}$ and $\mathcal{P}_{\text{giant}}$ in ER and RG graphs.

**Remark 2.3.** *One could obtain a tighter sufficient condition $\mathcal{P}_{\text{lop}}^{\text{L}}$ (and thus a tighter lower bound) by restricting cycles of length $k \geq 5$ instead of all cycles. We have not done so for the following reasons:* i) *the use of* HasCycleGeq *with $K=5$ will not produce an exact answer (but instead an upper bound on $\mathcal{P}_{\text{lop}}^{\text{L}}$), and* ii) *we are more concerned and satisfied with characterizing an upper bound for $\mathcal{P}_{\text{lop}}$ and its interaction with connectivity requirements.*

## 2.6 Numerical Results

The analytical results presented thus far are asymptotic ($n \to \infty$). In this section, we compare the analytical mutual exclusion of LoP and giant components with that of numerical results for finite network sizes and find that this exclusion occurs rather quickly as the network grows in size.

### 2.6.1 ER Graphs

In Fig. 2.4, we see that the numerical results generally match their analytical limits at $n = 10^4$. In particular, as $n \to \infty$, the numerical curves associated with $\mathcal{P}_{\text{giant}}(\beta)$ become increasingly sigmoidal

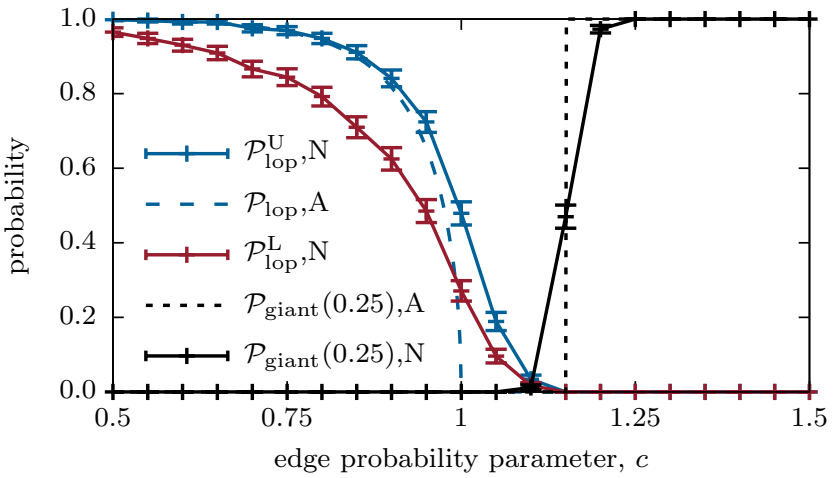


**Figure 2.4:** Probabilities of graph properties occurring in ER graphs are plotted as a function of $c$ where the edge probability is chosen according to $p(n) = c/n$. Asymptotic (as $n \to \infty$), analytical (A) probabilities are plotted in dashed lines. Numerical (N) probabilities are plotted in solid lines with 95% confidence intervals generated from $S = 10^3$ *i.i.d.* graphs of size $n = 10^4$. PLOPU was configured to use a maximum of $I = 10^4$ iterations.

about $c \approx 1.15$ when $\beta$ is set to a rather conservative value of 0.25. Also note that the effect of increasing the minimum required giant component size $\beta$ serves to shift the associated curves in Fig. 2.4 to the right, further negating any chance of both satisfying local pooling and having a giant component. Regarding $\mathcal{P}_{\text{lop}}$, when $c < 1$, we note that there is good agreement with the numerical upper bound and the gap with the lower bound is readily explained by Rem. 2.3. When $c > 1$, there are noticeable 'tails' on the numerical bounds, and we are inclined to attribute the existence of the tails to the notion that graphs of a finite size $n$ may only reliably capture the limiting behavior of small cycles, perhaps much smaller than $n$.[1]

In Fig. 2.5, we focus on edge probability functions $p(n) = c/n$ with parameter $1 \leq c \leq 1.15$, which falls between the asymptotic thresholds for $\mathcal{P}_{\text{lop}}$ and $\mathcal{P}_{\text{giant}}(0.25)$ (see Fig. 2.4). For each edge probability function within this regime, we plot the probability that an ER graph satisfies both $\mathcal{P}_{\text{lop}}^{\text{U}}$ and $\mathcal{P}_{\text{giant}}(0.25)$ as a function of the network size, $n$. We observe that the exclusion between $\mathcal{P}_{\text{lop}}^{\text{U}}$ and $\mathcal{P}_{\text{giant}}$ develops rather rapidly.

[1] By appropriately restricting conditions $\mathcal{P}_{\text{lop}}^{\text{L}}$ and $\mathcal{P}_{\text{lop}}^{\text{U}}$ to cycles of lengths less than finite $K \approx 20$, the resulting threshold distribution functions more closely match the presented numerical results.

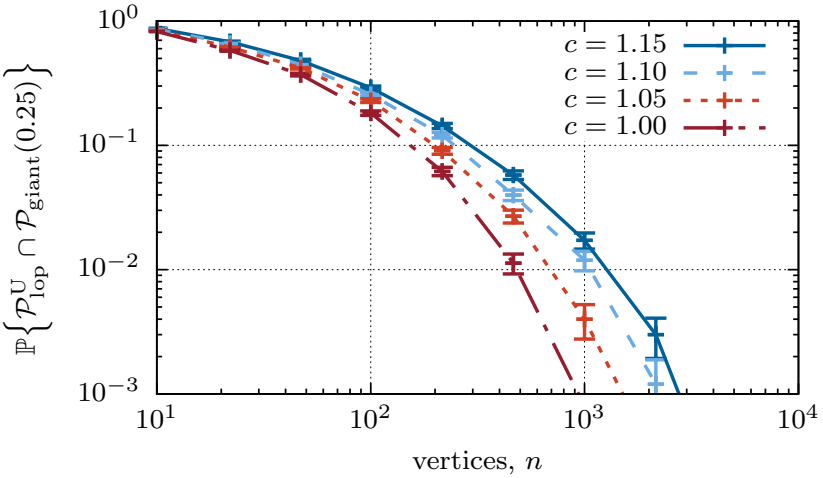


**Figure 2.5:** Numerical probability of satisfying both $\mathcal{P}^{\mathrm{U}}_{\mathrm{lop}}$ and $\mathcal{P}_{\mathrm{giant}}(0.25)$ in ER graphs plotted as a function of $n$ where the edge probability is chosen according to $p(n) = c/n$. Numerical probabilities are computed with 95% confidence intervals generated from $S = 10^4$ *i.i.d.* graphs. PLOPU was configured to use a maximum of $I = 10^3$ iterations.

### 2.6.2 RG Graphs

Unlike the case of ER graphs, we note that the RG graph bounds and thresholds for $\mathcal{P}_{\mathrm{lop}}$ and $\mathcal{P}_{\mathrm{giant}}(\beta)$ (respectively) must necessarily occur at edge radius functions of different orders of $n$. For this reason, we provide two subplots in Fig. 2.6 that are analogous to Fig. 2.4 and separately consider edge radius functions $r(n)^2 = c/n^{6/5}$ and $r(n)^2 = c/n$. Intuitively, for edge radius function $r(n)^2 = c/n^{6/5}$, we expect to see (and also observe) two phenomenon as the parameter $n$ increases: the probability of $\mathcal{P}^{\mathrm{U}}_{\mathrm{lop}}$ should show convergence towards a non-zero threshold distribution function (if Conj. 2.1 is true) while the probability of $\mathcal{P}_{\mathrm{giant}}(\beta)$ should converge to zero. Similarly, for edge radius function $r(n)^2 = c/n$ we observe the opposite phenomenon: the probability of $\mathcal{P}_{\mathrm{giant}}(\beta)$ begins to converge to a non-zero threshold distribution function (near $c = 1.5$) when $r(n)^2 = c/n$, while the probability of $\mathcal{P}^{\mathrm{U}}_{\mathrm{lop}}$ converges to zero for all $c$ at this choice of $r(n)^2$.

While we lack threshold distribution functions for both $\mathcal{P}^{\mathrm{U}}_{\mathrm{lop}}$ and $\mathcal{P}_{\mathrm{giant}}$, we include the established upper bound for $\mathcal{P}_{\mathrm{lop}}$ (Prop. 2.4) for comparison and plot each numerical curve for increasing network sizes $n = \{10^2, 10^3, 10^4\}$. We note that the bound in Prop. 2.4 forbids only vertex-induced complete graphs of order 6 ($K_6$) which is looser than $\mathcal{P}^{\mathrm{U}}_{\mathrm{lop}}$ which forbids edge-induced cycles of lengths $k \geq$

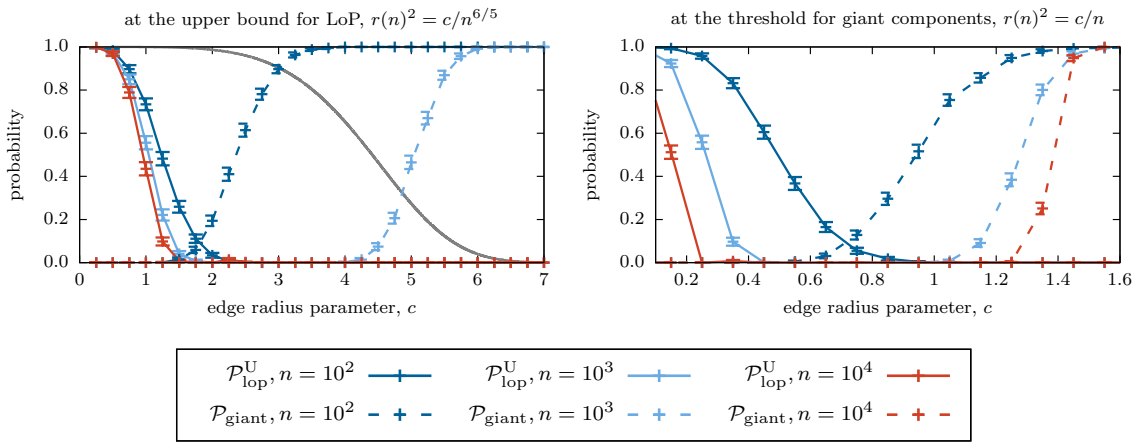


**Figure 2.6:** Probabilities of graph properties occurring in RG graphs are plotted as a function of $c$ where the edge radius is chosen according to $r(n)^2 = c/n^{6/5}$ (**left**) and $r(n)^2 = c/n$ (**right**). Numerical (N) probabilities are plotted according to the legend with 95% confidence intervals generated from $S = 10^3$ *i.i.d.* graphs of sizes $n = \{10^2, 10^3, 10^4\}$. PLOPU was configured to use a maximum of $I = 10^3$ iterations. An additional asymptotic upper bound for $\mathcal{P}_{\mathrm{lop}}$ is plotted in solid grey (**left**).

$6, k \neq 7$ from the set $\mathcal{F}$. The combination of plots in Fig. 2.6 serve to demonstrate the mutual exclusion between $\mathcal{P}_{\mathrm{lop}}$ and $\mathcal{P}_{\mathrm{giant}}$ as $n \to \infty$.

In Fig. 2.7, we focus on both edge radius functions selected for Fig. 2.6, and instead parameterize by $c$. Appropriate parameter values are chosen to explore the area in the gaps presented in Fig. 2.6. For each edge radius function within this regime, we plot the probability that an RG graph satisfies both $\mathcal{P}^{\mathrm{U}}_{\mathrm{lop}}$ and $\mathcal{P}_{\mathrm{giant}}(0.25)$ as a function of the network size, $n$. We observe that the exclusion between $\mathcal{P}^{\mathrm{U}}_{\mathrm{lop}}$ and $\mathcal{P}_{\mathrm{giant}}$ develops even more quickly than in the case of ER graphs. The increase in speed at which this exclusion develops is likely due to the separation in order between the thresholds functions that give rise to $\mathcal{P}_{\mathrm{lop}}$ and $\mathcal{P}_{\mathrm{giant}}$, which was not present in ER graphs.

## 2.7 Conclusions

In this chapter, we investigated the achievable fraction of the capacity region of Greedy Maximal Scheduling via an analytical tool known as Local Pooling. We provided rigorous characterizations of the LoP factor in large networks modeled as Erdős-Rényi (ER) and random geometric (RG) graphs under the primary interference model. We employed threshold functions to establish critical values

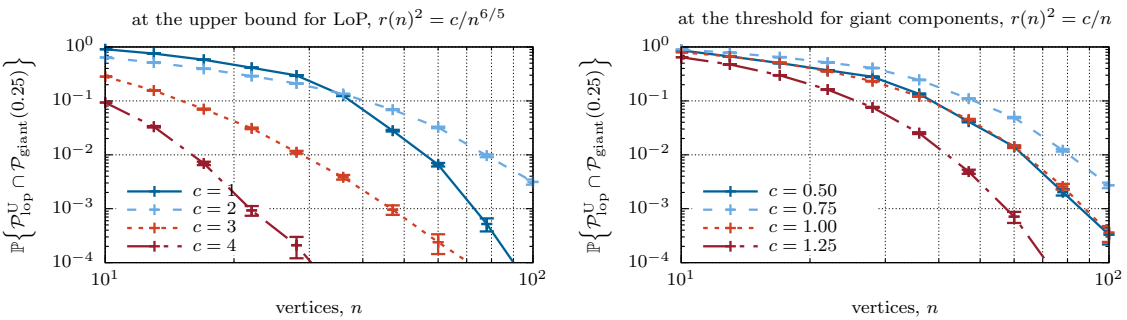


**Figure 2.7:** Numerical probability of satisfying both $\mathcal{P}^{\mathrm{U}}_{\mathrm{lop}}$ and $\mathcal{P}_{\mathrm{giant}}(0.25)$ in RG graphs plotted as a function of $n$ where the edge radius is chosen according to $r(n)^2 = c/n^{6/5}$ (**left**) and $r(n)^2 = c/n$ (**right**). Numerical probabilities are computed with 95% confidence intervals generated from $S = 10^5$ *i.i.d.* graphs. PLOPU was configured to use a maximum of $I = 10^3$ iterations.

for either the edge probability or communication radius to yield useful bounds on the range and expectation of the LoP factor as the network grows large in size. For sufficiently dense random graphs, we found that the LoP factor is bounded between 1/2 and 2/3, while sufficiently sparse random graphs permit GMS optimality (the LoP factor is 1) with high probability. We observed that edge densities permitting connectivity generally admit cycle subgraphs which forms the basis for the LoP factor upper bound of 2/3 and concluded with simulations that explored this aspect. In the regime of small network sizes, our simulation results suggest the probability that an ER or RG graph satisfies LoP and is connected decays rather quickly with the size of the network.

Avenues for future investigation of LoP include a more rigorous examination of the rate of convergence of the probabilities of these graph properties to their asymptotic values. Additionally, examining the fraction of nodes/edges/components in the network satisfying LoP ($\sigma = 1$) may help in identifying simple topology control techniques to increase the LoP factor (*e.g.*, removal of edges to break forbidden cycles in non-LoP satisfying components or addition of edges to patch smaller LoP-satisfying components together).

**Listing 1** Pseudo-code checking for $\mathcal{P}^{\mathrm{L}}_{\mathrm{lop}}$ and $\mathcal{P}^{\mathrm{U}}_{\mathrm{lop}}$

```
function HasCycleEq(G,k,I)
    return AYK(G,k,I)
function HasCycleGeq(G,K,I)
    T_DFS ← DFS(G)
    if LongestBackedge(T_DFS) ≥ (K − 1) then
        return true
    else
        for k = K to 2K − 4 do
            if HasCycleEq(G,k,I) then
                return true
        return false
function PlopL(G,I)
    return HasCycleGeq(G,3,I)
function PlopU(G,I)
    if HasCycleGeq(G,8,I) then
        return true
    else
        return HasCycleEq(G,6,I)
```

# Chapter 3: On the Joint Impact of Beamwidth and Orientation Error on Throughput in Directional Wireless Poisson Networks

## 3.1 Introduction

In a wireless communications network, directional antennas can help increase received signal power while simultaneously reducing interference. Antenna arrays that are steerable mechanically, electrically, or via switched-beams, can further improve networks performance by dynamically redirecting transmitted energy based on the network state. The performance analysis of directional antennas in large scale wireless communications systems over the last few decades has made use of a variety of models, assumptions, and analytical tools. However, much of the previous work assumes either perfect sector selection or beamsteering.

We anticipate the presence of several tradeoffs affecting network throughput and transmission capacity as antenna beamwidth decreases, stemming from sources of imperfect antenna configuration, beamforming, and selection [30, 31, 32, 33, 34]. Assuming constant transmitted power, decreasing beamwidth will result in a higher gain within the antenna's main beam. As the beamwidth decreases, fewer interferers significantly affect the typical receiver, but their individual effects are stronger. Additionally, as the beamwidth decreases, properly aligning the transmitter and receiver becomes more difficult, but when both are aligned, the desired signal strength increases.

In this work, we study these tradeoffs in an ad hoc wireless network setting, modeled by a bipolar Poisson Point Process (PPP). We employ stochastic geometry to investigate optimal beamwidths that maximize throughput-based metrics in the presence of an assumed orientation error distribution. We now categorize and review related work in this area.

### 3.1.1 Related Work

Early works [35, 36] have studied the maximum throughput and expected forward progress of ALOHA and Carrier Sense Multiple Access (CSMA) systems using the protocol model with appropriately chosen interference zones. In particular, under Poisson ALOHA networks with antenna

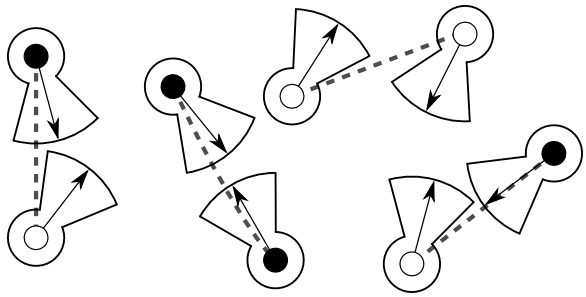

**Figure 3.1:** A wireless network with directional antennas employed on transmitter and receiver pairs (dotted lines). When subjected to orientation error, transmitters and receivers may correctly direct their beam (black nodes), or they may miss their intended counterpart (white nodes).

beamwidth $\beta$, C.-J. Chang and J.-F. Chang [35] found that certain routing schemes achieve a maximum throughput gain on the order of $\frac{1}{\beta}$. A second set of works [37, 38, 39, 40, 41] focused on throughput capacity of directional wireless networks, extending the seminal work of Gupta and Kumar [42]. Specifically, Yi *et al.* [38] found throughput gains of $O\left(\frac{1}{\alpha\beta}\right)$ in random networks employing the protocol interference model with transmitter and receiver beamwidths of $\alpha$ and $\beta$, respectively.

More recently, several works [43, 44, 45, 46] have analyzed directional wireless networks with stochastic geometry, which offers a rich framework [47, 48] for modeling effects such as physical interference (SINR) and fading. Hunter *et al.* [43] studied spatial diversity schemes in ad hoc networks and found that static transmit and receive beamforming with $M$ ideal sector antennas without sidelobes yields transmission capacity gains of $\Theta(M^2)$ over omni-directional antennas. Singh *et al.* [44] developed insights into medium access control design for highly directional networks by examining outage using protocol and physical interference models. Wang and Reed [45] incorporated directional antennas into the analysis of coverage in multi-tier heterogeneous cellular networks. Akoum *et al.* [46] were motivated by the rise of millimeter wave (mmWave) technology and studied achievable coverage and rates of mmWave beamsteering.

All of the works reviewed thus far assumed either perfect sector selection or perfect beamsteering. Even the *point-to-destination* scheme of C.-J. Chang and J.-F. Chang [35] modeled perfect orientation towards the destination, despite leading to outages when no feasible next hop falls within the transmitter's sector. We note that antenna orientation error can affect the distribution of gains

between interferers and the typical receiver. While gain distributions have been used to study the interaction between arbitrary interferers and the typical receiver [45, 46], we are aware of no work that incorporates orientation error into a stochastic geometry based analysis.

However, we note several works that do explicitly account for error in directional wireless networks [49, 50, 32, 51]. Specifically, the effect of beam-pointing error can be associated with an averaged, normalized radiation pattern with a wider main lobe and higher sidelobes than the original normalized pattern without error [49, 50]. Shen and Pearson [49] investigated coupled oscillator beam-steering arrays and the effects of per-array-element phase error on beam-pointing error. Li *et al.* [50] discussed uniform linear array (ULA) beamforming error stemming from direction of arrival (DOA) estimation, spatial (or angular) spread of the transmitted signal, antenna array element perturbation, and mutual coupling of array elements. They analyzed outage and noted a degradation in performance due to error sources of increasing magnitude. Vakilian *et al.* [51] studied the impact of DOA estimation error, angular spread, and beamwidth on bit error rate. They noted that narrow beamwidths can exhibit higher bit error rates than wider beamwidths when subjected to a large enough DOA error.

### 3.1.2 Contributions

The rest of this chapter is summarized as follows. §3.2 introduces our wireless network model. §3.3 explores the success probability of a typical transmitter under arbitrary radiation patterns (Prop. 3.1) and sectorized patterns (Cor. 3.2 and Cor. 3.3). §3.4 and §3.5 study network metrics spatial throughput and transmission capacity, respectively. We derive closed form expressions for spatial throughput (Prop. 3.2) and transmission capacity (Prop. 3.4) under ideal sector antennas without sidelobes and arbitrary orientation error distributions. We find that concavity of the cumulative orientation error distribution is sufficient for both monotonicity of spatial throughput (Prop. 3.3) and unimodality of transmission capacity (Prop. 3.5) when expressed as functions of antenna beamwidth. A comparison of our analytical results with that of numerical results involving more complex radiation patterns is provided in §3.6. We conclude our work and outline future avenues of research in §3.7. Finally, for clarity, long proofs are presented in App. B.

## 3.2 Model

We model a wireless network with $\hat{\Phi} = \{(x_i, m_i)\}$, a marked, homogeneous, bipolar Poisson Point Process (PPP) of intensity $\lambda > 0$. $\hat{\Phi}$ models the placement and orientation of transmitter-receiver pairs, where the members of each pair are separated by distance parameter $d > 0$. The ground set $\{x_i\} \subset \mathbb{R}^2$ represents the transmitter (TX) locations, while the *i.i.d.* marks $\{m_i\}$ (formally defined in §3.2.3) encode the receiver (RX) locations and antenna orientation errors. For notational convenience, we will denote the resulting RX locations with $\{y_i\} \subset \mathbb{R}^2$, where RX $i$ is associated (paired) with TX $i$. In the following subsections, we detail the rest of our model.

### 3.2.1 Gain Patterns

Each TX and RX is equipped with a 2-dimensional antenna gain pattern $G : [-\pi, \pi) \to \mathbb{R}^+$. The input angle to $G(\cdot)$ is provided relative to the antenna's boresight, or 'forward' direction. For simplicity, we will assume the gain pattern is symmetric about the boresight angle: $G(-\theta) = G(\theta)$. Further, we will consider parameterized antenna radiation patterns such that the total radiated power (TRP) remains constant over the parameter space; equivalently:

$$\text{TRP} \equiv \int_{-\pi}^{\pi} \frac{G(\theta)}{2\pi} \mathrm{d}\theta = 1. \tag{3.1}$$

### 3.2.2 Antenna Orientation & Error

Let $\hat{\theta}_{x,y} = \angle(y - x)$ be the angle of the vector from location $x$ to location $y$ relative to the positive $x$-axis. Thus, for a given TX-RX pair $i$, $\hat{\theta}_{x_i,y_i}$ is the orientation of the RX about its paired TX. We assume that each communication device may steer its gain pattern $G(\cdot)$ via a simple rotation of the pattern about the device's location. Thus, under the assumption of perfect orientation, the boresight of antennas on TX $i$ and RX $i$ would be aligned directly along $\hat{\theta}_{x_i,y_i}$ and $\hat{\theta}_{y_i,x_i}$ respectively. However, in order to study the effect of antenna misconfiguration on network performance, we introduce additive error $\epsilon_x$ into the orientation of a beam originating from location $x$, measured relative to the perfect orientation angle. For simplicity, we will consider error distributions symmetric about zero degrees. Finally, let $\theta_{x_i,y_j}$ and $\theta_{y_j,x_i}$ be the angles between TX $i$ and RX $j$ relative to their

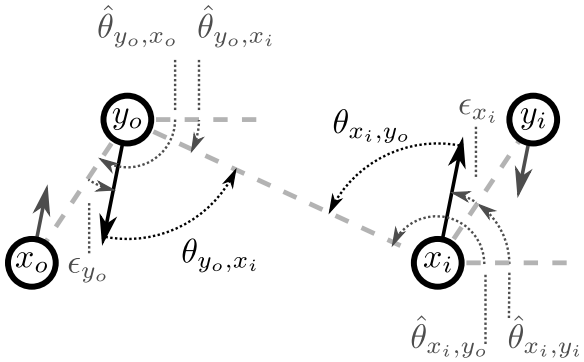


**Figure 3.2:** TX/RX positions are in circles with boresight angles marked by solid arrows. Relevant angles are marked by gray dashed arrows, while gain input angles are black dashed arrows.

respective boresight angle. These angles are the gain input angles used to compute the gain between two communication devices, and can be expressed as:

$$\begin{aligned}\theta_{x_i,y_j} &= \hat{\theta}_{x_i,y_j} - (\hat{\theta}_{x_i,y_i} + \epsilon_{x_i}) \\ \theta_{y_j,x_i} &= \hat{\theta}_{y_j,x_i} - (\hat{\theta}_{y_i,x_i} + \epsilon_{y_j}),\end{aligned} \tag{3.2}$$

and are visualized by Fig. 3.2. Note: if $i = j$, the gain input angles between TX-RX pair $i$ are simply $\theta_{x_i,y_i} = -\epsilon_{x_i}$ and $\theta_{y_i,x_i} = -\epsilon_{y_i}$.

### 3.2.3 Marks on the Process

The marks of the process are $\{m_i = (\hat{\theta}_{x_i,y_i}, \epsilon_{x_i}, \epsilon_{y_i})\}$ and consist of the following:

- $\{\hat{\theta}_{x_i,y_i} \sim [-\pi, \pi]\}$, the uniformly distributed orientation of each RX about its paired TX. Note: the marks encode the RX locations $\{y_i\} \subset \mathbb{R}^2$ via $\{\hat{\theta}_{x_i,y_i}\}$ and $d$,
- $\{\epsilon_{x_i} \sim f_\epsilon : [-\epsilon_{\max}, \epsilon_{\max}] \to \mathbb{R}^+\}$, the random orientation error of each TX's beam toward its paired RX, with zero-mean and bounded absolute error $\epsilon_{\max} \leq \pi$, and
- $\{\epsilon_{y_i} \sim f_\epsilon : [-\epsilon_{\max}, \epsilon_{\max}] \to \mathbb{R}^+\}$, the random orientation error of each RX's beam toward its paired TX, with zero-mean and bounded absolute error $\epsilon_{\max} \leq \pi$.

### 3.2.4 Communication Model

Finally, we model signal propagation using large-scale, distance-based pathloss with Rayleigh fading. The signal power at RX $j$ from TX $i$ is given by:

$$P_{i,j} = P_t H_{i,j} G(\theta_{x_i,y_j}) G(\theta_{y_j,x_i}) d_{i,j}^{-\alpha}, \tag{3.3}$$

where $P_t$ is a fixed global power assignment across all transmitters, $H_{i,j}$ is the Rayleigh fading coefficient between TX $i$ and RX $j$ with $H_{i,j} \sim \text{Exp}(1)$, $G(\theta_{x_i,y_j})$ and $G(\theta_{y_j,x_i})$ are the gains produced by TX $i$ and RX $j$ respectively in the direction of each other, $\alpha > 2$ is the large-scale pathloss constant, and $d_{i,j}$ is the distance from TX $i$ to RX $j$ (note: $d_{i,i} = d$).

A transmission between TX-RX pair $j$ is considered successful if the signal-to-interference-plus-noise ratio (SINR) falls above a defined SINR threshold $\beta > 0$: $\text{SINR}_j = P_{j,j}/(I_j + \eta)$, where $\eta \geq 0$ is the background noise power and $I_j = \sum_{i \neq j} P_{i,j}$ is the sum interference power at RX $j$. The probability of success $p_s$ of transmission $j$ is then given by $p_s = \mathbb{P}\{\text{SINR}_j \geq \beta\}$. Unless otherwise noted, common parameters used to generate all figures and numerical results are $\alpha = 3$, $\beta = 4$, $d = 100$ meters, $\eta = 10^{-12}$ Watts, and $P_t = 1$ Watt.

## 3.3 A Typical Transmission

In this section, we discuss the success probability of a typical TX-RX pair $o$ with the receiver located at the origin. This is possible due to Slivnyak's Theorem (Theorem 8.1 [52]) applied to the PPP $\hat{\Phi}$, which says that the reduced Palm distribution of $\hat{\Phi}$ is equivalent to the original distribution of $\hat{\Phi}$. Here, the reduced Palm distribution of interest first conditions $\hat{\Phi}$ on the locations of $x_o$ and $y_o$ and subsequently removes both points in order to provide analysis on the sum interference generated by $\hat{\Phi}$ and observed at $y_o$.

### 3.3.1 Induced Gain Distributions

As Wang and Reed [45] note, the antenna gains produced between arbitrary TX/RXs in a PPP are random variables due to their random positions. In this work, we additionally allow the TX/RX

orientations to vary independently of their positions via $\epsilon_{x_i}$ and $\epsilon_{y_i}$. As a consequence, the random gains produced between the typical TX-RX pair, denoted $G_{\mathrm{T}}$ and $G_{\mathrm{R}}$, are:

$$\begin{aligned} G_{\mathrm{T}}(\theta_{x_o,y_o}) &= G_{\mathrm{T}}(\epsilon_{x_o}), \quad \epsilon_{x_o} \sim f_{|\epsilon|} \\ G_{\mathrm{R}}(\theta_{y_o,x_o}) &= G_{\mathrm{R}}(\epsilon_{y_o}), \quad \epsilon_{y_o} \sim f_{|\epsilon|}. \end{aligned} \tag{3.4}$$

Equations in (3.4) are due to the simplification of (3.2) when $i = j = o$. It is sufficient to consider a distribution on the absolute orientation error, $f_{|\epsilon|}$, due to our assumption of a symmetric gain pattern $G(\cdot)$. Additionally, the random gains produced between an arbitrary TX at $x_i$ and the typical RX at $y_o$, denoted $G_{\mathrm{T_I}}$ and $G_{\mathrm{R_I}}$ are:

$$\begin{aligned} &G_{\mathrm{T_I}}(\theta_{x_i,y_o}), \quad \theta_{x_i,y_o} \sim [-\pi, \pi] \\ &G_{\mathrm{R_I}}(\theta_{y_o,x_i}), \quad \theta_{y_o,x_i} \sim [-\pi, \pi], \end{aligned} \tag{3.5}$$

due to fact that (3.2) contains the sum of circular *r.v.*'s, where one of the summands in each sum ($\hat{\theta}_{x_o,y_o}$ or $\hat{\theta}_{x_i,y_i}$) is uniformly distributed over the circle, thus the sum is also uniformly distributed over the circle [53]. In effect, the above four gains have been expressed independently of the geometry of the points in $\hat{\Phi}$. The distributions on the gains will be useful when computing the success probability of a typical transmission.

**Remark 3.1.** *In this chapter, we restrict our attention to absolute orientation error* c.d.f.*s, $F_{|\epsilon|}$, that are twice differentiable and concave over bounded support $[0, \epsilon_{\max}]$ with $\epsilon_{\max} \leq \pi$. Concave distributions are equivalently the set of monotonically decreasing distributions $F''_{|\epsilon|}(x) = f'_{|\epsilon|}(x) \leq 0, \forall x \in (0, \epsilon_{\max})$. This is a reasonable class of distributions to model sources of error, especially if increasingly large errors are expected to occur with decreasing likelihood. The assumption of twice differentiability is made to avoid distracting analytical corner cases. From the assumptions of concavity and the support, it follows that $f_{|\epsilon|}(x) > 0, \forall x \in [0, \epsilon_{\max})$ and $F_{|\epsilon|}(x) > 0, \forall x \in (0, \epsilon_{\max}]$. Finally, we will make use of truncated distributions (*e.g.*, exponential truncated to $[0, \pi]$) and parameterize*

*them by their mean (prior to truncation) in the text and figures.*

### 3.3.2 Success Probability

We begin with Prop. 3.1, which provides a general formulation of the typical transmission success probability under arbitrary gain patterns and error distributions.

**Proposition 3.1** (Success of a Typical Transmission)**.** *In a network modeled by $\hat{\Phi}$ with intensity $\lambda > 0$, TX-RX separation distance $d$, gain pattern $G(\cdot)$, pathloss constant $\alpha > 2$, background noise $\eta \geq 0$, SINR threshold $\beta$, orientation error distribution $f_{|\epsilon|}$, and Rayleigh fading, the success probability $p_s$ of a typical transmission can be expressed as:*

$$p_s = \int_{0^+}^{\infty} \int_{0^+}^{\infty} \exp\left( -\lambda \pi \kappa \left( \frac{\beta}{g_{\mathrm{T}} g_{\mathrm{R}}} \right)^{2/\alpha} \mathbb{E}\left[ G_{\mathrm{T_I}}^{2/\alpha} \right] \mathbb{E}\left[ G_{\mathrm{R_I}}^{2/\alpha} \right] d^2 \right) * \exp\left( -\frac{\beta d^{\alpha} \eta}{P_t g_{\mathrm{T}} g_{\mathrm{R}}} \right) f_{G_{\mathrm{T}}}(g_{\mathrm{T}})\, f_{G_{\mathrm{R}}}(g_{\mathrm{R}})\, \mathrm{d}g_{\mathrm{T}} \mathrm{d}g_{\mathrm{R}}, \tag{3.6}$$

*where $\kappa = \Gamma(1+2/\alpha)\Gamma(1-2/\alpha)$ and both $\mathbb{E}\left[ G_{\mathrm{T_I}}^{2/\alpha} \right]$ and $\mathbb{E}\left[ G_{\mathrm{R_I}}^{2/\alpha} \right]$ are the $2/\alpha$-moments of the random gains produced between an arbitrary interferer and the typical RX.*

*Proof.* See proof in App. B.1. □

As Wang and Reed [45] note, the joint gain distribution $f_{G_{\mathrm{T_I}}}(g_{\mathrm{T_I}})\, f_{G_{\mathrm{R_I}}}(g_{\mathrm{R_I}})$ can be interpreted as a thinning probability. The expression $\lambda f_{G_{\mathrm{T_I}}}(g_{\mathrm{T_I}})\, f_{G_{\mathrm{R_I}}}(g_{\mathrm{R_I}})$ represents the intensity of transmitters from $\hat{\Phi}$ that produce a combined gain of $g_{\mathrm{T_I}} g_{\mathrm{R_I}}$ with the typical receiver at $y_o$. Further, if we ignore fading and approximate the sum interference ($I_o$) with the dominant interference, [1] success under each such thinned PPP would require that no interferers exist within a void zone of radius $\left( \beta \frac{g_{\mathrm{T_I}} g_{\mathrm{R_I}}}{g_{\mathrm{T}} g_{\mathrm{R}}} \right)^{1/\alpha} d$ around the typical receiver. The integral inside the exponent can be interpreted as a product of void probabilities across the independent, thinned PPPs.

With the appropriate assumptions, Prop. 3.1 can be related back to the success probability under omni-directional antennas [47].

[1] See Prop. 3.6 and Prop 4.2 from [54]. Under these assumptions, $\kappa$ can be effectively treated as 1.

**Corollary 3.1** (Success with Omni-directional Antennas [47])**.** *Let an omni-directional antenna be described by* $G(\theta) = 1, \forall \theta \in [-\pi, \pi]$*. If such antennas are employed in a network described by Prop. 3.1, the success probability* $p_s$ *of a typical TX-RX pair is:*

$$p_s = e^{-\lambda \pi \kappa \beta^{2/\alpha} d^2} e^{-\frac{\beta d^\alpha \eta}{P_t}}, \tag{3.7}$$

*where* $\kappa = \Gamma(1 + 2/\alpha)\Gamma(1 - 2/\alpha)$*.*

*Proof.* Under omni-directional antennas $G(\theta) = 1$, the four gain distributions are equivalently: $G_{\mathrm{T}} \sim G_{\mathrm{R}} \sim G_{\mathrm{T_I}} \sim G_{\mathrm{R_I}} \sim f_G(g) = \delta(g - 1)$, where $\delta(\cdot)$ is the Dirac delta function. It immediately follows that $\mathbb{E}\left[G_{\mathrm{T_I}}^{2/\alpha}\right] = \mathbb{E}\left[G_{\mathrm{R_I}}^{2/\alpha}\right] = 1$. Finally, apply these gain distributions and moments into (3.6) of Prop. 3.1. □

### 3.3.3 Ideal Sectors

Let $G_{\mathrm{ideal}}(\theta)$ be an ideal sector antenna with a gain pattern defined by beamwidth $\omega \in (0, 2\pi)$, main beam gain $g_1$, and sidelobe gain $g_2$ with $0 \leq g_2 < 1 < g_1$:

$$G_{\mathrm{ideal}}(\theta) = \begin{cases} g_1 = \frac{2\pi - (2\pi - \omega) g_2}{\omega} & \text{if } |\theta| \leq \omega/2 \\ g_2 & \text{else} \end{cases}. \tag{3.8}$$

A visualization of this pattern is provided in Fig. 3.3. Note: the TRP of (3.8) is held constant at $P_t$ over the parameter space of $\omega$ and $g_2$. Lem. 3.1 provides the four distributions and $2/\alpha$-moments of the sector pattern gains between the typical RX and both the typical TX and an arbitrary interfering TX.

**Lemma 3.1** (Ideal Sector Gain Distributions)**.** *In a network modeled by* $\hat{\Phi}$ *with ideal sector antennas described by (3.8), the gain distributions are given by:*

$$f_{G_{\mathrm{T}}}(g) = f_{G_{\mathrm{R}}}(g) = \bar{u}\delta(g - g_2) + u\delta(g - g_1), \tag{3.9}$$

$$f_{G_{\mathrm{T_I}}}(g) = f_{G_{\mathrm{R_I}}}(g) = \bar{p}\delta(g - g_2) + p\delta(g - g_1), \tag{3.10}$$

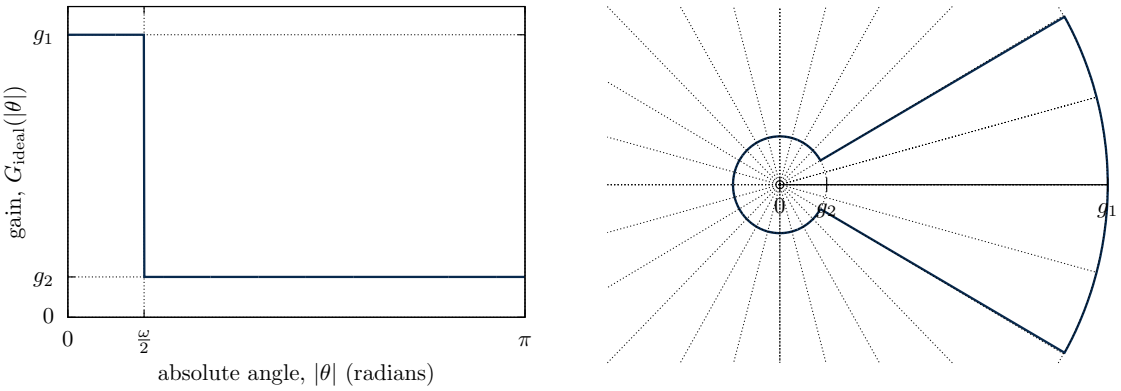


**Figure 3.3:** A symmetric, sector pattern with beamwidth $\omega$, mainbeam gain $g_1$, and sidelobe gain $g_2$.

*where* $p = \frac{\omega}{2\pi}$, $\bar{p} = 1 - p$, $u = F_{|\epsilon|}(\omega/2)$ *and* $\bar{u} = 1 - u$. *Further, the* $2/\alpha$*-moments of the gain distributions between an arbitrary interferer and the typical receiver are:*

$$\mathbb{E}\left[G_{\text{T}_\text{I}}^{2/\alpha}\right] = \mathbb{E}\left[G_{\text{R}_\text{I}}^{2/\alpha}\right] = \bar{p}g_2^{2/\alpha} + pg_1^{2/\alpha}. \tag{3.11}$$

*Proof.* Apply the ideal sector pattern (3.8) to the gain distributions in (3.4) and (3.5). Since (3.8) produces either gains $g_1$ and $g_2$ over all possible input angles, the resulting gain distributions are discrete. The moments of the discrete gain *r.v.*'s are readily computed. □

We note that $p$ and $\bar{p}$ can be interpreted as the main beam *hit rate* and *miss rate*, respectively, between interferers and the typical receiver ultimately due to their uniform orientation with respect to one another. On the other hand, $u$ and $\bar{u}$ are the main beam hit and miss rates, respectively, between the typical TX-RX pair solely determined by their orientation errors.

**Corollary 3.2** (Success with Ideal Sectors)**.** *If sectors described by (3.8) with non-zero sidelobes* ($g_2 > 0$) *are employed in a network described by Prop. 3.1, the success probability* $p_s$ *of a typical*

*TX-RX pair is:*

$$p_s = u^2 e^{-\lambda\pi\kappa\beta^{2/\alpha}d^2\left(p+\bar{p}\left(\frac{g_2}{g_1}\right)^{2/\alpha}\right)^2} e^{-\frac{\beta d^\alpha \eta}{P_t g_1^2}} + 2u\bar{u}e^{-\lambda\pi\kappa\beta^{2/\alpha}d^2\left(p\left(\frac{g_1}{g_2}\right)^{1/\alpha}+\bar{p}\left(\frac{g_2}{g_1}\right)^{1/\alpha}\right)^2} e^{-\frac{\beta d^\alpha \eta}{P_t g_1 g_2}} + \bar{u}^2 e^{-\lambda\pi\kappa\beta^{2/\alpha}d^2\left(p\left(\frac{g_1}{g_2}\right)^{2/\alpha}+\bar{p}\right)^2} e^{-\frac{\beta d^\alpha \eta}{P_t g_2^2}}. \tag{3.12}$$

*where $\kappa$, $p$, $\bar{p}$, $u$, and $\bar{u}$ are as defined in Prop. 3.1 and Lem. 3.1.*

*Proof.* Apply the gain distributions and moments from Lem. 3.1 to (3.6) of Prop. 3.1. □

From Cor. 3.2, the three summands in (3.12) correspond to cases involving the typical TX and RX; *i)* both the typical TX and RX *hit* each other *w.p.* $u^2$, *ii)* one *hits* and the other *misses w.p.* $2u\bar{u}$, or *iii)* both *miss* each other *w.p.* $\bar{u}^2$. In each summand, the last exponential term relates to the transmission failure rate due to noise under Rayleigh fading, $1 - e^{-\frac{\beta d^\alpha \eta}{P_t g_T g_R}}$, and differs due to the gains between the typical TX-RX pair. Finally, in each summand, the first exponential term contains a quadratic term in $p$ and $\bar{p}$. This term offers some intuitive interpretations once expanded, where $p^2$ and $2p\bar{p}$ and $\bar{p}^2$ represent the cases describing the hit/miss interaction between an arbitrary interferer and the typical RX and can be thought of as thinning probabilities of the interferers in $\hat{\Phi}$. If we ignore fading and approximate sum interference with dominant interference, the ratio of variables $g_1$ and $g_2$ represent adjustments to void distances/probabilities for the dominant interferer based on its hit/miss interaction with the typical RX.

Finally, if we assume perfect control over the strength of the sidelobes $g_2 = 0$, we can simplify the success probability further, as given by Cor. 3.3.

**Corollary 3.3** (Success with Ideal Sectors without Sidelobes)**.** *If sectors described by (3.8) with zero sidelobes ($g_2 = 0$) are employed in a network described by Prop. 3.1, the success probability $p_s$ of a typical TX-RX pair is:*

$$p_s = u^2 e^{-\lambda\pi\kappa\beta^{2/\alpha}d^2p^2} e^{-\frac{\beta d^\alpha \eta}{P_t g_1^2}}. \tag{3.13}$$

*Proof.* Apply the gain distributions and moments from Lem. 3.1 to (3.6). Note: $g_2 = 0$ and the

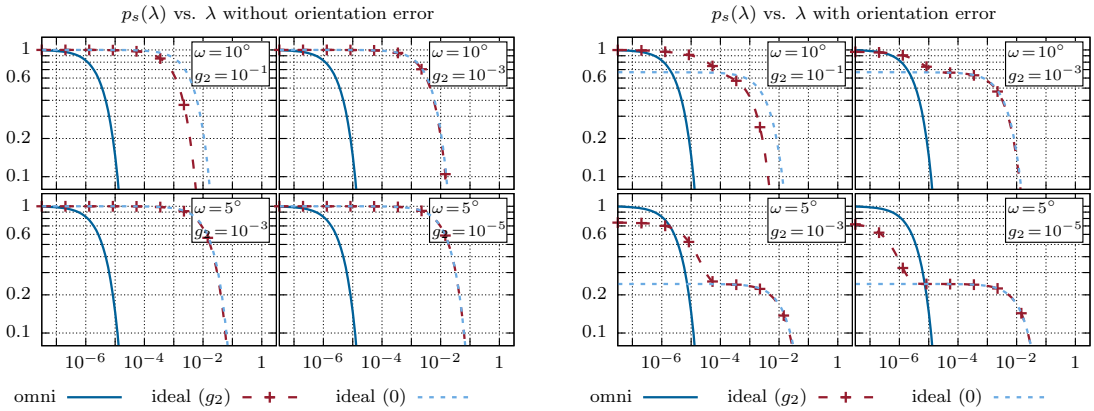


**Figure 3.4:** Sample success curves $p_s(\lambda)$ plotted against intensity of active transmitters $\lambda$. Orientation error $|\epsilon|$ is set to zero in the left set of grouped plots; in the right set of grouped plots, orientation error $|\epsilon|$ is modeled using a half-normal distribution with mean $\bar{\epsilon} = 3$ degrees. Curves include the cases of **omni**-directional antennas; **ideal** sector antennas with sidelobes ($g_2$) with beamwidth $\omega$ and sidelobe gain $g_2$ specified in each subplot; and ideal sector antennas without sidelobes ($g_2 = 0$) with the indicated beamwidth $\omega$ specified in each subplot.

lower limits of the double integration are $0^+$. □

The results of Cor. 3.3 offer a nice interpretation when compared to the omni-directional results of Cor. 3.1. First, an arbitrary interferer and the typical RX will hit each other *w.p.* $p^2$ which acts to thin the original process of interferers. Second, within this thinned process, the typical TX-RX pair will hit each other with rate $u^2$.

A comparison of the success probabilities established in Cor. 3.1, Cor. 3.2, and Cor. 3.3 can be seen in Fig. 3.4. The degree to which the success under ideal sector antennas with sidelobes can be approximated by that of sectors without sidelobes greatly depends on the system parameters $\omega$, $F_{|\epsilon|}$, and $g_2$. Without orientation error, the three types of radiation patterns in Fig. 3.4, omni-directional, sectors without sidelobes, and sectors with sidelobes produce neatly ordered success curves. Furthermore, success without sidelobes is the largest because any energy allocated to sidelobes is essentially wasted between the typical TX-RX pair in the absence of orientation error. Finally, $p_s \to 1$ as the network intensity $\lambda$ (and interference) approaches zero.

When orientation error is introduced, the success curves in Fig. 3.4 are no longer guaranteed to be ordered. In fact, the two sector types produce a crossing, where the presence of sidelobes is beneficial in low density networks, but harmful in high density networks. The presence of sidelobes not

only allows interference to be generated and received, but also permits successful communications when antennas are misaligned. In low density networks, interference is minimal, resulting in a net benefit from sidelobes. Regardless of the presence of error, sector antennas tend to increase a typical transmission's success for higher spatial intensities $\lambda$ over that of omni directional antennas. Additionally, sectors with and without sidelobes produce similar success curves when *i)* the beamwidth is sufficiently larger than the mean orientation error, or *ii)* the sector sidelobe is sufficiently suppressed. As the network intensity $\lambda$ approaches zero, success of sectors without sidelobes is upper bounded by the typical TX-RX hit rate $u^2 = F^2_{|\epsilon|}(\omega/2)$ which decreases as the beamwidth narrows.

## 3.4 Maximizing Spatial Throughput

The *spatial throughput* of a network described by Prop. 3.1 is the maximum spatial intensity of successful transmissions. Spatial throughput (TP) is found by the maximization of $\lambda p_s(\lambda)$ over the spatial intensity of active transmitters $\lambda$:

$$\mathrm{TP} = \max_{\lambda>0} \lambda p_s(\lambda). \tag{3.14}$$

Spatial throughput can be achieved by an appropriate tradeoff of the intensity of active transmitters $\lambda$ with the transmission success rate $p_s(\lambda)$ (a monotone decreasing function of $\lambda$). Prop. 3.2 provides the optimal spatial intensity of active transmitters $\lambda^*$ and the resulting success rate $p_s(\lambda^*)$ that achieves TP for networks that employ ideal sector without sidelobes.

**Proposition 3.2** (TP using Sectors without Sidelobes)**.** *If sectors described by (3.8) with zero sidelobes ($g_2 = 0$) are employed in a network described by Prop. 3.1, the network's spatial throughput is* $\mathrm{TP_s} = \lambda^* p_s(\lambda^*)$*, where:*

$$p_s(\lambda^*) = u^2 e^{-1-\frac{\beta d^\alpha \eta}{P_t g_1^2}}, \qquad \lambda^* = \frac{1}{p^2 \pi \kappa d^2 \beta^{2/\alpha}}. \tag{3.15}$$

*Proof.* See proof in App. B.2. □

Examining Prop. 3.2, the dependence of $p_s(\lambda^*)$ and $\lambda^*$ on $\omega$ is such that $p_s(\lambda^*) \to 0$ and $\lambda^* \to \infty$

as the beamwidth is decreased $\omega \to 0$. It stands to reason that if $p_s(\lambda)$ decreases slowly enough in $\omega$, the product (spatial throughput) may be driven higher by a narrowing beamwidth. Along these lines, we have found that spatial throughput $\mathrm{TP_s}$ can be increased arbitrarily, despite the presence of orientation error, under the class of concave, twice differentiable error distributions $F_{|\epsilon|}$. This notion is formalized by Prop. 3.3.

**Proposition 3.3** (Concave $F_{|\epsilon|}$ Implies Monotonicity of $\mathrm{TP_s}$ in Beamwidth)**.** *Let sectors described by (3.8) with zero sidelobes ($g_2 = 0$) be employed in a network described by Prop. 3.1. If the orientation error* c.d.f. $F_{|\epsilon|}$ *is concave over* $[0, \pi]$*, then* $\mathrm{TP_s}$ *is monotone increasing as* $\omega \to 0$*.*

*Proof.* See proof in App. B.3. □

In the proof of Prop. 3.3, we use the fact that concavity of $F_{|\epsilon|}$ implies $\frac{f_{|\epsilon|}(x)}{F_{|\epsilon|}(x)} \leq \frac{1}{x}$ before establishing $\mathrm{TP_s}$ monotonicity, producing the following nested subsets of error distributions:

$$\{F_{|\epsilon|} : F_{|\epsilon|} \text{ concave, twice diff.}\} \subset \left\{F_{|\epsilon|} : \frac{f_{|\epsilon|}(x)}{F_{|\epsilon|}(x)} \leq \frac{1}{x}, \forall x > 0\right\} \subset \{F_{|\epsilon|} : \mathrm{TP_s} \text{ monotone}\}. \quad (3.16)$$

The ratio, $\frac{f_{|\epsilon|}}{F_{|\epsilon|}} = \frac{\mathrm{d}}{\mathrm{d}x} \log\left(F_{|\epsilon|}\right)$, is also known as the logarithmic derivative of $F_{|\epsilon|}$. We point out that truncations of a distribution $F_{|\epsilon|}$ are simply a linear scaling, and thus preserve concavity and leave the logarithmic derivative of $F_{|\epsilon|}$ unchanged. As a result, we can classify some error distributions with infinite support (*e.g.*, exponential) as satisfying Prop. 3.3 without having to first truncate them. It is worth noting the possible connection with log-concavity for probability distributions, a well studied subject [55].

A sample of *c.d.f.*s in the class covered by Prop. 3.3 are the uniform, exponential, and normal *c.d.f.*s, all of which are concave, as stated by Cor. 3.4.

**Corollary 3.4** (Error Distributions with Monotone $\mathrm{TP_s}$)**.** *If sectors described by (3.8) with zero sidelobes ($g_2 = 0$) are employed in a network described by Prop. 3.1 with orientation error modeled by either i) uniform, ii) exponential, or iii) half-normal distributions, then* $\mathrm{TP_s}$ *is monotone decreasing in* $\omega$ *over* $[0, 2\pi]$*.*

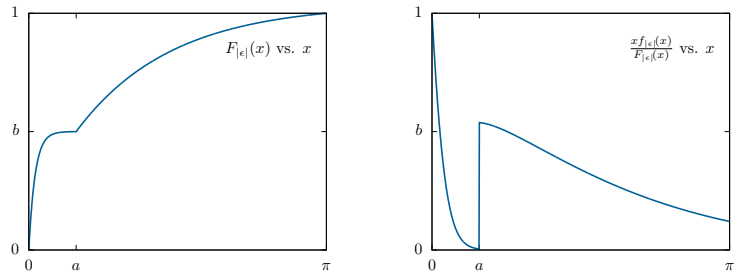


**Figure 3.5:** Sample distribution $F_{|\epsilon|}(x)$ given by (3.17) with $a = 0.5$, $b = 0.5$, $c_1 = 15$, $c_2 = 1$.

*Proof.* It is enough to show that $F_{|\epsilon|}(x)$ is concave over $x \in [0, \pi]$ (omitted for brevity). By Prop. 3.3, it follows that $\mathrm{TP_s}(\omega)$ is monotone decreasing in $\omega$ over $(0, 2\pi]$. □

**Remark 3.2.** *While sufficient, concavity of the error distribution $F_{|\epsilon|}$ is not necessary for throughput monotonicity. Consider the following error distribution on $[0, \pi]$ with a 'dimple' at $(a, b)$:*

$$F_{|\epsilon|}(x) = \begin{cases} \frac{b\left(1-e^{-c_1 x}\right)}{1-e^{-c_1 a}} & 0 \le x \le a \\ b + \frac{(1-b)\left(1-e^{-c_2(x-a)}\right)}{1-e^{-c_2(\pi-a)}} & a < x \le \pi \end{cases} \tag{3.17}$$

*Fig. 3.5 displays (3.17) with parameter values such that $F_{|\epsilon|}$ is non-concave. However, the example satisfies $\frac{xf_{|\epsilon|}(x)}{F_{|\epsilon|}(x)} \le 1, \forall x > 0$ and thus yields monotone* $\mathrm{TP_s}$.

For completeness, Cor. 3.5 provides the spatial throughput for networks employing omni-directional antennas, a well studied scenario [47, 54].

**Corollary 3.5** (TP using Omni-directional Antennas)**.** *If omni-directional antennas are employed in a network described by Prop. 3.1, the network's spatial throughput is* $\mathrm{TP_o} = \lambda^* p_s(\lambda^*)$*, where:*

$$p_s(\lambda^*) = e^{-1-\frac{\beta d^\alpha \eta}{P_t}}, \qquad \lambda^* = \frac{1}{\pi \kappa d^2 \beta^{2/\alpha}}. \tag{3.18}$$

*Proof.* See proof in App. B.4. □

Comparing Prop. 3.2 and Cor. 3.5 when background noise is negligible ($\eta \approx 0$), the gain in TP

by the use of sectors without sidelobes over omni-directional antennas is:

$$\frac{\mathrm{TP_s}}{\mathrm{TP_o}} = \frac{u^2}{p^2} \propto \frac{F^2_{|\epsilon|}(\omega/2)}{\omega^2}, \tag{3.19}$$

after expanding $g_1$, $u$, and $p$ in terms of $\omega$. As the main beam becomes narrower and stronger, $\omega \to 0$, the TP gain is affected by decreasing beamwidth in two opposing ways. First, the optimal spatial intensity of active transmitters is increased by factor $p^2 = \frac{4\pi^2}{\omega^2}$ equal to the interferer thinning probability. Second, the success rate at this intensity decreases by factor $u^2 = F^2_{|\epsilon|}(\omega/2)$ equal to the hit rate of the typical TX/RX pair. In the absence of orientation error ($u = 1$), the use of sectorized transmitters with omni-directional receivers produces a TP gain of $1/p \propto 1/\omega$, which mirrors similar throughput gains derived by C.-J. Chang and J.-F. Chang [35].

## 3.5 Maximizing Transmission Capacity

Spatial throughput is often achieved by increasing the spatial intensity of active transmitters at the expense of the success rate of the transmissions. The *transmission capacity* (TC) of a network described by Prop. 3.1 is the maximum spatial intensity of successful transmissions subject to a maximum outage constraint $p_e$:

$$\mathrm{TC} = \max_{\lambda>0, p_s(\lambda)\geq 1-p_e} \lambda p_s(\lambda). \tag{3.20}$$

As it has been well established for transmission capacity [54], the monotonicity of $p_s$ in $\lambda$ allows us to solve this maximization by taking the inverse of $p_s(\lambda)$, which yields the intensity of active transmitters that achieves success rate $1 - p_e$:

$$\mathrm{TC} = \lambda(p_e)(1 - p_e). \tag{3.21}$$

Prop. 3.4 extends the analysis of transmission capacity to networks with orientation error and ideal sector antennas without sidelobes.

**Proposition 3.4** (TC using Sectors without Sidelobes)**.** *If sectors described by (3.8) with zero sidelobes ($g_2 = 0$) are employed in a network described by Prop. 3.1, the transmission capacity subject to maximum outage $p_e$ is given by* $\mathrm{TC_s} = \lambda^*(1-p_e)$ *where:*

$$\lambda^* = \frac{\log\left(\frac{u^2(1-p_{\eta,s})}{1-p_e}\right)}{p^2\pi\kappa d^2\beta^{2/\alpha}}, \tag{3.22}$$

*and $p_{\eta,s} = 1 - e^{-\frac{\beta d^\alpha \eta}{P_t g_1^2}}$ is the failure rate due to background noise under Rayleigh fading.*

*Proof.* See proof in App. B.5. □

Unlike the monotonicity results obtained for spatial throughput in §3.4, the additional outage constraint of transmission capacity combined with antenna orientation error prohibits $\mathrm{TC_s}$ from being monotone increasing with the narrowing of antenna beamwidth $\omega \to 0$. Ignoring background noise ($\eta \approx 0$) for the moment, the argument to the logarithm in (3.22) is $F_{|\epsilon|}^2\left(\frac{\omega}{2}\right)/(1-p_e)$ when expanded in terms of $\omega$. It follows that when $\omega < 2F_{|\epsilon|}^{-1}\left(\sqrt{1-p_e}\right)$, the transmission capacity expression will be negative, $\mathrm{TC_s} < 0$. This can be interpreted in the following manner: there is a minimum threshold for beamwidth, beyond which the typical TX/RX hitting probability $u^2$ becomes smaller than the required success rate $1-p_e$. In this beamwidth regime, the transmission capacity outage constraint cannot be satisfied simply due to typical TX/RX misalignment, and transmission capacity can effectively be considered zero.

Along the lines of maximizing $\mathrm{TC_s}$ as a function of antenna beamwidth, we have found that transmission capacity $\mathrm{TC_s}$ is unimodal in $\omega$ under the class of concave, twice differentiable error distributions $F_{|\epsilon|}$. This notion is formalized by Prop. 3.5.

**Proposition 3.5** (Concavity of $F_{|\epsilon|}$ Implies Unimodality of $\mathrm{TC_s}$)**.** *Let sectors described by (3.8) with zero sidelobes ($g_2 = 0$) be employed in a network described by Prop. 3.1 with outage constraint $p_e > 0$. If the orientation error* c.d.f. *$F_{|\epsilon|}$ is concave over $[0,\pi]$, then there exists a unique maximizer of* $\mathrm{TC_s}$ *within $\omega \in \left(2F_{|\epsilon|}^{-1}\left(\sqrt{1-p_e}\right), 2\epsilon_{\max}\right]$.*

*Proof.* See proof in App. B.6. □

Prop. 3.5 relies on the fact that $\mathrm{TC_s}$ is monotone outside of the stated domain, while being quasi-concave (unimodal) inside, producing a unique maximizer.

Following the results of Prop. 3.5, the location of the unique maximizer $\omega^*$ of $\mathrm{TC_s}$ can be expressed based on conditions on $f_{|\epsilon|}$ evaluated at the *r.h.s.* of its support $\omega/2 = \epsilon_{\max}$.

**Corollary 3.6** (Conditions on the Maximizing $\omega^*$ for $\mathrm{TC_s}$)**.** *Let sectors described by (3.8) with zero sidelobes ($g_2 = 0$) be employed in a network described by Prop. 3.1 with outage constraint $p_e > 0$. If the orientation error* c.d.f. *$F_{|\epsilon|}$ is concave over $[0, \pi]$, then the unique maximizer $\omega^*$ of* $\mathrm{TC_s}$ *has the following properties:*

- *If $f_{|\epsilon|}(\epsilon_{\max}) \geq \frac{\log\left(\frac{1}{1-p_e}\right)}{\epsilon_{\max}}$, then $\omega^* = 2\epsilon_{\max}$.*
- *If $f_{|\epsilon|}(\epsilon_{\max}) < \frac{\log\left(\frac{1}{1-p_e}\right)}{\epsilon_{\max}}$, then $\omega^* \in \left(2F_{|\epsilon|}^{-1}\left(\sqrt{1-p_e}\right), 2\epsilon_{\max}\right)$, and $\omega^*$ is the unique solution to the equation:*

$$\frac{f_{|\epsilon|}(\omega/2)}{F_{|\epsilon|}(\omega/2)} = \frac{1}{\omega/2} \log\left(\frac{F_{|\epsilon|}^2(\omega/2)}{1-p_e}\right). \tag{3.23}$$

*Proof.* See proof in App. B.7. □

Interestingly, Cor. 3.6 indicates that $\omega^*$ depends only on the outage constraint $p_e$ and the error distribution $F_{|\epsilon|}$ and is independent of other system parameters $\alpha$, $\beta$, $\eta$, $d$, and $\lambda$.

**Remark 3.3.** *Cor. 3.6 implies that two opposite strategies may be required to separately maximize spatial throughput and transmission capacity. Let $F_{|\epsilon|}$ be concave with $\epsilon_{\max} = \pi$ and let $f_{|\epsilon|}(\epsilon_{\max}) \geq \log\left(\frac{1}{1-p_e}\right)/\epsilon_{\max}$. By concavity of $F_{|\epsilon|}$, Prop. 3.3 implies that maximizing spatial throughput is done with $\omega \to 0$. However, by the additional assumptions on $f_{|\epsilon|}(\epsilon_{\max})$, Cor. 3.6 implies that maximizing transmission capacity is achieved as $\omega \to 2\epsilon_{\max} = 2\pi$. Fig. 3.6 shows error distributions with parameter values such that the (normalized) spatial throughput and transmission capacity are maximized by opposite extremes of beamwidth, $\omega \to 0$ and $\omega \to 2\pi$.*

For completeness, Cor. 3.7 provides the transmission capacity for networks employing omni-directional antennas, a well studied scenario [54].

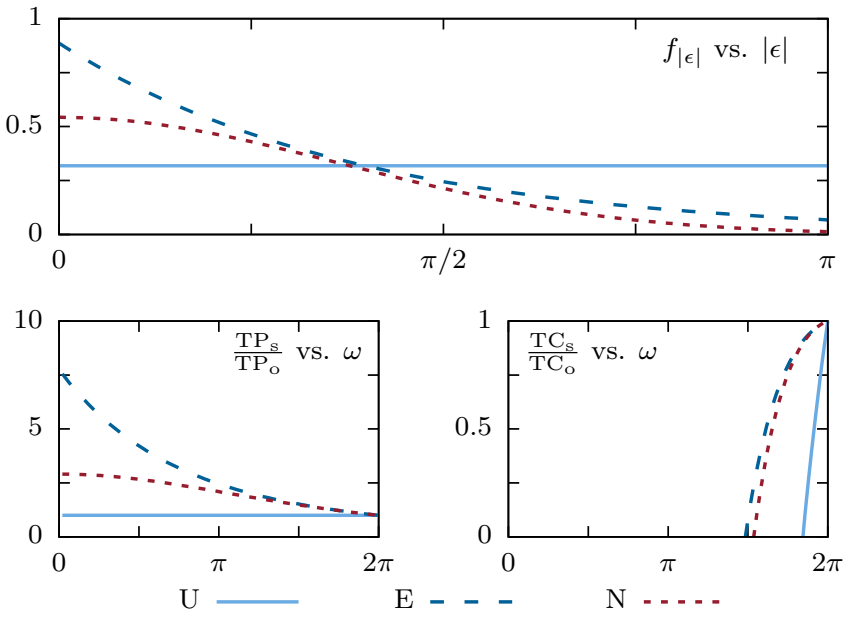


**Figure 3.6:** Sample error *p.d.f.*s, (**U**niform, **E**xponential, and half-**N**ormal) plotted over support $|\epsilon| \in [0, \pi]$ (**top**). Normalized spatial throughput $\text{TP}_\text{s}/\text{TP}_\text{o}$ (**bottom-left**) and normalized transmission capacity $\text{TC}_\text{s}/\text{TC}_\text{o}$ (**bottom-right**) with outage $p_e = 0.15$ plotted against antenna beamwidth $\omega$. The **U**niform has a mean of $\bar{\epsilon} = 90$ degrees, while the **E**xponential and half-**N**ormal are assigned a mean of $\bar{\epsilon} = 70$ degrees. Note: the mean must be set large enough to satisfy the first condition of Cor. 3.6.

**Corollary 3.7** (TC using Omni-directional Antennas)**.** *If omni-directional antennas are employed in a network described by Prop. 3.1, the transmission capacity subject to maximum outage $p_e$ is* $\text{TC}_\text{o} = \lambda^*(1-p_e)$ *where* $\lambda^* = \frac{\log\left(\frac{1-p_{\eta,o}}{1-p_e}\right)}{\pi\kappa d^2 \beta^{2/\alpha}}$ *and* $p_{\eta,o} = 1 - e^{-\frac{\beta d^\alpha \eta}{P_t}}$ *is the failure rate due to background noise under Rayleigh fading.*

Comparing Prop. 3.4 and Cor. 3.7 when background noise is negligible $\eta \approx 0$, we see that sector antennas without sidelobes increase the transmission capacity by a factor of:

$$\frac{\text{TC}_\text{s}}{\text{TC}_\text{o}} = \frac{1}{p^2} \frac{\log\left(\frac{u^2}{1-p_e}\right)}{\log\left(\frac{1}{1-p_e}\right)} \propto \frac{1}{\omega^2} \log\left(\frac{F_{|\epsilon|}^2\left(\frac{\omega}{2}\right)}{1-p_e}\right), \tag{3.24}$$

after expanding $g_1$, $u$, and $p$ in terms of $\omega$. As the main beam becomes narrower and stronger, $\omega \to 0$, the gain in transmission capacity differs from that of spatial throughput in (3.19). The success rate is fixed at $1-p_e$, thus the realized gain is purely a function of an adjustment to the spatial intensity of active transmitters. While this intensity contains a similar factor $1/p^2$ as (3.19), the numerator is

now $\log\left(F^2_{|\epsilon|}(\omega/2)/(1-p_e)\right)$, instead of simply $F^2_{|\epsilon|}(\omega/2)$, due to the fixed outage constraint. In the absence of orientation error ($u=1$) and the employment of sectorized transmitters, the transmission capacity gain is $1/p^2 \propto 1/\omega^2$. When the beamwidth $\omega$ is converted into an equivalent number of sectors $M$ covering the circle $\omega = \frac{2\pi}{M}$, we recover similar transmission capacity gains $\Theta(M^2)$ derived by Hunter *et al.* [43].

## 3.6 Results

In this section, we explore the relationship between mean orientation error, throughput maximizing beamwidths, and maximum throughput using sector patterns based on those of *i)* Baccelli and Błaszczyszyn [48] and Akoum *et al.* [46], and *ii)* the spatial channel model used by 3GPP standards [56]. Numerical methods are used to compute the success probability of the typical transmission as well as the derived throughput metrics.

Based on [46], let $G_{\text{trans}}(\theta)$ in (3.25) be an antenna gain pattern defined by 3dB-beamwidth $\omega$, main beam gain $g_1$, and sidelobe gain $g_2$ with $0 \leq g_2 < g_1$ and transition width $\gamma$:

$$G_{\text{trans}}(\theta) = \begin{cases} g_1 = \frac{2\pi-(2\pi-3/2\gamma-\omega)g_2}{\omega} & \text{if } |\theta| \leq \theta_1 \\ g_1 - \frac{g_1}{\gamma}\left(|\theta|-\theta_1\right) & \text{if } \theta_1 < |\theta| \leq \theta_2 \\ \frac{2g_2}{\gamma}\left(|\theta|-\theta_2\right) & \text{if } \theta_2 < |\theta| \leq \theta_3 \\ g_2 & \text{if } \theta_3 < |\theta| \leq \pi \end{cases}, \tag{3.25}$$

with $\theta_1 = \omega/2-\gamma/2$, $\theta_2 = \omega/2+\gamma/2$, and $\theta_3 = \omega/2+\gamma$. In order to yield constant TRP, we place the following restrictions on the pattern's parameterization. The beamwidth and transition width must jointly satisfy $\omega \in (0, 2\pi-2\gamma)$ and $\gamma \in (0, \min\{\omega, \pi-\omega/2\})$ so that the full transition from main beam gain $g_1$ to sidelobe gain $g_2$ occurs within $|\theta| \in [0,\pi]$. Finally, the sidelobe gain must satisfy $g_2 \in \left[0, 1/(1-\frac{3\gamma}{4\pi})\right)$ in order for the sidelobe to be smaller than the main lobe $g_2 < g_1$. See Fig. 3.7 for a visualization of this pattern and relevant parameters. As the transition width decreases ($\gamma \to 0$), we recover the ideal sector pattern from (3.8) with an identical beamwidth $\omega$. Similar to Lem. 3.1 we provide four gain distributions and relevant moments of the sector pattern with transition width $\gamma$

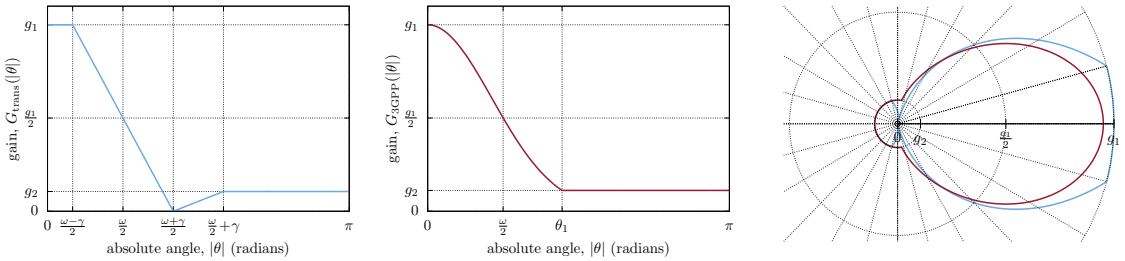


**Figure 3.7:** Sector patterns (3.25) (**left**) and (3.26) (**middle**) are plotted with 3-dB beamwidth of $\omega$, transition width $\gamma$, mainbeam gain $g_1$ and sidelobe gain $g_2$. Also shown is a superimposed polar plot (**right**) of both patterns for common $g_2 = 0.35$ and $\omega = 90$ degrees.

in Lem. 3.2. The fact that the $2/\alpha$-moments are closed form helps simplify the numerical integration needed to evaluate the typical transmission's probability of success provided in Prop. 3.1.

Based on a 3GPP channel model [56], let $G_{\text{3GPP}}(\theta)$ in (3.26) be an antenna gain pattern defined by 3dB-beamwidth $\omega$, max gain $g_1$, and sidelobe gain $g_2$ with $0 \leq g_2 < g_1$:

$$G_{\text{3GPP}}(\theta) = \begin{cases} g_1 10^{-\frac{3}{10}\left(\frac{|\theta|}{\omega/2}\right)^2} & \text{if } |\theta| \leq \theta_1 \\ g_2 & \text{if } \theta_1 < |\theta| \leq \pi \end{cases}, \tag{3.26}$$

with $\theta_1 = \omega/2\sqrt{10/3\log_{10}(g_1/g_2)}$ representing the angle at which the mainbeam falls off to the sidelobe level. Note: $g_1$ is solved for numerically to yield normalized TRP, and the parameter space of $\omega$ and $g_2$ is necessarily restricted so that $\theta_1$ falls within $[0, \pi]$. See Fig. 3.7 for a visualization of this pattern and relevant parameters.

**Lemma 3.2** (Gain Distributions using Sectors with Transition Width)**.** *In a network modeled by* $\hat{\Phi}$ *with sector antennas described by (3.25), the gain distributions are given by:*

$$f_{G_{\text{T}}}(g) = f_{G_{\text{R}}}(g) = \left(F_{|\epsilon|}(\pi) - F_{|\epsilon|}\left(\frac{\omega}{2} + \gamma\right)\right)\delta(g - g_2) + F_{|\epsilon|}\left(\frac{\omega}{2} - \frac{\gamma}{2}\right)\delta(g - g_1) + \begin{cases} \frac{\gamma}{2g_2} f_{|\epsilon|}\left(\frac{\gamma}{2} + \frac{\gamma g}{2g_2} + \frac{\omega}{2}\right) + \frac{\gamma}{g_1} f_{|\epsilon|}\left(\frac{\gamma}{2} - \frac{\gamma g}{g_1} + \frac{\omega}{2}\right) & \text{if } 0 < g < g_2 \\ \frac{\gamma}{g_1} f_{|\epsilon|}\left(\frac{\gamma}{2} - \frac{\gamma g}{g_1} + \frac{\omega}{2}\right) & \text{if } g_2 < g < g_1 \end{cases} \tag{3.27}$$

$$f_{G_{\mathrm{T_I}}}(g) = f_{G_{\mathrm{R_I}}}(g) = \left(1 - \frac{\omega + 2\gamma}{2\pi}\right)\delta(g - g_2) + \left(\frac{\omega - \gamma}{2\pi}\right)\delta(g - g_1) + \begin{cases} \frac{(g_1+2g_2)\gamma}{2\pi g_1 g_2} & \text{if } 0 < g < g_2 \\ \frac{\gamma}{\pi g_1} & \text{if } g2 < g < g_1 \end{cases}. \tag{3.28}$$

*Further, the $2/\alpha$-moments of the gain distributions between an arbitrary interferer and the typical receiver are:*

$$\mathbb{E}\left[G_{\mathrm{T_I}}^{2/\alpha}\right] = \mathbb{E}\left[G_{\mathrm{R_I}}^{2/\alpha}\right] = \left(1 - \frac{\omega + \gamma}{2\pi} - \frac{\gamma}{(2+\alpha)\pi}\right) g_2^{2/\alpha} + \left(\frac{\omega + \gamma}{2\pi} - \frac{2\gamma}{(2+\alpha)\pi}\right) g_1^{2/\alpha}. \tag{3.29}$$

*Proof.* (3.27) follows by transforming the error *c.d.f.* $F_{|\epsilon|}(\epsilon)$ by the gain pattern (3.25). (3.28) follows by transforming a uniform *c.d.f.* over $[0, \pi]$ by the gain pattern (3.25). Finally, (3.29) is evaluated by taking the $2/\alpha$-moment of the arbitrary interferer gain distribution in (3.28). □

In Fig. 3.8, we compare the network performance of several radiation patterns explored in this chapter. The success rate of a typical transmission (top-left of Fig. 3.8) is provided with inset and outset plots. The inset plot shows that the success curves generally tracked one another closely. The outset plot magnifies differences between the curves that occur at higher success rates ($\geq 95\%$). As the transition width $\gamma$ is decreased, we observe success rates fall, perhaps due to a 'broadening' of the antenna's main beam that interferes with other transmissions more than it helps cope with orientation error. As the sidelobe is decreased for all three sector patterns, the main beam is strengthened and we note increased success under higher TX intensities ($\lambda \geq 10^{-5}$).

The throughput of the network (top-right of Fig. 3.8) shows the spatial intensity of successful transmissions plotted against TX intensity for a fixed beamwidth of $\omega = 20$ degrees and fixed mean orientation error of $\bar{\epsilon} = 3$ degrees. Higher throughputs are achieved at higher TX intensities using the directional patterns over an omni-directional pattern. At this fixed beamwidth, the sidelobe strength $g_2$ appears to be the dominant factor (compare with transition width $\gamma$) in the behavior of throughput. Throughput curves for all three patterns corresponding to stronger sidelobes ($g_2 = 10^{-1}$) produce lower throughput and maximizing TX intensity than smaller sidelobes ($g_2 = 10^{-3}$).

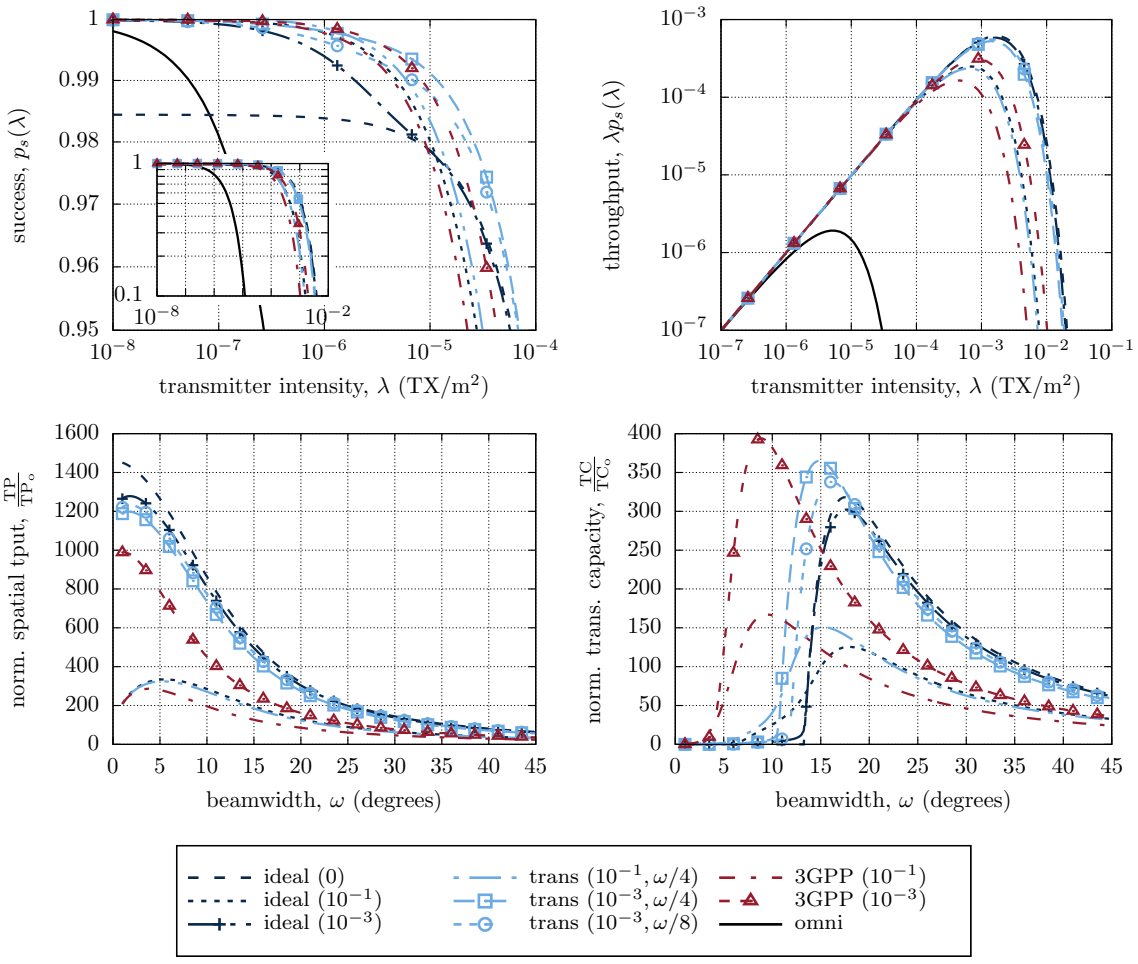


**Figure 3.8:** Plotted are success probability (**top-left**), throughput as a function of transmitter intensity $\lambda$ (**top-right**), throughput maximized over $\lambda$ (**bottom-left**), and outage-constrained throughput maximized over $\lambda$ (**bottom-right**). The legend includes **omni**-directional antennas; **ideal** sector with sidelobe strength ($g_2$); sector with sidelobe strength and **trans**ition width ($g_2, \gamma$); and the **3GPP** sector with sidelobe strength ($g_2$). Default parameters include $p_e = 0.15$, $\omega = 20$ degrees, and $g_2 = 0.1$. Orientation error $|\epsilon|$ is a half-normal distributed *r.v.* with a mean of $\bar{\epsilon} = 3$ degrees.

Spatial throughput (throughput maximized *w.r.t.* $\lambda$) plotted against antenna beamwidth $\omega$ (bottom-left of Fig. 3.8), is shown for a fixed mean orientation error. As beamwidth is decreased below 20 degrees, we begin to see a greater differentiation in TP achieved by each of the evaluated radiation patterns. While the analytical result of TP-monotonicity in Prop. 3.3 is reflected numerically for ideal sectors without sidelobes ($g_2 = 0$), the introduction of sidelobes and transition widths into the directional radiation pattern does not preserve spatial throughput monotonicity.

Transmission capacity (outage-constrained throughput maximized *w.r.t.* $\lambda$) plotted against antenna beamwidth $\omega$ (bottom-right of Fig. 3.8) is also shown for a fixed mean orientation error. For ideal sector patterns, as sidelobes are removed and transition width is narrowed, TC tends to increase and the maximizing $\omega$ decreases to match the results obtained by ideal sectors without sidelobes. For the 3GPP pattern, we note that the TC-maximizing beamwidth does not appear to vary with a change in sidelobe strength. Additionally, the TC-unimodality in Prop. 3.5 is reflected numerically for ideal sectors without sidelobes and appears to hold experimentally for all other shown radiations patterns.

The outage constraint $p_e$ appears to enforce a sharp falloff in TC as beamwidth narrows (compare with TP). This is explicitly observed in the ideal sector pattern without sidelobes. In this case, missing the main beam, even slightly, provides no throughput benefit. In all patterns with small sidelobes $g_2 = 10^{-3}$, the falloff in TC is very similar with the exception of a tail on the *l.h.s.*. The TC-maximizing beamwidth appears more sensitive to the pattern type (ideal, trans, 3GPP) while the maximum TC appears more sensitive to the sidelobe gain $g_2 \in \{10^{-1}, 10^{-3}\}$. Ultimately, the outage constraint prohibits blind throughput maximization *w.r.t.* $\lambda$ at the expense of success, thus lower throughput is realized with TC versus TP.

In Fig. 3.9, we explore the maximization of TP and TC (*w.r.t.* beamwidth $\omega$) plotted against mean orientation error (top-left and top-right of Fig. 3.9, respectively). In general, maximum spatial throughput $\mathrm{TP}^*$ and maximum transmission capacity $\mathrm{TC}^*$ decrease as the uncertainty in orientation increases and behave rather identically across radiation patterns. For the configurations plotted, the sidelobe strength $g_2$ is the dominant factor in separating the throughput curves.

The corresponding maximizing beamwidths $\omega^*$ for both maximum throughput metrics (bottom-left and bottom-right of Fig. 3.9) are also plotted against mean orientation error. Intuitively, the TP- and TC-maximizing beamwidths tend to increase with an increased uncertainty in antenna orientation. Also, as expected under ideal sectors without sidelobes, TP-monotonicity results in a maximizing beamwidth of zero regardless of the mean orientation error. The addition of sidelobes and transition widths into the sector pattern produces TP-maximizing beamwidths larger than zero, and

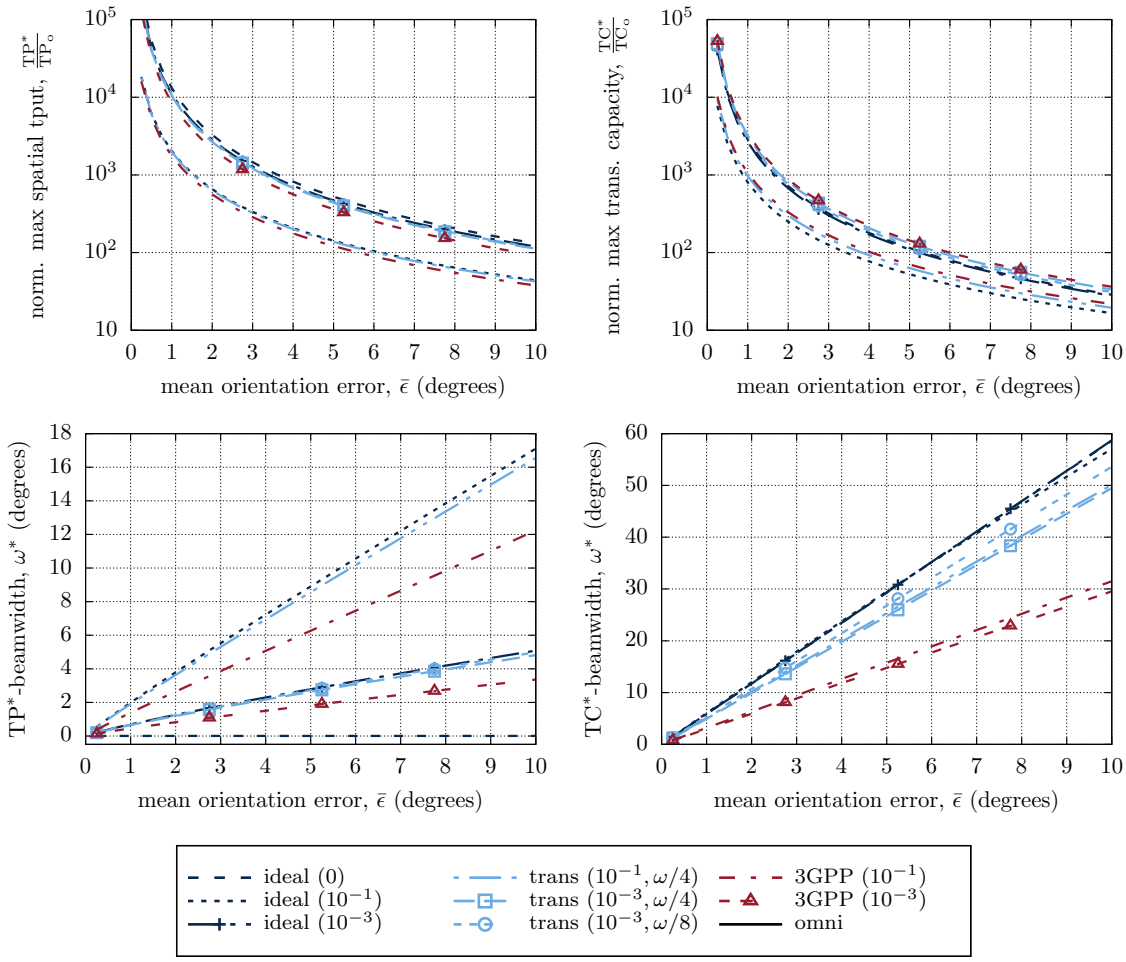


**Figure 3.9:** Plotted are spatial throughput TP maximized over beamwidth (**top-left**), the resulting TP-maximizing beamwidth (**bottom-left**), transmission capacity TC maximized over beamwidth (**top-right**), and the resulting TC-maximizing beamwidth (**bottom-right**). The legend, default parameters, and orientation error modeling are identical to that of Fig. 3.8.

the outage-constrained nature of TC$^*$ produces significantly larger optimal beamwidths than TP$^*$. The sidelobe strength $g_2$ seems to be the determining factor in grouping TP-maximizing beamwidth curves, while the radiation pattern type (ideal, trans, 3GPP) appears to be the more dominant factor in grouping TC-maximizing beamwidth curves. For the scenarios investigated, the TC-maximizing beamwidth for the ideal sector without sidelobes seems to provide a good approximation for all other ideal sectors with sidelobes and also serves as an upper bound for the remaining patterns (trans and 3GPP).

**Remark 3.4.** *Interestingly, we see that both* TP- *and* TC-*maximizing beamwidths have a nearly*

*linear relationship with the mean orientation error for all radiation patterns displayed. Assuming truncated exponential orientation error, the optimality constraint (3.23) can be reparameterized by the ratio $\omega/\bar{\epsilon}$, indicating that $\omega^*$ does indeed scale linearly with $\bar{\epsilon}$ under the assumption of ideal sectors without sidelobes.*

## 3.7 Conclusions

In this chapter, we introduced a model for capturing the effects of beam misdirection on coverage and throughput in a directional wireless network using stochastic geometry. In networks employing ideal sector antennas without sidelobes, we found that the moderate assumption of a concave orientation error *c.d.f.* was sufficient to prove monotonicity and quasi-concavity (both with respect to antenna beamwidth) of spatial throughput (TP) and outage-constrained transmission capacity (TC), respectively. Our numerical results confirm this, but also show that monotonicity of spatial throughput is not preserved for networks employing more complex antenna models. However, unimodality appears to be maintained across the various radiation patterns studied for both throughput metrics, which warrants further investigation.

While varying the sector pattern's sidelobe strength and 'sharpness' of the beamwidth, we found that the ideal sector pattern without sidelobes varied in its ability to approximate more complex patterns. For instance, while the antenna sidelobe strength could greatly influence transmission capacity maximized over antenna beamwidth, the resulting maximizing beamwidths for different sidelobe strengths tended to be well approximated by that of the sector without sidelobes. There exist possible opportunities for upper bounding metrics (*i.e.*, transmission capacity-maximizing beamwidth) for complex radiation patterns by the use of simpler patterns (*i.e.*, ideal sector antenna without sidelobes).

Finally, we noted an apparent linear relationship between mean orientation error and throughput maximizing beamwidths. This held across both throughput metrics and across the sector patterns explored in this chapter, suggesting another interesting future direction of inquiry.

# Chapter 4: Minimizing the Bayes Risk of the Protocol Interference Model in Wireless Poisson Networks

## 4.1 Introduction

Interference models are a key component in the simulation and design of large scale wireless networks due to the shared nature of the medium. Several models have seen extensive use over the past several decades, including the *physical* and *protocol* interference models [57]. Under the physical interference model, successful reception requires constraints on the sum interference power observed at the receiver, where the sum is taken over all sources of interference. In contrast, the protocol interference model places constraints on the max power observed at the receiver from any one source of interference.

Usage of the protocol model is typically parameterized by a guard zone distance around each receiver. When the guard zone contains any source of interference, the transmission is declared as being in outage; otherwise, for an empty guard zone, a transmission is declared as successful. As the guard zone increases, the protocol model will become more conservative in declaring transmission success (and falsely declaring outages with higher probability). As the guard zone decreases, the protocol model will become more aggressive in declaring transmission success (and falsely rejecting outages with higher probability). This invites the question: if one is to employ the protocol model to simulate or design wireless networks, how should one choose the guard zone radius?

In this work, we recognize that this tradeoff fits nicely within the framework of binary hypothesis testing. We treat the protocol interference model, parameterized by a guard zone distance, as a decision rule to evaluate/predict physical model success; given the simple observation of the distance from the receiver to the closest interferer, the protocol model must decide between success/outage under the physical model. Under this framework, we may assign unique costs to correct and incorrect protocol model decisions and employ Bayes estimation to find the guard zone that minimizes the expected cost of the protocol model. We may additionally use this framework as a natural basis for

comparing several intuitive guard zone sizes. We now categorize and review related work.

### 4.1.1 Related Work

Several works have explored how to employ the protocol model within the context of scheduling and higher layer network objectives [58, 59, 60]. Hasan and Andrews [58] study the protocol model as a scheduling algorithm in CDMA-based wireless ad hoc networks. They comment that a guard zone around each transmitter induces a natural tradeoff between interference and spatial reuse, affecting higher layer performance metrics such as transmission capacity. They employ stochastic geometry to derive a guard zone that maximizes transmission capacity. Shi *et al.* [59] examine the use of the protocol model within a cross-layer optimization framework and provide a strategy for correcting infeasible schedules generated under the protocol model by allowing transmission rate-adaptation to physical model SINR. The sensitivity of the gap in predicted network performance between the original and corrected schedules is measured against guard zone radius using simulations. Optimal guard zones derived in our work may provide efficient protocol model operating points for this algorithm. Zhang *et al.* [60] analyze the effectiveness of protocol model scheduling using a variety of analytical, simulation, and testbed measurements.

We differentiate our work in the following way. Assuming a set of concurrent transmissions has already been scheduled by the result of action of higher layers (MAC/NET), we focus on the physical layer (PHY) problem of modeling their success/failure. As such, we emphasize that this work analyzes the protocol model as an interference model, not as a feature of a communications protocol that may be integrated into the operation of a wireless network.

In this work, the analytical results are primarily centered around the protocol interference model accuracy in networks with active transmitter spatial distributions modeled by Poisson Point Processes (PPP). These type of networks may be observed when Aloha scheduling is employed on an initial PPP network, given that *i)* Aloha scheduling is analogous to independent thinning and *ii)* an independently thinned PPP yields another PPP [52, Thm. 2.36]. We note more sophisticated thinning processes on a PPP provide inroads to studying the spatial geometry of other scheduling algorithms. For example, dependently thinning a PPP based on nearest neighbor distance constraints

results in a Matérn Point Process (MPP) which draws a parallel with Carrier Sense Multiple Access (CMSA) scheduling techniques. This concept has been extended to RTS/CTS scheduling techniques, where the mean interference of such networks is analyzed by Zhong *et al.* [61]. Baccelli and Bermolen [62] extend the concept of additive interference to the construction of MPPs, where the condition for retaining points is refined to account for the additive effects of all nearby points.

We note works that deal directly with the protocol model as a model for interference [63, 64, 65]. Iyer *et al.* [64] compare several interference models in simulation and qualitatively discuss the sacrifices in accuracy associated with abstracted interference models, including the protocol model. Zorzi [63] analytically compare the outage rates under both the protocol and physical models and note a close approximation under guard zones configured using dominant interference. While a guard zone may be chosen to match the outage rates predicted by networks employing the physical interference model, it is not immediately clear if such a guard zone also yields a high degree of correlation between the subsets of transmissions that are predicted successful by both models. On this front, Kang *et al.* [65] study the accuracy of the protocol model via simulation and provide its false positive and false negative rates as a predictor for physical model feasibility. Their model makes use of a dynamic scaling of guard zones on a per-transmission basis based on SINR measurements, which differs from traditional scaling (via guard zone *factor*, $\Delta$) based on transmitter-receiver distances. Additionally, they touch upon the connection between the protocol model and graph-theory based scheduling (independent sets on the conflict graph). We note that while our work can be considered to use a global guard zone factor, we are able to express both error rates analytically for Poisson networks and combine them appropriately to express the Bayes risk associated with the protocol model. These error rates are key in understanding the correlation in predictions of both the physical and protocol interference models.

Finally, both the protocol and physical interference models have been studied within the framework of extremal and additive shot noise fields within stochastic geometry. Baccelli and Błaszczyszyn [47, Sec. 2.4] discuss the use of additive vs. extremal shot noise fields to model interference in wireless networks represented as point processes. Max (extremal) interference finds use in bounding outage

and transmission capacity under sum (additive) interference in PPPs with Aloha scheduling, as is done in [54, Sec. 2.5].

### 4.1.2 Contributions

The rest of this chapter is summarized as follows. In §4.2, we introduce our wireless network model, including both the physical and protocol interference models. In §4.3, we introduce a binary hypothesis testing framework for evaluating the protocol model. For a wireless Poisson network, we employ stochastic geometry to provide prior and posterior distributions (Lem. 4.1, Lem. 4.2, and Prop. 4.1) of the related decision problem. The resulting Bayes risk, parameterized by guard zone radius, is given in Prop. 4.2. We include a characterization of the optimal guard zone achieving minimum Bayes risk in Thm. 4.1 and find that under a natural cost assignment, the total risk is bounded above by the physical model's outage rate Prop. 4.6. In §4.4, we provide the missed detection and false alarm rates forming the receiver operating characteristic (ROC) curve associated with the protocol model and compare the minimum risk guard zone with several other intuitive operating points along the ROC curve. In regimes of low physical model outage, a guard zone radius based on dominant interference incurs little additional error over the optimal guard zone and correlates well with physical model feasibility. In §4.5, we extend this framework to directional wireless Poisson networks and note parallel observations on the minimum Bayes risk (Thm. 4.2) and bounds for the optimal and dominant interferer risks (Prop. 4.10). We conclude our work and outline other interesting avenues for future research in §4.6. Finally, for clarity, long proofs are presented in App. C.

## 4.2 Model

We model a wireless network with $\hat{\Phi} = \{(x_i, m_i)\}$, a marked, homogeneous, bipolar Poisson Point Process (PPP) of intensity $\lambda > 0$ in $d$-dimensional space $\mathbb{R}^d$. $\hat{\Phi}$ models the placement and orientation of transmitter-receiver pairs, where the members of each pair are separated by distance parameter $d_{\mathrm{T}} > 0$. The ground set $\{x_i\} \subset \mathbb{R}^d$ represents the transmitter (TX) locations, while the *i.i.d.* marks $\{m_i\}$ are the relative locations of each RX about its paired TX. Let the *p.d.f.* of $m_i$ be the

uniform distribution over the $d$-dimensional sphere with radius $d_{\mathrm{T}}$. Together the ground set and marks encode the RX locations $\{y_i \equiv x_i + m_i\}$. For notational convenience, we will refer to paired TX-RXs by their shared index $i$.

In the following sections, we discuss the success probability of a typical TX-RX pair $o$ with the receiver located at the origin. This is possible due to Slivnyak's Theorem [52, Thm. 8.1] applied to the PPP $\hat{\Phi}$, which says that the reduced Palm distribution of $\hat{\Phi}$ is equivalent to the original distribution of $\hat{\Phi}$. Here, the reduced Palm distribution of interest first conditions $\hat{\Phi}$ on the locations of $x_o$ and $y_o$ and subsequently removes both points in order to provide analysis on the sum interference generated by $\hat{\Phi}$ and observed at $y_o$.

In the following subsections, we detail the rest of our model.

### 4.2.1 Physical Interference Model

We model signal propagation using large-scale, distance-based pathloss with Rayleigh fading. The signal power at RX $o$ from TX $i$ is given by:

$$P_{i,o} \equiv F_{i,o} d_{i,o}^{-\alpha}, \tag{4.1}$$

where $F_{i,o} \sim \mathrm{Exp}(1)$ is the Rayleigh fading coefficient between TX $i$ and RX $o$, $\alpha > 2$ is the large-scale pathloss constant, and $d_{i,o}$ is the distance from TX $i$ to RX $o$ (note: $d_{o,o} = d_{\mathrm{T}}$).

A transmission between TX-RX pair $o$ is considered successful under the physical interference model if the signal-to-interference-plus-noise ratio (SINR) falls above a defined SINR threshold $\beta > 0$: $\mathrm{SINR}_o \equiv P_{o,o}/(I_o + \eta)$, where $\eta \geq 0$ is the background noise power and $I_o \equiv \sum_{i \neq o} P_{i,o}$ is the sum interference power at RX $o$. Let *r.v.* $H \equiv \mathbf{1}\{\mathrm{SINR}_o \geq \beta\}$ represent the physical model feasibility of a typical transmission $o$ in $\hat{\Phi}$ and let the events $\{\mathcal{H}_0, \mathcal{H}_1\}$ correspond to the two possible values for $H$: $\{0, 1\}$.

### 4.2.2 Protocol Interference Model

We will also consider the protocol interference model, characterized by a guard zone distance[1] $d_{\mathrm{I}}$. A transmission between TX-RX pair $o$ is considered successful under the protocol interference model iff there are no interfering TX's within distance $d_{\mathrm{I}}$ of RX $o$. In other words, all interferers must lie at least $d_{\mathrm{I}}$ away from RX $o$. Let *r.v.* $D \equiv \mathbf{1}\{d_{i,o} \geq d_{\mathrm{I}}, \forall i \neq o\}$ represent the protocol model feasibility of a typical transmission $o$ in $\hat{\Phi}$ and let the events $\{\mathcal{D}_0, \mathcal{D}_1\}$ correspond to the two possible values for $D$: $\{0, 1\}$. By appropriately setting the guard zone $d_{\mathrm{I}}$, one may change how aggressive/conservative the protocol model behaves when measuring transmission success. In the following sections, we will quantify this tradeoff within the framework of binary hypothesis testing.

### 4.2.3 Notation

For convenience, we will make use of the following notation:

- $c_d$, the volume of a $d$-dimensional unit ball, $\mathcal{B}(0, 1)$,
- $\kappa = \Gamma(1 + \delta)\Gamma(1 - \delta)$,
- $\delta = d/\alpha$,
- $s = \beta d_{\mathrm{T}}^{\alpha}$, and
- $I_\delta(x) \equiv (-1)^{1-\delta}\delta B_{-x}(1 + \delta, 0) = \int_0^x \delta t^\delta/(1 + t)\mathrm{d}t$ is a convenience function for a specific form of the incomplete Beta function for $x \geq 0$ and $\delta > 0$.

## 4.3 Binary Hypothesis Testing

By simply employing the protocol model in place of the physical model, one is implicitly treating protocol model feasibility $D$ *as the decision rule* for estimating typical transmission success. In fact, there are a family of decision rules parameterized by guard zone $d_{\mathrm{I}}$, and the suitability of $D(d_{\mathrm{I}})$ as a predictor for $H$ will vary with the choice of $d_{\mathrm{I}}$.

By employing a Bayesian hypothesis testing formulation, we may find a sophisticated choice for $d_{\mathrm{I}}$. Define a non-negative, $2 \times 2$ cost matrix where element $c_{ij} \geq 0$ is the cost of making decision

[1] Alternately, one may employ a guard zone factor $\Delta$ of the TX-RX distance $d_{\mathrm{T}}$, producing (potentially unique) guard zone distances: $d_{\mathrm{I}} = (1 + \Delta)d_{\mathrm{T}}$. Under our model with a fixed TX-RX $d_{\mathrm{T}}$, these formulations are equivalent.

$D = i$ when hypothesis $H = j$ is true. These costs may be chosen to suit the particular application at hand; in this chapter, we will frequently assume a uniform cost matrix that does not penalize correct decisions and uniformly penalizes incorrect decisions: $c_{01} = c_{10} = 1$ and $c_{00} = c_{11} = 0$.

Using the cost matrix, we may enumerate the conditional risks associated with the decision rule $D$ characterized by guard zone $d_{\mathrm{I}}$:

$$R_0(d_{\mathrm{I}}) = c_{10}\mathbb{P}\{\mathcal{D}_1|\mathcal{H}_0\} + c_{00}\mathbb{P}\{\mathcal{D}_0|\mathcal{H}_0\} \tag{4.2}$$

$$R_1(d_{\mathrm{I}}) = c_{11}\mathbb{P}\{\mathcal{D}_1|\mathcal{H}_1\} + c_{01}\mathbb{P}\{\mathcal{D}_0|\mathcal{H}_1\}\,. \tag{4.3}$$

These risks provide the expected costs of decision rule $D$ conditioned on the value of $H$, the *r.v.* to be estimated. Note, under a uniform cost model, $R_0(d_{\mathrm{I}})$ and $R_1(d_{\mathrm{I}})$ yield the false rejection (Type I error) rate and the false acceptance (Type II error) rate, respectively.

The total expected cost of decision rule $D$, otherwise known as the Bayes risk, is the weighted combination of conditional risks:

$$r(d_{\mathrm{I}}) = R_0(d_{\mathrm{I}})\mathbb{P}\{\mathcal{H}_0\} + R_1(d_{\mathrm{I}})\mathbb{P}\{\mathcal{H}_1\}\,. \tag{4.4}$$

Given that our decision space is parameterized by the guard zone distance, a Bayes decision rule $d_{\mathrm{I}}^*$ minimizes the incurred Bayes risk over all possible decision rules:

$$d_{\mathrm{I}}^* \in \operatorname{argmin}_{d_{\mathrm{I}} \geq 0} r(d_{\mathrm{I}}). \tag{4.5}$$

In the rest of this section, Lem. 4.1 and Lem. 4.2 provide the prior distributions on $H$ and $D$, while Prop. 4.1 provides the posterior distribution related to the estimation problem. Finally, Thm. 4.1 provides a characterization of the Bayes rule achieving minimum risk associated with the protocol model.

**Lemma 4.1** (Distribution on $H$)**.** *The distribution of $H$, the physical model feasibility of a typical*

*transmission $o$ in $\hat{\Phi}$ is given by:*

$$\mathbb{P}\{\mathcal{H}_1\} = \exp\left(-\lambda c_d \kappa s^\delta - s\eta\right), \qquad \mathbb{P}\{\mathcal{H}_0\} = 1 - \mathbb{P}\{\mathcal{H}_1\}. \tag{4.6}$$

*Proof.* This result follows from standard arguments in stochastic geometry [47, 48], but may also be obtained from Prop. C.1 by letting the void zone radius approach zero: $d_\mathrm{I} \to 0$. □

**Lemma 4.2** (Distribution on $D$)**.** *The distribution of $D$, the protocol model feasibility of a typical transmission $o$ in $\hat{\Phi}$ is given by:*

$$\mathbb{P}\{\mathcal{D}_1\} = \exp\left(-\lambda c_d d_\mathrm{I}^d\right), \qquad \mathbb{P}\{\mathcal{D}_0\} = 1 - \mathbb{P}\{\mathcal{D}_1\}. \tag{4.7}$$

*Proof.* $\mathbb{P}\{\mathcal{D}_1\}$ is the void probability of the $d$-dimensional guard zone of radius $d_\mathrm{I}$ [52, Thm. 2.24]. □

**Proposition 4.1** (Posterior Distribution)**.** *The posterior distribution of $H$ given $D$ is:*

$$\mathbb{P}\{\mathcal{H}_1|\mathcal{D}_1\} = \mathrm{e}^{-A-C(d_\mathrm{I})+B(d_\mathrm{I})} \tag{4.8}$$

$$\mathbb{P}\{\mathcal{H}_0|\mathcal{D}_1\} = 1 - \mathbb{P}\{\mathcal{H}_1|\mathcal{D}_1\} \tag{4.9}$$

$$\mathbb{P}\{\mathcal{H}_1|\mathcal{D}_0\} = \frac{\mathbb{P}\{\mathcal{H}_1\} - \mathbb{P}\{\mathcal{H}_1|\mathcal{D}_1\}\,\mathbb{P}\{\mathcal{D}_1\}}{\mathbb{P}\{\mathcal{D}_0\}} \tag{4.10}$$

$$\mathbb{P}\{\mathcal{H}_0|\mathcal{D}_0\} = 1 - \mathbb{P}\{\mathcal{H}_1|\mathcal{D}_0\}, \tag{4.11}$$

*where $A = \lambda c_d \kappa s^\delta + s\eta$, $B(d_\mathrm{I}) = \lambda c_d d_\mathrm{I}^d$, and $C(d_\mathrm{I}) = \lambda c_d s^\delta I_\delta(d_\mathrm{I}^\alpha/s)$.*

*Proof.* See proof in App. C.1. □

**Remark 4.1.** *Note that the posterior distributions are not well defined for $d_\mathrm{I} = \{0, \infty\}$. When $d_\mathrm{I} = 0$, the event $\mathcal{D}_0$ occurs* w.p. *0. Alternately, when $d_\mathrm{I} \to \infty$, $\mathcal{D}_1$ occurs* w.p. *0. However, neither of these cases will affect our analysis of Bayes risk. Also, note that the chosen variables $A$, $B(d_\mathrm{I})$, and $C(d_\mathrm{I})$ yield the following: $\mathbb{P}\{\mathcal{H}_1\} = \mathrm{e}^{-A}$, $\mathbb{P}\{\mathcal{D}_1\} = \mathrm{e}^{-B(d_\mathrm{I})}$, and $\mathbb{P}\{\mathcal{D}_1|\mathcal{H}_1\} = \mathrm{e}^{-C(d_\mathrm{I})}$ (derived from (4.8)).*

**Proposition 4.2** (Bayes Risk)**.** *The Bayes risk of the protocol model decision rule $d_{\mathrm{I}}$ for a typical transmission in $\hat{\Phi}$ is given by:*

$$r(d_{\mathrm{I}}) = c_{00} + (c_{01} - c_{00})\mathrm{e}^{-A} + (c_{10} - c_{00})\mathrm{e}^{-B(d_{\mathrm{I}})} + (c_{11} + c_{00} - c_{10} - c_{01})\mathrm{e}^{-A-C(d_{\mathrm{I}})}, \tag{4.12}$$

*where $A = \lambda c_d \kappa s^{\delta} + s\eta$, $B(d_{\mathrm{I}}) = \lambda c_d d_{\mathrm{I}}^{d}$, and $C(d_{\mathrm{I}}) = \lambda c_d s^{\delta} I_{\delta}(d_{\mathrm{I}}^{\alpha}/s)$.*

*Proof.* The expression (4.4) for the Bayes risk may be expanded to obtain:

$$r(d_{\mathrm{I}}) = c_{00} + (c_{01} - c_{00})\mathbb{P}\{\mathcal{H}_1\} + (c_{10} - c_{00})\mathbb{P}\{\mathcal{D}_1\} + (c_{11} + c_{00} - c_{01} - c_{10})\mathbb{P}\{\mathcal{H}_1 \cap \mathcal{D}_1\}, \tag{4.13}$$

where we additionally substitute expressions from Lem. 4.1, Lem. 4.2, and Prop. 4.1 to achieve (4.12). □

**Theorem 4.1** (Minimum Bayes Risk)**.** *When $c_{10} > c_{00}$, the Bayes rule $d_{\mathrm{I}}^{*}$ minimizing Bayes risk (4.5) is given by the solution to:*

$$\frac{c_{00} - c_{10}}{c_{11} + c_{00} - c_{10} - c_{01}}(1 + s d_{\mathrm{I}}^{-\alpha}) = \mathrm{e}^{-A-C(d_{\mathrm{I}})+B(d_{\mathrm{I}})}. \tag{4.14}$$

*The resulting Bayes risks under the Bayes rule $d_{\mathrm{I}}^{*}$ is:*

$$r(d_{\mathrm{I}}^{*}) = c_{00} + (c_{01} - c_{00})\mathrm{e}^{-A} - (c_{10} - c_{00}) s \frac{\mathrm{e}^{-B(d_{\mathrm{I}}^{*})}}{(d_{\mathrm{I}}^{*})^{\alpha}}, \tag{4.15}$$

*where $A = \lambda c_d \kappa s^{\delta} + s\eta$, $B(d_{\mathrm{I}}) = \lambda c_d d_{\mathrm{I}}^{d}$, and $C(d_{\mathrm{I}}) = \lambda c_d s^{\delta} I_{\delta}(d_{\mathrm{I}}^{\alpha}/s)$.*

*Proof.* See proof in App. C.2. □

**Remark 4.2.** *First, the condition $c_{10} > c_{00}$ can be roughly interpreted to mean the assigned cost of making a wrong decision is higher than the assigned cost of making a correct decision. This is a rather benign condition and may be assumed common of typical applications of a Bayes estimation framework. Second, a closed form expression for $d_{\mathrm{I}}^{*}$ satisfying (4.14) is not currently known to us,*

*but the proof for Thm. 4.1 assures us of its uniqueness. In all numerical examples tested thus far, we have noted that (4.14) does indeed exist and is the Bayes rule. Finally, the uniform cost model results in coefficient ratio* $1/2$ *on the* l.h.s. *of (4.14).*

## 4.4 Uniform Cost ROC Curve

Given Thm. 4.1, we now know how to find the guard zone $d_{\mathrm{I}}^*$ that minimizes the protocol model's Bayes risk associated with predicting physical model feasibility. Clearly, deviating from $d_{\mathrm{I}}^*$ in either direction will result in an increase in the average risk, but will also trade off the two types of conditional risk, $R_0(d_{\mathrm{I}})$ and $R_1(d_{\mathrm{I}})$. We analyze this tradeoff under a uniform cost model, which reduces to one between the Type I rate (False Rejection Rate) and Type II rate (False Acceptance Rate), denoted:

$$p_{\mathrm{I}} \equiv \mathbb{P}\{\mathcal{D}_1|\mathcal{H}_0\} \qquad\qquad p_{\mathrm{II}} \equiv \mathbb{P}\{\mathcal{D}_0|\mathcal{H}_1\}\,. \tag{4.16}$$

Note: in this formulation, the null hypothesis $\mathcal{H}_0$ is equivalent to physical model *infeasibility.*

**Proposition 4.3** (False Rejection Rate - Type I)**.** *The rate at which the null hypothesis* $\mathcal{H}_0$ *is falsely rejected is given by:*

$$p_{\mathrm{I}} = \frac{\mathrm{e}^{-B(d_{\mathrm{I}})} - \mathrm{e}^{-A-C(d_{\mathrm{I}})}}{1-\mathrm{e}^{-A}}, \tag{4.17}$$

*where* $A = \lambda c_d \kappa s^\delta + s\eta$*,* $B(d_{\mathrm{I}}) = \lambda c_d d_{\mathrm{I}}^d$*, and* $C(d_{\mathrm{I}}) = \lambda c_d s^\delta I_\delta(d_{\mathrm{I}}^\alpha/s)$*.*

*Proof.* Apply Bayes Theorem and substitute in remaining expressions from Lem. 4.1, Lem. 4.2, and Prop. 4.1:

$$p_{\mathrm{I}} = \mathbb{P}\{\mathcal{D}_1|\mathcal{H}_0\} = \frac{(1-\mathbb{P}\{\mathcal{H}_1|\mathcal{D}_1\})\,\mathbb{P}\{\mathcal{D}_1\}}{1-\mathbb{P}\{\mathcal{H}_1\}}. \tag{4.18}$$

□

**Proposition 4.4** (False Acceptance Rate - Type II)**.** *The rate at which the null hypothesis* $\mathcal{H}_0$ *is falsely accepted is given by:*

$$p_{\mathrm{II}} = 1 - \mathrm{e}^{-C(d_{\mathrm{I}})}, \tag{4.19}$$

*where* $C(d_{\mathrm{I}}) = \lambda c_d s^{\delta} I_{\delta}(d_{\mathrm{I}}^{\alpha}/s)$.

*Proof.* Take the complement, apply Bayes Theorem, and substitute in remaining expressions from Lem. 4.1, Lem. 4.2, and Prop. 4.1:

$$p_{\mathrm{II}} = \mathbb{P}\{\mathcal{D}_0|\mathcal{H}_1\} = 1 - \frac{\mathbb{P}\{\mathcal{H}_1|\mathcal{D}_1\}\,\mathbb{P}\{\mathcal{D}_1\}}{\mathbb{P}\{\mathcal{H}_1\}}. \tag{4.20}$$

□

Under the uniform cost model, we obtain the following Bayes risk expression from (4.4), now an expression for the average probability of error, $p_{\mathrm{E}}$, of the protocol model as a function of the guard zone:

$$p_{\mathrm{E}}(d_{\mathrm{I}}) = p_{\mathrm{I}}\mathbb{P}\{\mathcal{H}_0\} + p_{\mathrm{II}}\mathbb{P}\{\mathcal{H}_1\}\,. \tag{4.21}$$

The total error rate, $p_{\mathrm{E}}$, provides a measure of how well $H$ and $D$ correlate with one another – it is the average fraction of transmissions whose feasibility is predicted incorrectly by the protocol model.

**Proposition 4.5** (Total Error)**.** *The rate at which protocol model feasibility* $D$ *incorrectly predicts physical model feasibility is given by:*

$$p_{\mathrm{E}}(d_{\mathrm{I}}) = \mathrm{e}^{-A} + \mathrm{e}^{-B(d_{\mathrm{I}})} - 2\mathrm{e}^{-A-C(d_{\mathrm{I}})}, \tag{4.22}$$

*where* $A = \lambda c_d \kappa s^{\delta} + s\eta$, $B(d_{\mathrm{I}}) = \lambda c_d d_{\mathrm{I}}^{d}$, *and* $C(d_{\mathrm{I}}) = \lambda c_d s^{\delta} I_{\delta}(d_{\mathrm{I}}^{\alpha}/s)$.

*Proof.* The result is obtained immediately from substituting uniform costs into (4.12). □

**Remark 4.3** (Limiting Behavior in $d_{\mathrm{I}}$)**.** *As* $d_{\mathrm{I}} \to 0$ *and* $d_{\mathrm{I}} \to \infty$*, we observe a tradeoff between Type I and Type II errors (see Fig. 4.1). For simplicity, we discuss this further under the assumption of a uniform costs model. As* $d_{\mathrm{I}} \to 0$*, the protocol model will declare all transmissions successful (rejecting the null hypothesis* w.p. *1); however, the protocol model will* falsely *reject* $\mathcal{H}_0$ w.p. $\mathbb{P}\{\mathcal{H}_0\}$*, the probability of physical model outage. On the other hand, as* $d_{\mathrm{I}} \to \infty$*, the protocol model will declare all transmissions in outage (accepting the null hypothesis* w.p. *1); however, the protocol model will*

falsely *accept* $\mathcal{H}_0$ w.p. $\mathbb{P}\{\mathcal{H}_1\}$. *Thus, in these limiting cases of* $d_\mathrm{I}$*, the total risk (4.21), is confined by the success/failure probability of the protocol model (green dashed/dotted lines in Fig. 4.1).*

### 4.4.1 Operating Points

Given the family of protocol model decision rules parameterized by guard zone radius $d_\mathrm{I}$, we wish to compare the optimal guard zone $d_\mathrm{I}^*$ to a few alternative operating points of the decision rule given by Lem. 4.3, Lem. 4.4, and Lem. 4.5.

**Lemma 4.3** (Dominant Interferer (DI) Guard Zone)**.** *A guard zone* $d_\mathrm{I,DI}$ *set to exclude dominant interferers is given by:*

$$d_\mathrm{I,DI} = \left(\frac{d_\mathrm{T}^{-\alpha}}{\beta} - \eta\right)^{-1/\alpha}. \tag{4.23}$$

*Proof.* Such a guard zone should prevent the existence of a dominant interferer, *i.e.* an interferer whose interference contribution is enough to violate the SINR threshold $\beta$. We consider the case without fading and solve the following for $d_\mathrm{I}$:

$$\mathrm{SINR}_o = \frac{d_\mathrm{T}^{-\alpha}}{d_\mathrm{I}^{-\alpha} + \eta} = \beta. \tag{4.24}$$

□

**Lemma 4.4** (Mean-Matched (MM) Guard Zone)**.** *The guard zone* $d_\mathrm{I,MM}$ *that matches the first moment of* $D$ *with that of* $H$ *is given by:*

$$d_\mathrm{I,MM} = \left(\kappa s^\delta + \frac{s\eta}{\lambda c_d}\right)^{1/d}. \tag{4.25}$$

*Proof.* Set the means of $D$ and $H$ equal to one another and solve for $d_\mathrm{I}$, making use of Lem. 4.1 and Lem. 4.2:

$$\mathbb{E}[D] = \mathbb{E}[H] \tag{4.26}$$

$$\mathbb{P}\{\mathcal{D}_1\} = \mathbb{P}\{\mathcal{H}_1\} \tag{4.27}$$

□

**Lemma 4.5** (Equal Error (EE) Rate Guard Zone)**.** *The guard zone $d_{\mathrm{I,EE}}$ that achieves equal Type I and Type II error rates is given by:*

$$d_{\mathrm{I,EE}} : 1 = \mathrm{e}^{-A} + \mathrm{e}^{-B(d_{\mathrm{I}})} + \mathrm{e}^{-C(d_{\mathrm{I}})} - 2\mathrm{e}^{-A-C(d_{\mathrm{I}})}. \tag{4.28}$$

*where $A = \lambda c_d \kappa s^{\delta} + s\eta$, $B(d_{\mathrm{I}}) = \lambda c_d d_{\mathrm{I}}^{d}$, and $C(d_{\mathrm{I}}) = \lambda c_d s^{\delta} I_{\delta}(d_{\mathrm{I}}^{\alpha}/s)$.*

*Proof.* Set $p_{\mathrm{I}} = p_{\mathrm{II}}$ and solve for $d_{\mathrm{I}}$. □

**Remark 4.4** (Operating Point Ordering)**.** *In the absence of background noise ($\eta = 0$), we may readily obtain $d_{\mathrm{I,DI}} \leq d_{\mathrm{I,MM}}$, since $\kappa \geq 1$. We then find that this hold true for all $\eta \geq 0$. If $\beta \geq 1$, then we may further conclude that $d_{\mathrm{T}} \leq d_{\mathrm{I,DI}} \leq d_{\mathrm{I,MM}}$. However, the remaining points are hard to place within this ordering as we do not have closed form solutions for $d_{\mathrm{I}}^{*}$ and $d_{\mathrm{I,EE}}$.*

**Proposition 4.6** (Protocol Model Error Bounds)**.** *The risk (total error rate) associated with the dominant interferer guard zone $d_{\mathrm{I,DI}}$ may be bounded by the minimum Bayes risk and the outage rate of the physical model:*

$$p_{\mathrm{E}}(d_{\mathrm{I}}^{*}) \leq p_{\mathrm{E}}(d_{\mathrm{I,DI}}) \leq 1 - \mathrm{e}^{-A} = \mathbb{P}\{\mathcal{H}_0\}\,. \tag{4.29}$$

*where $A = \lambda c_d \kappa s^{\delta} + s\eta$.*

*Proof.* See proof in App. C.3. □

**Remark 4.5** (Limiting Behavior in $\lambda$, $\beta$)**.** *As a consequence of Prop. 4.6, the risk under both the optimal guard zone $d_{\mathrm{I}}^{*}$ and the dominant interferer guard zone $d_{\mathrm{I,DI}}$ are bounded above the the physical model outage rate $\mathbb{P}\{\mathcal{H}_0\}$. Thus, any environmental parameter that yields lower outage rates will necessarily lead to lower protocol model prediction error rates. In particular, this occurs with decreasing transmitter density $\lambda \to 0$ and decreasing SINR threshold $\beta \to 0$.*

These operating points are now plotted and discussed in the next subsection.

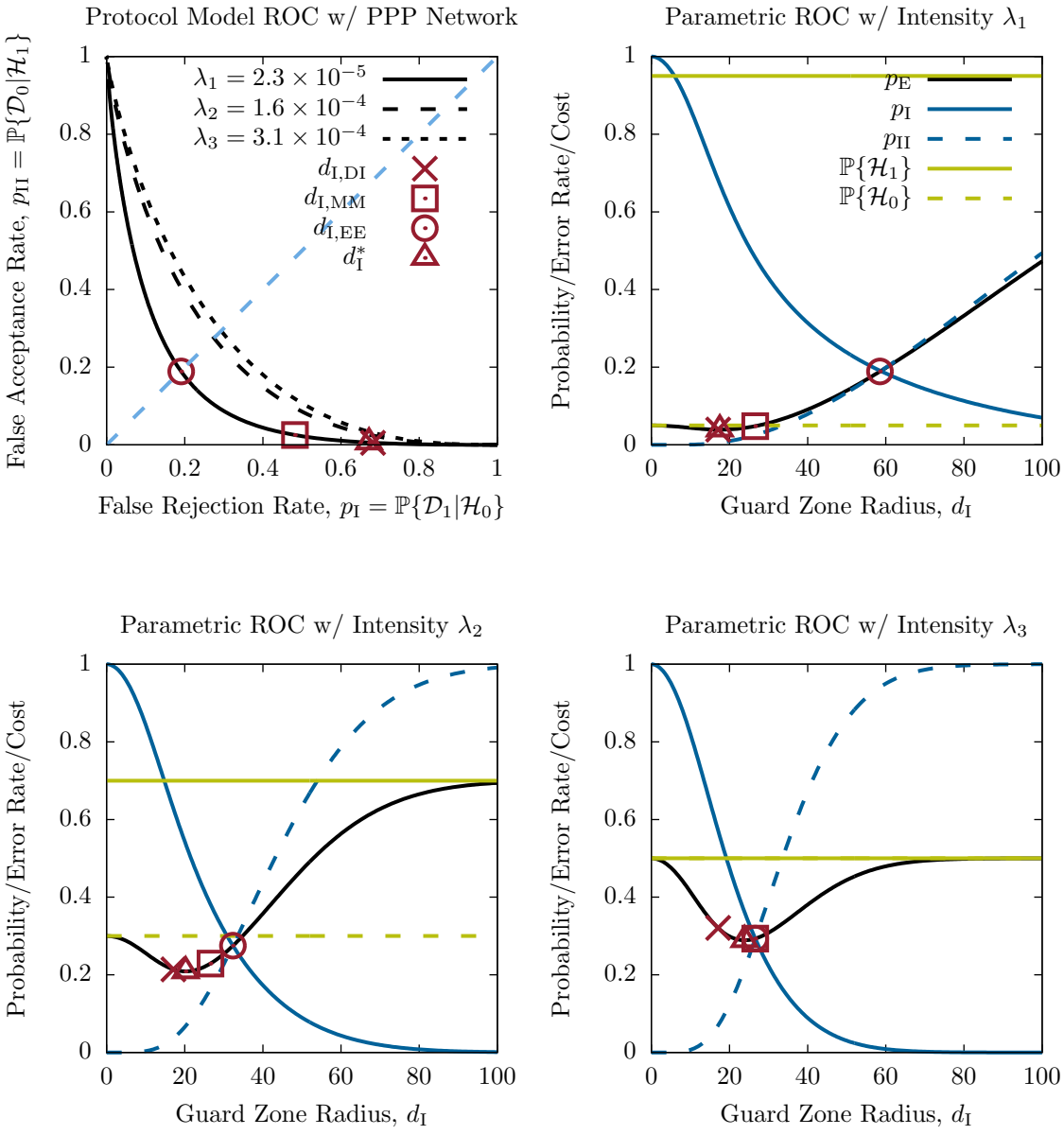


**Figure 4.1:** The protocol model ROC curve under a PPP is plotted (**top-left**) in black solid and dashed lines for three outage rates (5%, 25%, 50%) and the equal error rate curve is plotted in light blue dashes. Each protocol model ROC curve is plotted (**top-right**, **bottom-left**, and **bottom-right**) component-wise against guard zone parameter $d_{\mathrm{I}}$; Type I and II conditional error rates are plotted in blue, and total error rate in black. The physical model success and failure rates are plotted in green dashes and dots to provide references for the asymptotic Bayes risk as $d_{\mathrm{I}} \to 0$ and $d_{\mathrm{I}} \to \infty$. In all plots, operating points $d_{\mathrm{I,DI}}$, $d_{\mathrm{I,MM}}$, $d_{\mathrm{I,EE}}$, and $d_{\mathrm{I}}^*$ are plotted as red markers.

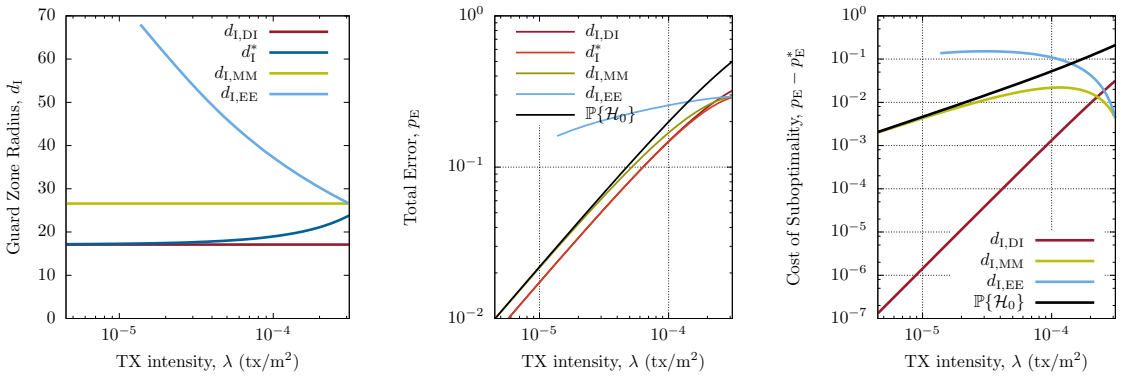


**Figure 4.2:** On the **left**, the guard zone operating points are plotted as a function of the network density $\lambda$, covering network densities producing physical model outages between 1% and 50%. On the **middle**, we show the total incurred by each of the operating points as a function of network density. On the **right**, we show the cost of suboptimality, that is the difference in risks between a suboptimal operating point and the optimal guard zone $d_{\mathrm{I}}^*$.

### 4.4.2 Results

In Fig. 4.1, we provide a sample plot of the protocol model ROC curve under a PPP in two forms using parameters from Tab. 4.1. As the guard zone $d_{\mathrm{I}}$ is increased, the ROC curve travels from bottom-right to top-left as the false rejection rate is reduced in exchange for a higher rate of false acceptance. As the network density is increased, the ROC curves indicate a drop in detection performance, that is, the ROC curve are located further away from the origin. The intuition for this effect comes from the increased significance of aggregate interference in dense networks. In the parametric versions of the ROC curve in Fig. 4.1, we may observe the tradeoff in the Type I and II conditional errors more clearly as a function of the guard zone. In high outage environments, the total error rate becomes more sensitive to choices of protocol model guard zone in high outage environments, and the optimal guard zone incurs an error rate as high as $\sim 30\%$ when the physical model outage rate is 50%. In this extreme case, the feasibility of nearly a third of the transmissions in the network are incorrectly predicted by the protocol model under the optimal guard zone. In low outage environments, both the dominant interferer guard zone and the optimal guard zone perform quite well. Finally, we note that the tradeoff between Type I and Type II errors, as well as the limiting behavior of Bayes risk, both respect the remarks made in Rem. 4.3 and Rem. 4.5.

**Table 4.1:** Environment Parameters

| Parameter | Value | Description |
|---|---|---|
| $A$ | 2500 | arena side length (m) |
| $d$ | 2 | dimension of the arena |
| $c_{d=2}$ | $\pi$ | volume of 2-dimensional unit ball |
| $\lambda$ | $5 * 10^{-4}$ | initial Poisson TX intensity, (per sq. m) |
| $\alpha$ | 3 | pathloss constant |
| $d_{\mathrm{T}}$ | 10 | typical TX-RX distance (m) |
| $\beta$ | 5 | SINR threshold (W/W) |
| $\eta$ | 0 | background noise power (W) |

In Fig. 4.2, we show how the operating points and their associated risks behave has a function of the network density on a finer granularity of network densities. We note that for the displayed intensities (yielding physical model outage rates from 1% to 50%), there is a proper ordering of guard zones, and two constant guard zones (dominant interferer $d_{\mathrm{I,DI}}$ and mean-matched $d_{\mathrm{I,MM}}$) serve as bounds for the optimal guard zone $d_{\mathrm{I}}^{*}$. As the network density (and outage) decrease, we observe that the error rate of the protocol model under the optimal guard zone is bounded by the outage rate, predicted by Prop. 4.6. Further, we note that the dominant interferer guard zone, while suboptimal, serves as a good approximation to the Bayes rule guard zone in low network density regimes, where the additional cost of using the dominant interferer guard zone decays linearly in decreasing network intensity and is quite small in low outage regimes of interest.

## 4.5 Directional Antennas

In this section, we extend the previous framework to the case of wireless Poisson networks employing directional antennas. We note that the concept of a single guard zone must be relaxed to account for the different antenna gains that are possible between the typical receiver and the interferers. As a result, the guard zone distance $d_{\mathrm{I}}$ is relaxed to a guard zone factor $\Delta$ that is applied multiplicatively

to the distance associated with dominant interferers (updated to reflect directional antennas). $\Delta$ can alternatively be thought of as a link budget margin added to or subtracted from the SINR threshold $\beta$, which would also effectively adjust the dominant interferer distance. Once the guard zone factor has been updated to reflect directional antenna patterns, we may compute the prior and posterior distributions of $H$ and $D$, as well as the posterior distribution of $H$ given $D$, using a similar strategy as in the previous case of omni-directional antennas. We note that the forms of the distributions do not change significantly and only require minor updating of the exponents.

Let us now proceed and assume a network deployment where transmitters and receivers are equipped with antennas with gain patterns $G_T(\theta) = G_R(\theta)$. These gain patterns, combined with the random orientations of the typical receiver and interferers in $\hat{\Phi}$ will induce gain distributions denoted $f_G$ and $F_G$ over support $G \in [0, \infty)$. Under these distributions, it will be convenient to define notation for the $\delta$th moment of the antenna gain pattern $G_i(\theta)$ normalized by its maximum boresight gain $G_i(0) = g_{\max}$, in a similar fashion to [45]:

$$\tilde{G}_i \equiv \mathbb{E}\left[\left(\frac{G_i}{g_{\max}}\right)^{\delta}\right] \tag{4.30}$$

**Remark 4.6.** *Under omni-directional antennas, $G_i(\theta) = 1, \forall\theta$ and the normalized moment must also be $\tilde{G}_i = 1$.*

As in the omni-directional physical interference model, the event $\mathcal{H}_1$ corresponds to the SINR falling above threshold $\beta$:

$$\mathbb{P}\{\mathcal{H}_1\} = \mathbb{P}\{\text{SINR}_o \geq \beta\}, \tag{4.31}$$

with:

$$P_{i,o} \equiv F_{i,o} G_{T,i,o} G_{R,i,o} d_{i,o}^{-\alpha} \tag{4.32}$$

$$I_o \equiv \sum_{i \neq o} P_{i,o} \tag{4.33}$$

$$\text{SINR}_o \equiv \frac{P_{o,o}}{I_o + \eta} = \frac{F_{o,o} g_{\max}^2 d_{\text{T}}^{-\alpha}}{\sum_{i \neq o} F_{i,o} G_{T,i,o} G_{R,i,o} d_{i,o}^{-\alpha} + \eta}, \tag{4.34}$$

where $P_{i,o}$ represents the received power from transmitter $i$ at receiver $o$ and accounts for the antenna gains between TX $i$ and RX $o$, $I_o$ represents the sum interference power at RX $o$, and $\text{SINR}_o$ is the updated signal-to-interference-plus-noise-ratio. Note that perfect orientation is assumed between each paired transmitter and receiver, hence gains $g_{\max}$ are employed in the numerator of the SINR.

We now introduce a slightly modified protocol interference model, where the event $\mathcal{D}_1$ corresponds to the absence of any interferers producing a *significant level* of interference, tuned by guard zone factor $\Delta$:

$$\mathbb{P}\{\mathcal{D}_1\} = \mathbb{P}\left\{ d_{i,o} \geq \Delta \left( \frac{G_{T,i,o} G_{R,i,o}}{g_{\max}^2} \right)^{1/\alpha} \beta^{1/\alpha} d_{\mathrm{T}}, \forall i \neq o \right\}. \tag{4.35}$$

In this case, the dominant interferer distance is derived without background noise and fading. We additionally replace an explicit guard zone radius $d_{\mathrm{I}}$ with a guard zone factor $\Delta$ that scales the dominant interferer distance. Note that the dominant interferer distance is itself a function of the gain levels associated with each interferer.

**Remark 4.7.** *Under omni-directional antennas, we have $g_{\max} = G_{T,i,o} = G_{R,i,o} = 1$ and we recover the condition $d_{i,o} \geq \Delta \beta^{1/\alpha} d_{\mathrm{T}}$. This represents a circular guard zone that is comprised of a multiplicative factor $\Delta$ of the dominant interferer distance.*

### 4.5.1 Priors and Posterior

In this section, we derive the prior and posterior distributions of the related estimation problem under directional antennas. Lem. 4.6 and Lem. 4.7 provide the prior distributions on $H$ and $D$, while Prop. 4.7 provides the posterior distribution.

**Lemma 4.6** (Distribution on $H$ w/ Directional Antennas)**.** *The distribution of $H$, the physical model feasibility of a typical transmission $o$ in $\hat{\Phi}$ is given by:*

$$\mathbb{P}\{\mathcal{H}_1\} = \exp\left( -\lambda c_d \kappa s^{\delta} \tilde{G}^2 - \frac{s\eta}{g_{\max}^2} \right). \tag{4.36}$$

*Proof.* The success rate follows from the success rates established in Ch. 3, appropriately simplified to the case of perfect orientation (*r.v.*'s $G_T$ and $G_R$ of Prop. 3.1 are now constants equal to $g_{\max}$)

and extended from the two-dimensional case to arbitrary dimension $d$. □

**Lemma 4.7** (Distribution on $D$ w/ Directional Antennas)**.** *The distribution of $D$, the protocol model feasibility of a typical transmission $o$ in $\hat{\Phi}$ is given by:*

$$\mathbb{P}\{\mathcal{D}_1\} = \exp\Big(-\lambda c_d s^\delta \tilde{G}^2 \Delta^d\Big). \tag{4.37}$$

*Proof.* In moving away from the case of omnidirectional antennas, the single circular guard zone has now been turned into multiple guard zones, each with a radius $d_{\mathrm{I}}$ tailored to a specific pair of realizable gains between the typical rx and an arbitrary interferer:

$$d_{\mathrm{I}}(G_i, G_j) = \Delta \left(\frac{G_i G_j}{g_{\max}^2}\right)^{1/\alpha} \beta^{1/\alpha} d_{\mathrm{T}}. \tag{4.38}$$

Each guard zone is applied to an independently thinned version of $\hat{\Phi}$ with thinning rate equal to the probability associated with the gain pair: $f_G(G_i) f_G(G_j)$.

$$\begin{aligned}
\mathbb{P}\{\mathcal{D}_1\} &= \prod_{i,j} \exp(-\left(\lambda f_G(G_i) f_G(G_j)\right) c_d d_{\mathrm{I}}(G_i, G_j)) && (4.39)\\
&= \exp\left(-\sum_{i,j} \left(\lambda f_G(G_i) f_G(G_j)\right) c_d d_{\mathrm{I}}(G_i, G_j)\right) && (4.40)\\
&= \exp\Big(-\lambda c_d s^\delta \tilde{G}^2 \Delta^d\Big). && (4.41)
\end{aligned}$$

□

**Remark 4.8.** *Complementary to the explanation in the proof of Lem. 4.7, the event $\mathcal{D}_1$ can be stochastically viewed as excluding all interferers from a ball around the typical receiver with radius:*

$$d_{\mathrm{I}} = \Big(s^\delta \tilde{G}^2 \Delta^d\Big)^{1/d} = \Delta \tilde{G}^{2/d} \beta^{1/\alpha} d_{\mathrm{T}}. \tag{4.42}$$

*This radius can be obtained from the exponent of the void probability of (4.37).*

**Proposition 4.7** (Posterior Distribution w/ Directional Antennas)**.** *The posterior distribution of $H$ given $D$ is:*

$$\mathbb{P}\{\mathcal{H}_1|\mathcal{D}_1\} = \mathrm{e}^{-A-C(\Delta)+B(\Delta)}, \tag{4.43}$$

*where* $A = \lambda c_d \kappa s^\delta \tilde{G}^2 + \frac{s\eta}{g_{\max}^2}$, $B(\Delta) = \lambda c_d s^\delta \tilde{G}^2 \Delta^d$, *and* $C(\Delta) = \lambda c_d s^\delta \tilde{G}^2 I_\delta(\Delta^\alpha)$.

*Proof.* See proof in App. C.4. □

### 4.5.2 Bayes Risk

We now appropriately quantify the Bayes risk as a function of the guard zone factor, $\Delta$.

**Proposition 4.8** (Bayes Risk w/ Directional Antennas)**.** *The Bayes risk of the protocol model decision rule $\Delta$ for a typical transmission in $\hat{\Phi}$ is given by:*

$$r(\Delta) = c_{00} + (c_{01} - c_{00})\mathrm{e}^{-A} + (c_{10} - c_{00})\mathrm{e}^{-B(\Delta)} + (c_{11} + c_{00} - c_{10} - c_{01})\mathrm{e}^{-A-C(\Delta)}, \tag{4.44}$$

*where* $A = \lambda c_d \kappa s^\delta \tilde{G}^2 + \frac{s\eta}{g_{\max}^2}$, $B(\Delta) = \lambda c_d s^\delta \tilde{G}^2 \Delta^d$, *and* $C(\Delta) = \lambda c_d s^\delta \tilde{G}^2 I_\delta(\Delta^\alpha)$.

*Proof.* The result is immediate from (4.13) and substituting expressions from Lem. 4.6, Lem. 4.7, and Prop. 4.7. □

**Theorem 4.2** (Minimum Bayes Risk w/ Directional Antennas)**.** *When $c_{10} > c_{00}$, the Bayes rule $\Delta^*$ minimizing Bayes risk (4.5) is given by the solution to:*

$$\frac{c_{00} - c_{10}}{c_{11} + c_{00} - c_{10} - c_{01}}(1 + \Delta^{-\alpha}) = \mathrm{e}^{-A-C(\Delta)+B(\Delta)}. \tag{4.45}$$

*The resulting Bayes risks under the Bayes rule $\Delta^*$ is:*

$$r(\Delta^*) = c_{00} + (c_{01} - c_{00})\mathrm{e}^{-A} - (c_{10} - c_{00})\frac{\mathrm{e}^{-B(\Delta^*)}}{(\Delta^*)^\alpha} \tag{4.46}$$

*where* $A = \lambda c_d \kappa s^\delta \tilde{G}^2 + \frac{s\eta}{g_{\max}^2}$, $B(\Delta) = \lambda c_d s^\delta \tilde{G}^2 \Delta^d$, *and* $C(\Delta) = \lambda c_d s^\delta \tilde{G}^2 I_\delta(\Delta^\alpha)$.

*Proof.* See proof in App. C.5. □

### 4.5.3 Uniform Cost ROC Curve and Operating Points

Under uniform costs, the error rates and operating points of the protocol model decision rule may be extended to the case of networks with directional antennas as well.

**Proposition 4.9** (Error Rates w/ Directional Antennas)**.** *In a PPP with directional antennas, the Type I, Type II, and total error rates of the protocol model as a detector for physical model outage $\mathcal{H}_0$ are given by:*

$$p_{\mathrm{I}}(\Delta) = \frac{\mathrm{e}^{-B(\Delta)} - \mathrm{e}^{-A-C(\Delta)}}{1 - \mathrm{e}^{-A}} \tag{4.47}$$

$$p_{\mathrm{II}}(\Delta) = 1 - \mathrm{e}^{-C(\Delta)} \tag{4.48}$$

$$p_{\mathrm{E}}(\Delta) = \mathrm{e}^{-A} + \mathrm{e}^{-B(\Delta)} - 2\mathrm{e}^{-A-C(\Delta)}, \tag{4.49}$$

*where $A = \lambda c_d \kappa s^{\delta} \tilde{G}^2 + \frac{s\eta}{g_{\max}^2}$, $B(\Delta) = \lambda c_d s^{\delta} \tilde{G}^2 \Delta^d$, and $C(\Delta) = \lambda c_d s^{\delta} \tilde{G}^2 I_{\delta}(\Delta^{\alpha})$.*

*Proof.* Proof strategies mirror those of networks with omni-directional antennas and are updated with new exponents $A$, $B(\Delta)$, and $C(\Delta)$ accordingly following the proofs of Prop. 4.3, Prop. 4.4, and Prop. 4.5. □

**Lemma 4.8** (Operating Points w/ Directional Antennas)**.** *In a PPP with directional antennas, the Dominant Interferer (DI), Mean-Matched (MM), and Equal-Error (EE) Rate guard factors are given by:*

$$\Delta_{\mathrm{DI}} = 1 \tag{4.50}$$

$$\Delta_{\mathrm{MM}} = \left( \kappa + \frac{s^{\delta-1}\eta}{\lambda c_d \tilde{G}^2 g_{\max}^2} \right)^{1/d} \tag{4.51}$$

$$\Delta_{\mathrm{EE}} : 1 = \mathrm{e}^{-A} + \mathrm{e}^{-B(\Delta)} + \mathrm{e}^{-C(\Delta)} - 2\mathrm{e}^{-A-C(\Delta)}, \tag{4.52}$$

*where $A = \lambda c_d \kappa s^{\delta} \tilde{G}^2 + \frac{s\eta}{g_{\max}^2}$, $B(\Delta) = \lambda c_d s^{\delta} \tilde{G}^2 \Delta^d$, and $C(\Delta) = \lambda c_d s^{\delta} \tilde{G}^2 I_{\delta}(\Delta^{\alpha})$.*

*Proof.* The dominant interferer guard factor is simply 1 due to the construction of the protocol model for wireless networks with directional antennas. The mean-matched guard factor and equal-error

guard factor are updated accordingly following the proofs of Lem. 4.4 and Lem. 4.5. □

**Proposition 4.10** (Protocol Model Error Bounds w/ Directional Antennas)**.** *In a PPP with directional antennas, the risk (total error rate) associated with the dominant interferer guard zone* $d_{\mathrm{I,DI}}$ *may be bounded by the minimum Bayes risk and the outage rate of the physical model:*

$$p_{\mathrm{E}}(\Delta^*) \leq p_{\mathrm{E}}(\Delta_{\mathrm{DI}}) \leq 1 - \mathrm{e}^{-A} = \mathbb{P}\{\mathcal{H}_0\}\,. \tag{4.53}$$

*where* $A = \lambda c_d \kappa s^{\delta} \tilde{G}^2 + \frac{s\eta}{g_{\max}^2}$.

*Proof.* See proof in App. C.6. □

### 4.5.4 Results

In this section, we study the sensitivity of the protocol model decision rule to changing antenna beamwidth in networks employing directional antennas. For simplicity, we will assume the network employs ideal sector antennas, as shown in (3.8) and Fig. 3.3, with no sidelobes ($g_2 = 0$). In this case, the gain moments shown in (4.30) simplify to $\tilde{G} = \frac{\omega}{2\pi}$, establishing the dependence of the Type I and II error rates on the antenna beamwidth employed within the network.

In Fig. 4.3, we provide a sample plot of the protocol model ROC curve under a PPP in two forms using parameters from Tab. 4.1. As the guard zone factor $\Delta$ is increased, the ROC curve travels from bottom-right to top-left as the false rejection rate is reduced in exchange for a higher rate of false acceptance. As the antenna beamwidth is decreased, the ROC curves move closer to the origin, indicating improved detection performance. The intuition is that in the regime of narrower beamwidths, transmissions become isolated from one another and outage is typically caused by a single interferer close to the typical receiver. In the parametric versions of the ROC curve of Fig. 4.3, we observe very similar patterns as in the case of omni-directional antennas (Fig. 4.1), further supporting the notion that protocol model detection performance is tightly keyed to the outage rates predicted by the physical interference model.

In Fig. 4.4, we show how the operating points and their associated risks behave has a function of the antenna beamwidth. We note that for the displayed beamwidths (yielding physical model

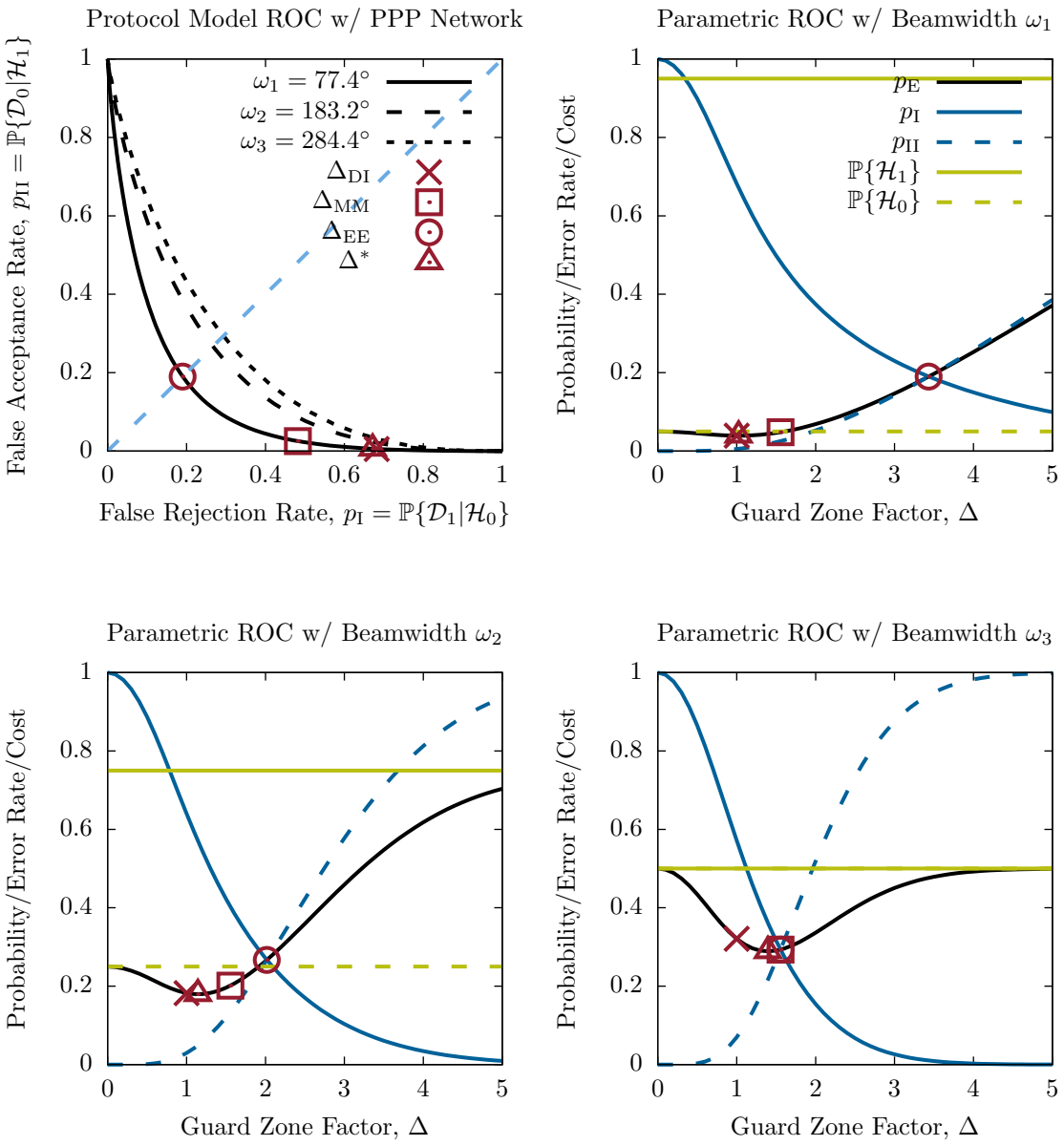


**Figure 4.3:** The protocol model ROC curve under a PPP network with directional antennas is plotted (**top-left**) in black solid and dashed lines for three outage rates (5%, 25%, 50%) and the equal error rate curve is plotted in light blue dashes. Each protocol model ROC curve is plotted (**top-right**, **bottom-left**, and **bottom-right**) component-wise against guard zone factor $\Delta$; Type I and II conditional error rates are plotted in blue, and total error rate in black. The physical model success and failure rates are plotted in green dashes and dots to provide references for the asymptotic Bayes risk as $\Delta \to 0$ and $\Delta \to \infty$. In all plots, operating points $\Delta_{\mathrm{DI}}$, $\Delta_{\mathrm{MM}}$, $\Delta_{\mathrm{EE}}$, and $\Delta^*$ are plotted as red markers.

outage rates from 1% to 50%), there is a proper ordering of guard zones factors, and the two constant operating points (dominant interferer $\Delta_{\mathrm{DI}}$ and mean-matched $\Delta_{\mathrm{MM}}$) again serve as bounds for the

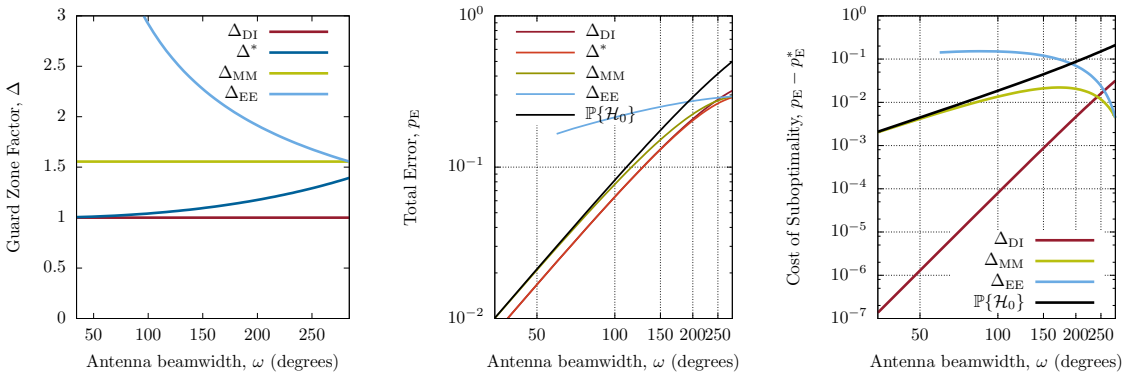


**Figure 4.4:** On the **left**, the guard zone operating points are plotted as a function of antenna beamwidth $\omega$, covering network densities producing physical model outages between 1% and 50%. On the **middle**, we show the total prediction error incurred by each of the decision rule operating points as a function of antenna beamwidth. On the **right**, we show the cost of suboptimality, that is the difference in risks between a suboptimal operating point and the optimal guard zone $\Delta^*$.

optimal guard zone factor $\Delta^*$. As antenna beamwidth (and outage) decreases, we observe that the error rate of the protocol model under the optimal guard zone is bounded by the outage rate, predicted by Prop. 4.10. Further, we note that the dominant interferer guard zone, while suboptimal, serves as a good approximation to the Bayes rule guard zone in low network density regimes, where the additional cost of using the dominant interferer guard zone decays linearly in decreasing network intensity and is quite small in low outage regimes of interest.

## 4.6 Conclusions

In this chapter, we studied the application of the protocol interference model in place of the more complex physical interference model in order to evaluate transmission success/outage in wireless networks. Under the protocol model, a transmission is successful iff there are no interferers within a specified guard zone around the receiver. While a guard zone may be chosen to match the outage rates predicted by networks employing the physical interference model, it was not immediately clear if such a guard zone also yields a high degree of correlation between the subsets of transmissions that are predicted successful by both models. To study this question, we recognize that the protocol model, parameterized by a guard zone radius, forms a family of decision rules for estimating the physical model feasibility of a typical transmission and cast the problem as binary hypothesis testing

framework. For wireless Poisson networks, we employ stochastic geometry to determine the estimation problem's prior and posterior distributions, and proceed to characterize the optimal guard zone that minimizes the protocol model prediction error. Finally, several intuitive guard zones for the protocol model, based on natural constraints and modeling objectives, are compared with the optimal guard zone. We find that error rates under the optimal guard zone are tightly coupled to the underlying physical model outage rates of the network. Additionally, in low outage regimes, we show that a guard zone based on dominant interference not only serves as a good approximation for the physical model outage probability, but it can also achieve close to optimal performance as a predictor of the feasibility of individual transmission attempts.

# Chapter 5: Conclusions

In this thesis, we addressed questions with the high-level goal to increase our understanding of the throughput performance and limitations of existing wireless communications techniques, as well as to characterize how our modeling assumptions influence the predicted throughput performance of such systems. The thesis was organized into three tasks that are primarily concerned with characterizing and maximizing throughput performance in such networks, with a secondary focus on the interference models employed therein. These tasks were investigated using random graph theory and stochastic geometry as a core set of analytical tools.

In Ch. 2, we studied the throughput ratio of a low-complexity, greedy scheduling technique in wireless communications networks. The randomized structure of wireless networks was hypothesized to be prohibitive to the throughput optimality of such a scheduling algorithm called Greedy Maximal Scheduling (GMS). In investigating this position, we employed threshold functions to characterize the sensitivity of the throughput ratio to the density of edges in large networks modeled as ER and RG graphs under the primary interference model. For sufficiently dense, large random graphs, we found that the throughput ratio is bounded between 1/2 and 2/3 and concluded that GMS is suboptimal with high probability in this regime. However, in the opposite regime of sparse random graphs, we demonstrated that GMS optimality, if permitted, must necessarily come at the cost of network connectivity.

While this work provides some needed answers regarding performance guarantees of greedy maximal scheduling (GMS) in random graph families of interest, there are several logical next steps forward. Our results suggest that if a network designer wanted to construct a random graph via its natural construction parameter (*e.g.*, edge communication radius), he or she cannot achieve both throughput optimality and connectivity simultaneously. Relevant here would be more advanced topology construction depending on the initial edge density of the network, such as the addition of edges to enable connectivity while preserving throughput optimality, or the removal of edges to

break up forbidden subgraphs while maintaining connectivity. However, adjusting the topology of a given graph also changes the dimensions of the stability region under the assumed single-hop traffic model. Of primary importance is an enhanced framework for comparing the stability regions (*i.e.*, throughput ratios) of a network graph with two different sets of edges. Work in this area will also likely require a relaxation of the model to study stability regions under multi-hop traffic, which itself contains many open and difficult questions.

In Ch. 3, we focused on the maximization of spatial throughput in large wireless networks employing directional antennas subject to orientation error. We proposed that such maximization over a configurable antenna beamwidths would result in an optimal beamwidth that navigated a trade-off between interference reduction and transmitter/receiver antenna misalignment. To this end, we defined a stochastic geometry based model that captured the effects of beam misdirection on coverage and throughput in large wireless networks. This framework yielded explicit expressions for communication outage as a function of network density and antenna beamwidth for idealized sector antenna patterns, which confirmed the existence of a throughput-optimizing antenna beamwidth. We additionally supplemented our analytical findings with matching numerical trends across more realistic antenna patterns.

This work represents a significant first step in incorporating beamsteering and orientation errors into stochastic geometry based approaches to analyze the throughput performance of wireless networks. In order to increase the relevance of this work to network designers, there are several directions to pursue. First, the assumption of Rayleigh fading, originally made for analytical tractability, may be relaxed to more general fading models. While this relaxation may result in increased computational complexity, it is appropriate in the regime of highly directional antennas and/or high frequency antenna arrays whose fading profiles may differ significantly from the multipath characterization associated with Rayleigh fading. Additionally, it is of great interest to characterize orientation error distributions for existing and emerging algorithms and techniques for antenna beamsteering, mode selection, pointing, etc. New error distributions may then be incorporated into the outage model developed in this work.

In Ch. 4, we turned our attention to the reconciliation of the protocol and physical interference models, both of which are heavily used in the simulation and design of scheduling and networking algorithms employed in wireless networks. We noted that that while a guard zone may be chosen to match the outage rate (and thus, spatial throughput) predicted by networks employing the physical interference model, it was not immediately clear if such a guard zone would also yield a high degree of correlation between the subsets of transmissions that are predicted successful by both models. We hypothesized that a properly configured protocol interference model can achieve both objectives for most regimes of interest. In our investigation, we modeled the protocol interference model as a binary decision rule to evaluate/predict physical model success of a typical transmission. Under this framework, we employed Bayes estimation and stochastic geometry to characterize the optimal guard zone that minimizes the prediction error rate associated with the protocol model decision rule. In regimes of low physical model outage, we demonstrated that a guard zone radius based on dominant interference incurs little additional error over the optimal guard zone and correlates well with physical model feasibility, in support of our hypothesis. This framework was then extended to the case of directional networks, where we were able to draw identical conclusions.

In regimes of higher physical model outage rates, it would be of interest to extend the protocol model to account for secondary (or more) sources of interference to improve the protocol model's prediction error rates. This may involve parameterizing inner and outer guard zones such that no interferers exist within the inner zone and one interferer may exist within the annulus formed by both radii. Such an extension draws parallels with conflict hypergraphs that encode the effects of multiple interferers on the feasibility of another transmission attempt via directed hyperedges. Also of interest is the extension of the Poisson Point Process (PPP) assumption to more general point processes that model more advanced scheduling algorithms. While PPPs are a natural model for capturing the spatial characteristics of an Aloha scheduling algorithm, they lack spatial separation between concurrent transmission attempts that is common of carrier sensing based scheduling techniques. An alternative is the Matérn Point Process, which clears out interferer-free zones around each transmitter in the spirit of modeling the carrier sensing process. However, MPPs are decidedly

less tractable in this context, meaning that bounds or numerical explorations of the protocol model prediction error rate are desirable first-order approaches.

# Bibliography


[1] L. Tassiulas and A. Ephremides, "Stability properties of constrained queueing systems and scheduling policies for maximum throughput in multihop radio networks," *IEEE Trans. Autom. Control*, vol. 37, no. 12, pp. 1936–1949, Dec. 1992. DOI: 10.1109/9.182479.

[2] S. Sarkar and K. Kar, "Queue length stability in trees under slowly convergent traffic using sequential maximal scheduling," *IEEE Trans. Autom. Control*, vol. 53, no. 10, pp. 2292–2306, Nov. 2008. DOI: 10.1109/TAC.2008.2006819.

[3] X. Lin and N. B. Shroff, "The impact of imperfect scheduling on cross-layer congestion control in wireless networks," *IEEE/ACM Trans. Netw.*, vol. 14, no. 2, pp. 302–315, Apr. 2006. DOI: 10.1109/TNET.2006.872546.

[4] A. Israeli and A. Itai, "A fast and simple randomized parallel algorithm for maximal matching," *Inform. Process. Lett.*, vol. 22, no. 2, pp. 77–80, Jan. 1986. DOI: 10.1016/0020-0190(86)90144-4.

[5] X. Lin and S. B. Rasool, "Constant-time distributed scheduling policies for ad hoc wireless networks," *IEEE Trans. Autom. Control*, vol. 54, no. 2, pp. 231–242, Feb. 2009. DOI: 10.1109/TAC.2008.2010888.

[6] A. Dimakis and J. Walrand, "Sufficient conditions for stability of longest-queue-first scheduling: Second-order properties using fluid limits," *Advances in Appl. Probability*, vol. 38, no. 2, pp. 505–521, Jun. 2006. DOI: 10.1239/aap/1151337082.

[7] B. Birand, M. Chudnovsky, B. Ries, P. Seymour, G. Zussman, and Y. Zwols, "Analyzing the performance of greedy maximal scheduling via local pooling and graph theory," *IEEE/ACM Trans. Netw.*, vol. 20, no. 1, pp. 163–176, Feb. 2012. DOI: 10.1109/TNET.2011.2157831.

[8] C. Joo, X. Lin, and N. B. Shroff, "Understanding the capacity region of the greedy maximal scheduling algorithm in multihop wireless networks," *IEEE/ACM Trans. Netw.*, vol. 17, no. 4, pp. 1132–1145, Aug. 2009. DOI: 10.1109/TNET.2009.2026276.

[9] G. Zussman, A. Brzezinski, and E. Modiano, "Multihop local pooling for distributed throughput maximization in wireless networks," in *Proc. 27th Annu. IEEE Conf. Comput. Commun. (INFOCOM)*, Apr. 2008, pp. 1139–1147. DOI: 10.1109/INFOCOM.2008.169.

[10] C. Joo, X. Lin, and N. B. Shroff, "Greedy maximal matching: Performance limits for arbitrary network graphs under the node-exclusive interference model," *IEEE Trans. Autom. Control*, vol. 54, no. 12, pp. 2734–2744, Dec. 2009. DOI: 10.1109/TAC.2009.2031719.

[11] B. Li, C. Boyaci, and Y. Xia, "A refined performance characterization of longest-queue-first policy in wireless networks," *IEEE/ACM Trans. Netw.*, vol. 19, no. 5, Oct. 2011. DOI: 10.1109/TNET.2011.2108314.

[12] M. Leconte, J. Ni, and R. Srikant, "Improved bounds on the throughput efficiency of greedy maximal scheduling in wireless networks," *IEEE/ACM Trans. Netw.*, vol. 19, no. 3, pp. 709–720, Jun. 2011. DOI: 10.1109/TNET.2010.2089534.

[13] A. Brzezinski, G. Zussman, and E. Modiano, "Local pooling conditions for joint routing and scheduling," in *Proc. 3rd Annu. Inform. Theory and Appl. Workshop (ITA)*, Jan. 2008, pp. 499–506. DOI: 10.1109/ITA.2008.4601094.

[14] ——, "Distributed throughput maximization in wireless mesh networks via pre-partitioning," *IEEE/ACM Trans. Netw.*, vol. 16, no. 6, pp. 1406–1419, Dec. 2008. DOI: 10.1109/TNET.2008.918109.

[15] X. Kang, J. J. Jaramillo, and L. Ying, "Stability of longest-queue-first scheduling in linear wireless networks with multihop traffic and one-hop interference," *Springer Queueing Syst.*, Apr. 2015. DOI: 10.1007/s11134-015-9441-2.

[16] R. Diestel, *Graph Theory*, 3rd. Springer, 2005, ISBN: 978-3642142789.

[17] B. Bollobás, *Random Graphs*, 2nd, ser. Cambridge Studies in Advanced Mathematics. Cambridge University Press, 2001, vol. 73, ISBN: 978-0521797221.

[18] S. Janson, T. Łuczak, and A. Ruciński, *Random Graphs*, ser. Series in Discrete Mathematics and Optimization. Wiley-Interscience, 2000, ISBN: 978-0471175414.

[19] P. Erdős and A. Rényi, "On the evolution of random graphs," *Publication Math. Inst. Hungarian Academy of Sci.*, vol. 5, pp. 17–61, 1960.

[20] T. H. Cormen, C. E. Leiserson, R. L. Rivest, and C. Stein, *Introduction to Algorithms*, 3rd. The MIT Press, 2009, ISBN: 978-0262033848.

[21] G. L. McColm, "Threshold functions for random graphs on a line segment," *Combinatorics, Probability, and Computing*, vol. 13, no. 3, pp. 373–387, May 2004. DOI: 10.1017/S0963548304006121.

[22] G. Han and A. M. Makowski, "A very strong zero-one law for connectivity in one-dimensional geometric random graphs," *IEEE Commun. Lett.*, vol. 11, no. 1, pp. 55–57, Jan. 2007. DOI: 10.1109/LCOMM.2007.061142.

[23] E. Friedgut and G. Kalai, "Every monotone graph property has a sharp threshold," *Proc. Amer. Math. Soc.*, vol. 124, no. 10, pp. 2993–3002, Oct. 1996. DOI: 10.1090/S0002-9939-96-03732-X.

[24] A. Goel, S. Rai, and B. Krishnamachari, "Monotone properties of random geometric graphs have sharp thresholds," *The Ann. of Appl. Probability*, vol. 15, no. 4, pp. 2535–2552, Nov. 2005. DOI: 10.1214/105051605000000575.

[25] P. Erdős and A. Rényi, "On random graphs, I," *Publicationes Mathematicae (Debrecen)*, vol. 6, pp. 290–297, 1959.

[26] M. Penrose, *Random Geometric Graphs*, ser. Oxford Studies in Probability. Oxford University Press, 2003, vol. 5, ISBN: 978-0198506263.

[27] D. F. Gleich, "Models and algorithms for pagerank sensitivity," Chapter 7 on MatlabBGL, PhD thesis, Stanford University, Sep. 2009.

[28] N. Alon, R. Yuster, and U. Zwick, "Color-coding," *J. ACM (JACM)*, vol. 42, no. 4, pp. 844–856, Jul. 1995. DOI: 10.1145/210332.210337.

[29] H. N. Gabow and S. Nie, "Finding long directed cycles," *ACM Trans. on Algorithms (TALG)*, vol. 4, no. 1, pp. 49–58, Mar. 2008. DOI: 10.1145/1328911.1328918.

[30] R. Ramanathan, J. Redi, C. Santivanez, D. Wiggins, and S. Polit, "Ad hoc networking with directional antennas: A complete system solution," *IEEE J. Sel. Areas Commun.*, vol. 23, no. 3, pp. 496–506, Mar. 2005. DOI: 10.1109/JSAC.2004.842556.

[31] S. D. Milner, J. Llorca, and C. C. Davis, "Autonomous reconfiguration and control in directional mobile ad hoc networks," *IEEE Circuits Syst. Mag.*, vol. 9, no. 2, pp. 10–26, Jun. 2009. DOI: 10.1109/MCAS.2008.931736.

[32] J. Yu, Y.-D. Yao, A. F. Molisch, and J. Zhang, "Performance evaluation of CDMA reverse links with imperfect beamforming in a multicell environment using a simplified beamforming model," *IEEE Trans. Veh. Technol.*, vol. 55, no. 3, pp. 1019–1031, May 2006. DOI: 10.1109/TVT.2006.874556.

[33] B. Epple, "Using a gps-aided inertial system for coarse-pointing of free-space optical communication terminals," in *Proc. SPIE*, vol. 6304, Sep. 2006. DOI: 10.1117/12.680502.

[34] B. L. Wilkerson, D. Giggenbach, and B. Epple, "Concepts for fast acquisition in optical communications systems," in *Proc. SPIE*, vol. 6304, Sep. 2006. DOI: 10.1117/12.680487.

[35] C.-J. Chang and J.-F. Chang, "Optimal design parameters in a multihop packet radio network using random access techniques," *Elsevier Comput. Networks and ISDN Syst.*, vol. 11, no. 5, pp. 337–351, May 1986. DOI: 10.1016/0169-7552(86)90040-1.

[36] C. Lau and C. Leung, "Throughput of slotted ALOHA channel with multiple antennas and receivers," *IET Electron. Lett.*, vol. 28, no. 25, pp. 1540–1542, Dec. 1988.

[37] A. Spyropoulos and C. S. Raghavendra, "Asymptotic capacity bounds for ad-hoc networks revisited: The directional and smart antenna cases," in *Proc. IEEE Global Telecommun. Conf. (GLOBECOM)*, vol. 3, Dec. 2003, pp. 1216–1220. DOI: 10.1109/GLOCOM.2003.1258432.

[38] S. Yi, Y. Pei, S. Kalyanaraman, and B. Azimi-Sadjadi, "How is the capacity of ad hoc networks improved with directional antennas?" *Springer Wireless Networks*, vol. 13, no. 5, pp. 635–648, Oct. 2007. DOI: 10.1007/s11276-006-8147-0.

[39] J. Wang, L. Kong, and M.-Y. Wu, "Capacity of wireless ad hoc network using practical directional antennas," in *Proc. IEEE Wireless Commun. and Networking Conf. (WCNC)*, Apr. 2010, pp. 1–6. DOI: 10.1109/WCNC.2010.5506381.

[40] P. Li, C. Zhang, and Y. Fang, "The capacity of wireless ad hoc networks using directional antennas," *IEEE Trans. Mobile Comput.*, vol. 10, no. 10, pp. 1374–1387, Oct. 2011. DOI: 10.1109/TMC.2010.243.

[41] Y. Chen, J. Liu, X. Jiang, and O. Takahashi, "Throughput analysis in mobile ad hoc networks with directional antennas," *Elsevier Ad Hoc Networks*, vol. 11, no. 3, pp. 1122–1135, May 2013. DOI: 10.1016/j.adhoc.2012.12.003.

[42] P. Gupta and P. R. Kumar, "The capacity of wireless networks," *IEEE Trans. Inf. Theory*, vol. 46, no. 2, pp. 388–404, Mar. 2000. DOI: 10.1109/18.825799.

[43] A. M. Hunter, J. G. Andrews, and S. Weber, "Transmission capacity of ad hoc networks with spatial diversity," *IEEE Trans. Wireless Commun.*, vol. 7, no. 12, pp. 5058–5071, Dec. 2008. DOI: 10.1109/T-WC.2008.071047.

[44] S. Singh, R. Mudumbai, and U. Madhow, "Interference analysis for highly directional 60-GHz mesh networks: The case for rethinking medium access control," *IEEE/ACM Trans. Netw.*, vol. 19, no. 5, pp. 1513–1527, Oct. 2011. DOI: 10.1109/TNET.2011.2122343.

[45] H. Wang and M. C. Reed, "Tractable model for heterogeneous cellular networks with directional antennas," in *Proc. Australian Commun. Theory Workshop (AusCTW)*, Feb. 2012, pp. 61–65. DOI: 10.1109/AusCTW.2012.6164907.

[46] S. Akoum, O. E. Ayach, and R. W. Heath Jr., "Coverage and capacity in mmWave cellular systems," in *Proc. 46th IEEE Asilomar Conf. Signals, Syst., and Comput. (Asilomar)*, Nov. 2012, pp. 688–692. DOI: 10.1109/ACSSC.2012.6489099.

[47] F. Baccelli and B. Błaszczyszyn, *Stochastic Geometry and Wireless Networks: Volume I Theory*, ser. Foundations and Trends in Networking 3-4. NOW Publishers, Jan. 2010, vol. 3, pp. 249–449. DOI: 10.1561/1300000006.

[48] ——, *Stochastic Geometry and Wireless Networks: Volume II Applications*, ser. Foundations and Trends in Networking 1-2. NOW Publishers, Jan. 2010, vol. 4, pp. 1–312. DOI: 10.1561/1300000026.

[49] J. Shen and L. W. Pearson, "The phase error and beam-pointing error in coupled oscillator beam-steering arrays," *IEEE Trans. Antennas Propag.*, vol. 53, no. 1, pp. 386–393, Jan. 2005. DOI: 10.1109/TAP.2004.838792.

[50] H. Li, Y.-D. Yao, and J. Yu, "Outage probabilities of wireless systems with imperfect beamforming," *IEEE Trans. Veh. Technol.*, vol. 55, no. 5, pp. 1503–1515, Sep. 2006. DOI: 10.1109/TVT.2006.878611.

[51] V. Vakilian, J.-F. Frigon, and S. Roy, "Effects of angle-of-arrival estimation errors, angular spread and antenna beamwidth on the performance of reconfigurable SISO systems," in *Proc. IEEE Pacific Rim Conf. Commun., Comput. and Signal Process. (PacRim)*, Aug. 2011, pp. 515–519. DOI: 10.1109/PACRIM.2011.6032947.

[52] M. Haenggi, *Stochastic Geometry for Wireless Networks*. Cambridge University Press, 2013, ISBN: 978-1107014695.

[53] K. M. Mardia and P. E. Jupp, *Directional Statistics*, ser. Wiley Series in Probability and Statistics. John Wiley & Sons, LTD, 2000, ISBN: 978-0471953333.

[54] S. Weber and J. G. Andrews, *Transmission Capacity of Wireless Networks*, ser. Foundations and Trends in Networking 2-3. NOW Publishers, Jan. 2012, vol. 5, pp. 109–281. DOI: 10.1561/1300000032.

[55] M. Bagnoli and T. Bergstrom, "Log-concave probability and its applications," *Springer-Verlag Economic Theory*, vol. 26, no. 2, pp. 445–469, Aug. 2005. DOI: 10.1007/s00199-004-0514-4.

[56] "UMTS; spatial channel model for MIMO simulations," ETSI 3rd Generation Partnership Project (3GPP), Tech. Rep. 25.996 version 11.0.0 Release 11, Sep. 2012. [Online]. Available: http://www.3gpp.org/DynaReport/25996.htm.

[57] P. Cardieri, "Modeling interference in wireless ad hoc networks," *IEEE Commun. Surveys Tuts.*, vol. 12, no. 4, pp. 551–572, 2010. DOI: 10.1109/SURV.2010.032710.00096.

[58] A. Hasan and J. G. Andrews, "The guard zone in wireless ad hoc networks," *IEEE Trans. Wireless Commun.*, vol. 6, no. 3, pp. 897–906, Mar. 2007. DOI: 10.1109/TWC.2007.04793.

[59] Y. Shi, Y. T. Hou, J. Liu, and S. Kompella, "Bridging the gap between protocol and physical models for wireless networks," *IEEE Trans. Mobile Comput.*, vol. 12, no. 7, pp. 1404–1416, Jul. 2013. DOI: 10.1109/TMC.2012.118.

[60] H. Zhang, X. Che, X. Liu, and X. Ju, "Adaptive instantiation of the protocol interference model in wireless networked sensing and control," *ACM Trans. Sensor Networks*, vol. 10, no. 2, 28:1–28:48, Jan. 2014. DOI: 10.1145/2530286.

[61] Y. Zhong, W. Zhang, and M. Haenggi, "Stochastic analysis of the mean interference for the RTS/CTS mechanism," in *Proc. IEEE Int. Conf. Commun. (ICC)*, Sydney, NSW, Australia, Jun. 2014, pp. 1996–2001. DOI: 10.1109/ICC.2014.6883616.

[62] F. Baccelli and P. Bermolen, "Extremal versus additive Matérn point processes," *Springer Queueing Systems*, vol. 71, no. 1–2, pp. 179–197, Mar. 2012. DOI: 10.1007/s11134-012-9280-3.

[63] M. Zorzi, "Accuracy of the dominant interferer method for outage probability evaluations in a mobile radio environment," in *Proc. Int. Conf. Telecommun. (ICT)*, 1995.

[64] A. Iyer, C. Rosenberg, and A. Karnik, "What is the right model for wireless channel interference?" *IEEE Trans. Wireless Commun.*, vol. 8, no. 5, pp. 2662–2671, May 2009. DOI: 10.1109/TWC.2009.080720.

[65] G. Kang, Y. Taniguchi, G. Hasegawa, and H. Nakano, "Extending the protocol interference model considering SINR for wireless mesh networks," in *Proc. 7th Advanced Int. Conf. Telecommun. (AICT)*, St. Maarten, The Netherlands Antilles, Mar. 2011, pp. 26–31. [Online]. Available: http://www.thinkmind.org/index.php?view=article&articleid=aict_2011_2_10_10033.

[66] S. Boyd and L. Vandenberghe, *Convex Optimization*. Cambridge University Press, 2004, ISBN: 978-0521833783.

# Appendix A: Proofs of Ch. 2

## A.1 Ancillary Lemmas

Lem. A.1 and Lem. A.2 are used to prove Thm. 2.2 (App. A.6), while Lem. A.3 and Lem. A.4 are used in the proof of Prop. 2.3 (App. A.12).

**Lemma A.1** (Expected Forbidden Cycles in $G_{n,p(n)}$)**.** *When $p(n) \sim c/n, c < 1$, the expected number of forbidden cycles of $\mathcal{F}$ in $G_{n,p(n)}$ obeys:*

$$\lim_{n\to\infty} \sum_{\substack{6\leq k\leq n,\\ k\neq 7}} \mathbb{E}[G(C_k)] = -\log(\sqrt{1-c}) - \sum_{k\in\mathcal{K}} \frac{c^k}{2k}. \tag{A.1}$$

*Proof.* Given the choice of $p(n)$, it follows that:

$$\forall \delta > 0, \exists n_\delta > 0 : \frac{c-\delta}{n} \leq p(n) \leq \frac{c+\delta}{n}, \forall n > n_\delta. \tag{A.2}$$

The expected number of copies of a $k$-length cycle, $C_k$ in $G_{n,p(n)}$ can be expressed as a product between the number of possible unlabelled cycles and the probability that each forms the desired cycle, $\mathbb{E}[G(C_k)] = n^{\underline{k}}/(2k) * p(n)^k$. Incorporating the bounds in (A.2) yields:

$$\frac{n^{\underline{k}}}{2k}\frac{(c-\delta)^k}{n^k} \leq \mathbb{E}[G(C_k)] \leq \frac{n^{\underline{k}}}{2k}\frac{(c+\delta)^k}{n^k}. \tag{A.3}$$

Next evaluate the following series when $c < 1$ and $\delta \in (0, 1-c)$:

$$\lim_{n\to\infty} \sum_{k=1}^{n} \frac{n^{\underline{k}}}{n^k}\frac{(c+\delta)^k}{2k} \overset{(a)}{=} \sum_{k=1}^{\infty} \frac{(c+\delta)^k}{2k} \tag{A.4}$$

$$\overset{(b)}{=} -\log(\sqrt{1-(c+\delta)}) \tag{A.5}$$

$$\overset{(c)}{\leq} -\log(\sqrt{1-c}) + \epsilon. \tag{A.6}$$

where we apply $(a)$ the monotone convergence theorem, $(b)$ series convergence when $c+\delta<1$, and $(c)$ continuity and monotonicity of $\log(\sqrt{1-c})$ at $c$.

By a similar process on the lower bound series, and by controlling $\epsilon$ by choice of $\delta$, we establish:

$$\lim_{n\to\infty}\sum_{\substack{6\leq k\leq n,\\ k\neq 7}}\mathbb{E}[G(C_k)] = -\log(\sqrt{1-c}) - \sum_{k\in\mathcal{K}}\frac{c^k}{2k}, \tag{A.7}$$

where we subtract out a finite number of terms ($\mathcal{K}=\{1,2,3,4,5,7\}$) that were originally included in (A.4) but do not correspond to forbidden cycle lengths. □

**Lemma A.2** (Expected Forbidden Dumbbells in $G_{n,p(n)}$)**.** *When $p(n)\sim c/n, c<1$, the expected number of forbidden dumbbells of $\mathcal{F}$ in $G_{n,p(n)}$ obeys:*

$$\lim_{n\to\infty}\sum_{k=0}^{n}\left(\mathbb{E}\Big[G(D_k^{5,5})\Big]+\mathbb{E}\Big[G(D_k^{5,7})\Big]+\mathbb{E}\Big[G(D_k^{7,7})\Big]\right)=0. \tag{A.8}$$

*Proof.* Given $p(n)$, it follows that:

$$\forall\delta>0, \exists n_\delta>0 : p(n)\leq\frac{c+\delta}{n}, \forall n>n_\delta. \tag{A.9}$$

The expected number of dumbbells, $D_k^{s,t}$ (unions of cycles of lengths $s$ and $t$ joined by a $k$-edge path), assuming $s\neq t$ and $k\geq 1$ is:

$$\begin{aligned}\mathbb{E}\big[G(D_k^{s,t})\big] &= \frac{n^{\underline{s}}}{2s}\frac{(n-s)^{\underline{t}}}{2t}s(n-s-t)^{\underline{k-1}}tp(n)^{s+t+k}\\ &< \frac{(c+\delta)^{s+t+k}}{4n}.\end{aligned} \tag{A.10}$$

where there are $n^{\underline{s}}/(2s)$ unlabelled cycles $C_s$, $(n-s)^{\underline{t}}/(2t)$ unlabelled cycles $C_t$ from the remaining $n-s$ vertices, and $s(n-s-t)^{\underline{k-1}}t$ ways of connecting $C_s$ to $C_t$ with a $k$-edge path using the remaining $n-s-t$ vertices. The probability that such a selection of vertices forms $D_k^{s,t}$ is $p(n)^{p+q+k}$.

In the event the path contains no edges, $k = 0$, then the cycles share a common vertex:

$$\mathbb{E}\big[G(D_0^{s,t})\big] = \frac{n^{\underline{s}}}{2s}\frac{(n-s)^{\underline{t-1}}}{2}sp(n)^{s+t} < \frac{(c+\delta)^{s+t}}{4n} \tag{A.11}$$

In this case, $C_t$ is created using one vertex from $C_s$ and a $(t-1)$-edge path from the remaining $n-s$ vertices.

Finally, if $s = t$, then $\mathbb{E}\big[G(D_k^{s,t})\big]$ contains an additional factor of $1/2$ due to symmetry, but nevertheless is upper bounded by the expressions in (A.10) and (A.11).

It remains to show that expected number of all forbidden dumbbells is zero. Let $\hat{c} = c + \delta < 1$ for an appropriate choice of $\delta \in (0, 1-c)$:

$$\lim_{n\to\infty}\sum_{k=0}^{n}\Big(\mathbb{E}\Big[G(D_k^{5,5})\Big] + \mathbb{E}\Big[G(D_k^{5,7})\Big] + \mathbb{E}\Big[G(D_k^{7,7})\Big]\Big) \overset{(a)}{<} \lim_{n\to\infty}\frac{\hat{c}^{10}+\hat{c}^{12}+\hat{c}^{14}}{4n}\sum_{k=0}^{\infty}\hat{c}^k \overset{(b)}{=} 0, \tag{A.12}$$

where we $(a)$ apply bounds derived above and collect common factors, and $(b)$ apply geometric series convergence and evaluate the limit. □

**Lemma A.3** (Expected Edges in $G_{n,r(n)}$)**.** *If $r(n)^2 \in 2c/(\pi n) + x2\sqrt{cn}/(\pi n^2)$ with $x \in \mathbb{R}$, then the mean number of edges $M_{n,r(n)}$ in $G_{n,r(n)}$ is:*

$$\mathbb{E}\big[M_{n,r(n)}\big] \in cn + x\sqrt{cn} + o\big(\sqrt{n}\big)\,. \tag{A.13}$$

*Proof.* This follows from a specialization of [26, Prop. 3.1] which provides the asymptotic mean of a subgraph count of $G_{n,r(n)}$ when $r(n) \in o(1)$. We will not recreate the theory here, but instead provide enough direction to allow the reader to follow along with [26]. The expected number of edges ($\mathbb{E}\big[M_{n,r(n)}\big]$) is given as:

$$\mathbb{E}\big[M_{n,r(n)}\big] \sim \mu_{K_2,\mathbb{R}^2} r(n)^{d(k-1)} n^k, \tag{A.14}$$

where the subgraph $K_2$ (the complete graph on 2 vertices, *i.e.*, an edge) has $k = 2$ vertices, $d = 2$ is

the dimension of the space in which the points of $G_{n,r(n)}$ reside, and $\mu_{K_2,\mathbb{R}^2}$ is computed as follows:

$$\mu_{K_2,\mathbb{R}^2} \overset{(a)}{=} \frac{1}{2!}\int_{\mathbb{R}^2} f(x)^2 \mathrm{d}x \int_{\mathbb{R}^2} h_{K_2}(\{0,x_1\})\mathrm{d}x_1 \tag{A.15}$$

$$\overset{(b)}{=} \frac{1}{2}\int_{\mathbb{R}^2} h_{K_2}(\{0,x_1\})\mathrm{d}x_1 \overset{(c)}{=} \frac{\pi}{2}. \tag{A.16}$$

where $(a)$ is simplified from [26] for the subgraph type $K_2$, $(b)$ follows from $f(x)$ being the uniform distribution over the unit square $[-1/2,1/2]^2$ used to generate *i.i.d.* vertex positions, and $(c)$ follows from $h_{K_2}(0,x_1)$ being the indicator function on whether or not two vertices (one at the origin and the other at $x_1$) with unit edge distance form $K_2$. To form $K_2$, $x_1$ must be within the unit disk centered at the origin to connect to the vertex at the origin.

Finally, expanding $\mu_{K_2} r(n)^2 n^2$ and grouping $o(\sqrt{n})$ terms is sufficient. □

**Lemma A.4** (CLT for Edges in $G_{n,r(n)}$)**.** *If $r(n)^2 \in 2c/(\pi n) + 2\sqrt{cn}x/(\pi n^2)$ with $x \in \mathbb{R}$, then the centered and scaled number of edges $M_{n,r(n)}$ in $G_{n,r(n)}$ converges in distribution to that of a centered normal* r.v.*:*

$$\frac{M_{n,r(n)} - \mathbb{E}\big[M_{n,r(n)}\big]}{n^{1/2}} \overset{\mathcal{D}}{\sim} \mathcal{N}(0,c). \tag{A.17}$$

*Proof.* This follows from a specialization of [26, Thm. 3.13] which provides a central limit theorem for collections of subgraph counts of $G_{n,r(n)}$ when $\lim_{n\to\infty} nr(n)^d \to \rho \in (0,\infty)$. The distribution of the centered and scaled number of edges $(M_{n,r(n)} - \mathbb{E}\big[M_{n,r(n)}\big])/\sqrt{n}$ is an asymptotic centered normal with variance:

$$\left(\sum_{j=1}^{k} \rho^{2k-j-1}\Phi_j(K_2,K_2)\right) - k^2\rho^{2k-2}\mu_{K_2}^2, \tag{A.18}$$

where the subgraph $K_2$ (the complete graph on 2 vertices, *i.e.*, an edge) has $k=2$ vertices, $d=2$ is the dimension of the space in which the points of $G_{n,r(n)}$ reside, $\mu_{K_2,\mathbb{R}^2} = \pi/2$ is computed as shown in the proof of Lem. A.3, and $\Phi_1(K_2,K_2)$ simplifies to:

$$\Phi_1(K_2,K_2) = \int_{\mathbb{R}^2} h_{K_2}(0,x_2)\mathrm{d}x_2 \int_{\mathbb{R}^2} h_{K_2}(0,x_3)\mathrm{d}x_3 = \pi^2, \tag{A.19}$$

and $\Phi_2(K_2, K_2) = \mu_{K_2}$.

Finally, note that for the given $r(n)^2$, $nr(n)^2 \sim \rho = 2c/\pi$. Substituting $\Phi_1$, $\Phi_2$, $\mu_{K_2}$, and $\rho$ into (A.18), we obtain the asymptotic variance:

$$\rho^2\Phi_1(K_2, K_2) + \rho\Phi_2(K_2, K_2) - 4\rho^2\mu_{K_2}^2 = \rho\mu_{K_2} = c. \tag{A.20}$$

□

## A.2 Lem. 2.2 ($\mathcal{P}_{\text{lop}}$ Monotonicity)

*Proof.* Let $G \in \mathcal{P}_{\text{lop}}$. From Thm. 2.1, $G$ contains no edge-induced forbidden subgraphs from $\mathcal{F}$. Let $H \subset G$ by an appropriate removal of edges. The removal of edges from $G$ cannot possibly create edge-induced forbidden subgraphs where none existed before, therefore $H \in \mathcal{P}_{\text{lop}}$ and $\mathcal{P}_{\text{lop}}$ is monotone decreasing as described by Def. 2.2. □

## A.3 Lem. 2.3 (Separate Sufficient and Necessary Cond. for $\mathcal{P}_{\text{lop}}$)

*Proof.* Since all forbidden subgraphs in $\mathcal{F}$ (Thm. 2.1) contain cycles, it immediately follows that forbidding all cycles ($\mathcal{P}_{\text{lop}}^{\text{L}}$) is sufficient for $\mathcal{P}_{\text{lop}}$. Separately, forbidding any subset of subgraphs in $\mathcal{F}$ is a necessary condition for $\mathcal{P}_{\text{lop}}$, therefore forbidding cycles of lengths $k \geq 6, k \neq 7$ ($\mathcal{P}_{\text{lop}}^{\text{U}}$) is necessary for $\mathcal{P}_{\text{lop}}$. Thus, the subsets of graphs on $n$ vertices that satisfy $\mathcal{P}_{\text{lop}}^{\text{L}}$, $\mathcal{P}_{\text{lop}}$, $\mathcal{P}_{\text{lop}}^{\text{U}}$ can be nested in that order. □

## A.4 Lem. 2.4 (Probability Bounds for $\mathcal{P}_{\text{lop}}$)

*Proof.* Given $p(n)$ (or $r(n)$) and $n \in \mathbb{Z}^+$, $G_{n,p(n)}$ (or $G_{n,r(n)}$) is a random graph generated from a distribution on $\mathcal{G}_n$. Interpreted as events, the nesting of subsets $\mathcal{P}_{\text{lop}}^{\text{L}}$, $\mathcal{P}_{\text{lop}}$, $\mathcal{P}_{\text{lop}}^{\text{U}}$ by Lem. 2.3 provides the desired ordering of probabilities. □

## A.5 Prop. 2.1 (Reg. Sharp Threshold for $\mathcal{P}_{\text{edge}}$ in $G_{n,p(n)}$)

*Proof.* Let the *r.v.* $M_{n,p(n)}$ (shortened to $M$) be the number of edges in graph $G_{n,p(n)}$. We show for the given choice of $(p^*(n) = 2c/n, \alpha(n) = 2\sqrt{cn}/n^2)$ and $F(x) = \Phi(-x)$ that:

$$p(n) \sim p^*(n) + x\alpha(n) \Rightarrow \lim_{n\to\infty} \mathbb{P}\{M \leq cn\} = F(x), \tag{A.21}$$

holds for every point of continuity of $F(x)$, $x \in \mathbb{R}$.

$M_{n,p(n)}$ has a binomial *p.d.f.*; for $p(n) \sim p^*(n) + x\alpha(n)$, $M_{n,p(n)}$ has mean and variance:

$$\mathbb{E}\big[M_{n,p(n)}\big] = \binom{n}{2} p(n) = cn + x\sqrt{cn} + o\big(\sqrt{n}\big) \tag{A.22}$$

$$\text{Var}\big(M_{n,p(n)}\big) = \binom{n}{2} p(n)(1-p(n)) = cn + o(n)\,, \tag{A.23}$$

by using the additional facts $p(n) = 2c/n + o(1/n)$ and $p(n)^2 = o(1/n)$.

Finally, for $p(n) \sim p^*(n) + x\alpha(n)$:

$$\mathbb{P}\{M \leq cn\} \overset{(a)}{=} \mathbb{P}\left\{ \frac{M - \mathbb{E}[M]}{\sqrt{\text{Var}(M)}} \leq \frac{cn - \mathbb{E}[M]}{\sqrt{\text{Var}(M)}} \right\} \tag{A.24}$$

$$\overset{(b)}{=} \mathbb{P}\left\{ \frac{M - \mathbb{E}[M]}{\sqrt{\text{Var}(M)}} \leq \frac{-x\sqrt{cn} + o(\sqrt{n})}{\sqrt{cn + o(n)}} \right\} \tag{A.25}$$

$$\overset{(c)}{=} \Phi\left(-x + o(1)\right) + o(1) \tag{A.26}$$

$$\overset{(d)}{=} \Phi(-x) + o(1)\,, \tag{A.27}$$

where we $(a)$ standardize $M_{n,p(n)}$, $(b)$ expand using (A.22) and (A.23), $(c)$ asymptotically simplify the inequality's *r.h.s.* and apply the CLT to the standardized $M_{n,p(n)}$, and $(d)$ apply continuity of the standard normal *c.d.f.*, $\Phi(x)$.

Thus, for the specific case when $c = 2$, we conclude:

$$\lim_{n\to\infty} \mathbb{P}\big\{G_{n,p(n)} \in \mathcal{P}_{\text{edge}}\big\} = \lim_{n\to\infty} \mathbb{P}\{M \leq 2n\} = \Phi\left(-x\right). \tag{A.28}$$

□

## A.6 Thm. 2.2 (Reg. Threshold for $\mathcal{P}_{\text{lop}}$ in $G_{n,p(n)}$)

*Proof.* Let $\Gamma$ be a connected graph. Let the *r.v.* $G(\Gamma)$ be the number of copies of $\Gamma$ in graph $G_{n,p(n)}$. Let $A_\Gamma = \{G(\Gamma) > 0\}$ be the event that there are one or more copies of $\Gamma$ in $G_{n,p(n)}$. We show for the given $p^*(n)$ and $F(x)$, that:

$$p(n) \sim xp^*(n) \Rightarrow \lim_{n\to\infty} \mathbb{P}\{\mathcal{P}_{\text{lop}}\} = F(x), \tag{A.29}$$

holds for every point of continuity of $F(x)$, $x \in \mathbb{R}$.

Suppose $p(n) \sim xp^*(n)$. We first upper bound $\mathbb{P}\{\mathcal{P}_{\text{lop}}\}$:

$$\lim_{n\to\infty} \mathbb{P}\{\mathcal{P}_{\text{lop}}\} \overset{(a)}{\leq} \lim_{n\to\infty} \mathbb{P}\left\{ \bigcap_{\substack{6\leq k\leq K,\\ k\neq 7}} \overline{A_{C_k}} \right\} \overset{(b)}{=} \exp\left( -\sum_{\substack{6\leq k\leq K,\\ k\neq 7}} \frac{x^k}{2k} \right), \tag{A.30}$$

where $(a)$ follows by forbidding only cycles in $\mathcal{F}$ up to length $K \leq n$, and $(b)$ is a consequence of [17, Cor. 4.9] which shows that when $p(n) \sim x/n$, a finite-length random vector of cycle subgraph counts $\{G(C_k)\}$ converges in distribution to that of independent Poisson *r.v.*'s with means $\{\lambda_k = x^k/(2k)\}$.

Now, considering the upper bound, suppose $x \geq 1$. The series $\sum_{k=1}^{\infty} x^k/(2k)$ diverges to $\infty$, thus $\mathbb{P}\{\mathcal{P}_{\text{lop}}\}$ can be upper-bounded by arbitrarily small $\epsilon$ by a large enough choice of $K$. Note when $x = 1$, the series becomes the harmonic series, which also diverges, albeit more slowly. Thus,

$$p(n) \sim xp^*(n), x \geq 1 \Rightarrow \lim_{n\to\infty} \mathbb{P}\{\mathcal{P}_{\text{lop}}\} = 0. \tag{A.31}$$

Alternatively, consider the upper bound when $x < 1$. The series $\sum_{k=1}^{\infty} x^k/(2k)$ converges to $-\log(\sqrt{1-x})$. Thus, for arbitrarily small $\epsilon$, a sufficiently large choice for $K$ will yield:

$$-\sum_{\substack{6\leq k\leq K,\\ k\neq 7}} \frac{x^k}{2k} \leq \log(\sqrt{1-x}) + \sum_{k\in\mathcal{K}} \frac{x^k}{2k} + \epsilon \tag{A.32}$$

where $\mathcal{K} = \{1, 2, 3, 4, 5, 7\}$. Substituting (A.32) into (A.30), we obtain the following upper bound for $\lim_{n\to\infty} \mathbb{P}\{\mathcal{P}_{\text{lop}}\}$:

$$\lim_{n\to\infty} \mathbb{P}\{\mathcal{P}_{\text{lop}}\} < \sqrt{1-x}\exp\left(\sum_{k\in\mathcal{K}} \frac{x^k}{2k}\right) + \epsilon', \tag{A.33}$$

where $\exp(\epsilon) \leq 1 + (e-1)\epsilon$ and the constants in front of $\epsilon$ can be rolled into $\epsilon' > 0$.

It remains to provide a lower bound when $x < 1$. We start by lower bounding $\mathbb{P}\{\mathcal{P}_{\text{lop}}\}$:

$$\mathbb{P}\{\mathcal{P}_{\text{lop}}\} = \mathbb{P}\left\{\bigcap_{\Gamma\in\mathcal{F}} \overline{A_\Gamma}\right\} \overset{(a)}{\geq} \prod_{\Gamma\in\mathcal{F}} \mathbb{P}\{\overline{A_\Gamma}\} \tag{A.34}$$

$$\overset{(b)}{\geq} \prod_{\Gamma\in\mathcal{F}} \exp\left(-\frac{\mathbb{E}[G(\Gamma)]}{1-p(n)}\right) \tag{A.35}$$

$$= \exp\left(-\frac{1}{1-p(n)} \sum_{\Gamma\in\mathcal{F}} \mathbb{E}[G(\Gamma)]\right) \tag{A.36}$$

where $(a)$ follows from the FKG Inequality applied to the set of monotone decreasing properties $\overline{A_\Gamma}$ on $\mathcal{G}_{n,p(n)}$ [18, Thm. 2.12], and $(b)$ is the result of applying [18, Cor. 2.13] to each multiplicand to obtain an exponential lower bound.

First, we note that:

$$\lim_{n\to\infty} \frac{1}{1-p(n)} = 1 \tag{A.37}$$

Second, by Lem. A.1 and Lem. A.2 (with $p(n) \sim x/n, x < 1$), the limit of the sum of the expected forbidden subgraph counts depends solely on cycles:

$$\lim_{n\to\infty} \sum_{\Gamma\in\mathcal{F}} \mathbb{E}[G(\Gamma)] = -\log(\sqrt{1-x}) - \sum_{k\in\mathcal{K}} \frac{x^k}{2k}, \tag{A.38}$$

with $\mathcal{K} = \{1, 2, 3, 4, 5, 7\}$.

Thus, by making use of (A.37) and (A.38) in (A.36), the limiting probability of satisfying $\mathcal{P}_{\text{lop}}$ is lower bounded by:

$$\lim_{n\to\infty} \mathbb{P}\{\mathcal{P}_{\text{lop}}\} \geq \sqrt{1-x}\exp\left(\sum_{k\in\mathcal{K}} \frac{x^k}{2k}\right) \tag{A.39}$$

Finally, combining (A.33) and (A.39) produces our desired limit when $x < 1$. □

## A.7 Cor. 2.1 (Threshold Function for $\mathcal{P}_{\text{lop}}$ in $G_{n,p(n)}$)

*Proof.* This, follows directly from the Thm. 2.2 and the monotonicity of property $\mathcal{P}_{\text{lop}}$. If $p(n) \in \omega(p^*(n))$, there exists $x > 1$ for which $p(n)$ is asymptotically greater than $x/n$. Alternately, if $p(n) \in o(p^*(n))$, then $p(n)$ is asymptotically less than $x/n$ for all $x > 0$. □

## A.8 Prop. 2.2 ($\sigma$-LoP Bounds in $G_{n,p(n)}$)

*Proof.* Let $G = G_{n,p(n)}$. Let $\Gamma$ and $A_\Gamma$ be as defined in App. A.6.

$$\lim_{n\to\infty} \mathbb{P}\{1/2 \leq \sigma(G) \leq 2/3\} \overset{(a)}{=} \lim_{n\to\infty} \mathbb{P}\{\sigma(G) \leq 2/3\} \overset{(b)}{\geq} 1 - \lim_{n\to\infty} \mathbb{P}\left\{ \bigcap_{k=1}^{\infty} \overline{A_{C_{6k}}} \right\} \overset{(c)}{=} 1, \tag{A.40}$$

where $(a)$ the lower bound is always true by Lem. 2.5, $(b)$ the presence of any $C_{6k}$ is sufficient for $\sigma(G) \leq 2/3$ by Lem. 2.6, and $(c)$ $p(n)$ is above the joint threshold for the appearance of all $C_{6k}$ by appropriate 'thinning' of the argument of Thm. 2.2 in App. A.6 to $C_{6k}$ and divergence of the series for $c > 1$. □

## A.9 Thm. 2.3 ($\mathbb{E}[\sigma]$ Bounds in $G_{n,p(n)}$)

*Proof.* For convenience, let $G = G_{n,p(n)}$. We first consider the lower bound:

$$\mathbb{E}[\sigma(G)] = \mathbb{E}[\sigma(G)|G \in \mathcal{P}_{\text{lop}}]\,\mathbb{P}\{G \in \mathcal{P}_{\text{lop}}\} + \mathbb{E}[\sigma(G)|G \notin \mathcal{P}_{\text{lop}}]\,\mathbb{P}\{G \notin \mathcal{P}_{\text{lop}}\} \tag{A.41}$$

$$\overset{(a)}{=} \mathbb{P}\{G \in \mathcal{P}_{\text{lop}}\} + \mathbb{E}[\sigma(G)|G \notin \mathcal{P}_{\text{lop}}]\,(1 - \mathbb{P}\{G \in \mathcal{P}_{\text{lop}}\}) \tag{A.42}$$

$$\overset{(b)}{\geq} \mathbb{P}\{G \in \mathcal{P}_{\text{lop}}\} + \frac{1}{2}(1 - \mathbb{P}\{G \in \mathcal{P}_{\text{lop}}\}) \tag{A.43}$$

$$= \frac{1}{2}\left(1 + \mathbb{P}\{G \in \mathcal{P}_{\text{lop}}\}\right), \tag{A.44}$$

where $(a)$ $\sigma(G) = 1$ when $G \in \mathcal{P}_{\text{lop}}$, and $(b)$ $\sigma(G) \geq 1/2$ when $G \notin \mathcal{P}_{\text{lop}}$. Finally, take the limit as $n \to \infty$ and apply $\mathbb{P}\{G \in \mathcal{P}_{\text{lop}}\} \to F_l(x)$ from Thm. 2.2.

We now apply a similar argument to the upper bound, but partition on the presence of the class of cycles $\{C_{6k}, k \in \mathbb{N}_+\}$, all of which result in $\sigma \leq 2/3$. Let $\Gamma$ and $A_\Gamma$ be as defined in App. A.6,

and let $\overline{\mathcal{A}} \equiv \{\cap_{k=1}^{\infty} \overline{A_{C_{6k}}}\}$ be the event that there exist no cycles $C_{6k}$ within $G$:

$$\mathbb{E}[\sigma(G)] = \mathbb{E}[\sigma(G)|\mathcal{A}]\,\mathbb{P}\{\mathcal{A}\} + \mathbb{E}\big[\sigma(G)|\overline{\mathcal{A}}\big]\,\mathbb{P}\big\{\overline{\mathcal{A}}\big\} \tag{A.45}$$

$$\overset{(a)}{\leq} \frac{2}{3}(1 - \mathbb{P}\big\{\overline{\mathcal{A}}\big\}) + \mathbb{P}\big\{\overline{\mathcal{A}}\big\} = \frac{1}{3}\left(2 + \mathbb{P}\big\{\overline{\mathcal{A}}\big\}\right), \tag{A.46}$$

where $(a)$ $\sigma(G) \leq 2/3$ when $\mathcal{A}$, and $\sigma(G) \leq 1$ is always true. Evaluating the limit of $\mathbb{P}\big\{\overline{\mathcal{A}}\big\}$ can be done using the same approach as the argument of Thm. 2.2 in App. A.6:

$$\lim_{n\to\infty} \mathbb{P}\left\{\bigcap_{k=1}^{K} C_{6k} \nsubseteq G\right\} = \prod_{k=1}^{K} \exp\left(-\frac{x^{6k}}{12k}\right) = \exp\left(-\sum_{k=1}^{K} \frac{x^{6k}}{12k}\right) \tag{A.47}$$

$$= \exp\left(\frac{1}{12}\log(1-x^6)\right) + \epsilon_K = (1-x^6)^{1/12} + \epsilon_K, \tag{A.48}$$

when $x \leq 1$ where $\epsilon_K$ can be driven lower by a larger choice of $K$. Otherwise, when $x > 1$, the series in the exponent diverges (*i.e.*, $G$ is sure to contain a cycle in $\{C_{6k}\}$). □

## A.10 Cor. 2.2 (Reg. Threshold for $\mathcal{P}_{\text{giant}}(\beta)$ in $G_{n,p(n)}$)

*Proof.* Given $\beta^* \in (0,1)$, construct $p^*(n) = c(\beta^*)/n$ using (2.13). We show that:

$$p(n) \sim x p^*(n) \Rightarrow \lim_{n\to\infty} \mathbb{P}\big\{G_{n,p(n)} \in \mathcal{P}_{\text{giant}}(\beta^*)\big\} = F(x), \tag{A.49}$$

where $F(x) = \mathbf{1}\{x > 1\}$ for all continuity points of $F(x)$: $\mathbb{R} \setminus \{1\}$.

Suppose $p(n) \sim x p^*(n)$, with $x > 1$. $p(n)$ is asymptotically larger than $p^*(n)$ and by monotonicity of (2.13), there exists $\beta \in (\beta^*, 1)$ such that:

$$\exists n_0 > 0, \forall n > n_0 : p(n) > \frac{c(\beta)}{n} > \frac{c(\beta^*)}{n}. \tag{A.50}$$

Apply part *ii)* of [18, Thm. 5.4] to establish that the size of the largest component, denoted as

$L_{n,p(n)}$, converges in probability to $\beta n$:

$$\forall \epsilon > 0, \lim_{n\to\infty} \mathbb{P}\left\{ \left| \frac{L_{n,p(n)}}{\beta n} - 1 \right| < \epsilon \right\} = 1. \tag{A.51}$$

By choosing $\epsilon$ such that $\beta^* = (1-\epsilon)\beta$, the event $\left|L_{n,p(n)}/(\beta n) - 1\right| < \epsilon$ is a subset of the event that $L_{n,p(n)} \geq \beta^* n$, giving us the upper bound:

$$\mathbb{P}\left\{ \left| \frac{L_{n,p(n)}}{\beta n} - 1 \right| < \epsilon \right\} \leq \mathbb{P}\left\{ \frac{L_{n,p(n)}}{n} \geq \beta^* \right\}. \tag{A.52}$$

Since $\lim_{n\to\infty} \mathbb{P}\left\{\left|L_{n,p(n)}/(\beta n) - 1\right| < \epsilon\right\} = 1$ and probabilities are bounded above by 1, we apply the squeeze theorem and conclude that $\lim_{n\to\infty} \mathbb{P}\left\{L_{n,p(n)}/n > \beta^*\right\} = 1$.

Alternately, suppose $p(n) \sim xp^*(n)$, with $x < 1$. $p(n)$ is asymptotically smaller than $p^*(n)$ and by monotonicity of (2.13), there exists $\beta \in (0, \beta^*)$ such that:

$$\exists n_0 > 0, \forall n > n_0 : p(n) < \frac{c(\beta)}{n} < \frac{c(\beta^*)}{n}. \tag{A.53}$$

Again, we use [18, Thm. 5.4] to show that $L_{n,p(n)}$ converges in probability to $\beta n$:

$$\forall \epsilon > 0, \lim_{n\to\infty} \mathbb{P}\left\{ \left| \frac{L_{n,p(n)}}{\beta n} - 1 \right| < \epsilon \right\} = 1. \tag{A.54}$$

By choosing $\epsilon$ such that $(1+\epsilon)\beta = \beta^*$, the event $\left|L_{n,p(n)}/(\beta n) - 1\right| < \epsilon$ is a subset of the event that $L_{n,p(n)} < \beta^* n$, giving us the upper bound:

$$\mathbb{P}\left\{ \left| \frac{L_{n,p(n)}}{\beta n} - 1 \right| < \epsilon \right\} \leq 1 - \mathbb{P}\left\{ \frac{L_{n,p(n)}}{n} \geq \beta^* \right\} \tag{A.55}$$

Since $\lim_{n\to\infty} \mathbb{P}\left\{\left|L_{n,p(n)}/(\beta n) - \right| < \epsilon\right\} = 1$ and probabilities are bounded below by 0, we apply the squeeze theorem and conclude that $\lim_{n\to\infty} \mathbb{P}\left\{L_{n,p(n)}/n \geq \beta^*\right\} = 0$. □

## A.11 Thm. 2.4 (Mutual Excl. of $\mathcal{P}_{\text{lop}}$ and $\mathcal{P}_{\text{giant}}(\beta)$ in $G_{n,p(n)}$)

*Proof.* By Thm. 2.2, $p(n) \sim c/n, c > 1$ implies that $\mathcal{P}_{\text{lop}}$ holds *a.a.n.*. Therefore, $p(n) \sim c/n, c \leq 1$ is a necessary condition for $\mathcal{P}_{\text{lop}}$ to hold *a.a.s.*. Under this necessary condition, we see that $p(n)$ is asymptotically less than $c(\beta)/n$ since $c(\beta) > 1$ and by Cor. 2.2, $\mathcal{P}_{\text{giant}}(\beta)$ holds *a.a.n.*.

Thus, for $p(n) \sim c/n, \forall c \leq 1$:

$$0 \leq \lim_{n\to\infty} \mathbb{P}\{\mathcal{P}_{\text{giant}}(\beta) \cap \mathcal{P}_{\text{lop}}\} \leq \lim_{n\to\infty} \mathbb{P}\{\mathcal{P}_{\text{giant}}(\beta)\} = 0 \tag{A.56}$$

Alternately, for $p(n) \sim c/n, \forall c > 1$:

$$0 \leq \lim_{n\to\infty} \mathbb{P}\{\mathcal{P}_{\text{giant}}(\beta) \cap \mathcal{P}_{\text{lop}}\} \leq \lim_{n\to\infty} \mathbb{P}\{\mathcal{P}_{\text{lop}}\} = 0 \tag{A.57}$$

In both cases, we can conclude that $\lim_{n\to\infty} \mathbb{P}\{\mathcal{P}_{\text{giant}}(\beta) \cap \mathcal{P}_{\text{lop}}\} = 0$. □

## A.12 Prop. 2.3 (Reg. Sharp Threshold for $\mathcal{P}_{\text{edge}}$ in $G_{n,r(n)}$)

*Proof.* Let the *r.v.* $M_{n,r(n)}$ (shortened to $M$) be the number of edges in graph $G_{n,r(n)}$. We show that for the given choice of $(r^*(n)^2 = 2c/(\pi n), \alpha(n) = 2\sqrt{cn}/(\pi n^2)$ and $F(x) = \Phi(-x)$ that:

$$r(n)^2 \sim r^*(n)^2 + x\alpha(n) \Rightarrow \lim_{n\to\infty} \mathbb{P}\{M \leq cn\} = F(x), \tag{A.58}$$

where $F(x) = \Phi(-x)$ for all continuous points of $F(x)$: $\mathbb{R}$.

For $r(n)^2 \sim r^*(n)^2 + x\alpha(n)$:

$$\mathbb{P}\{M \leq cn\} \overset{(a)}{=} \mathbb{P}\left\{ \frac{M - \mathbb{E}[M]}{\sqrt{n}} \leq \frac{cn - \mathbb{E}[M]}{\sqrt{n}} \right\} \tag{A.59}$$

$$\overset{(b)}{=} \mathbb{P}\left\{ \frac{M - \mathbb{E}[M]}{\sqrt{n}} \leq -x\sqrt{c} + o(1) \right\} \tag{A.60}$$

$$\overset{(c)}{=} \Phi\left( \frac{-x\sqrt{c} + o(1)}{\sqrt{c}} \right) + o(1) \tag{A.61}$$

$$\overset{(d)}{=} \Phi\left(-x + o(1)\right) + o(1) \tag{A.62}$$

$$\overset{(e)}{=} \Phi\left(-x\right) + o(1)\,, \tag{A.63}$$

where we $(a)$ standardize $M_{n,r(n)}$, $(b)$ apply Lem. A.3, $(c)$ apply Lem. A.4 and standardize the argument to the *c.d.f.*, $(d)$ results from asymptotic simplification, and $(e)$ apply continuity of the standard normal *c.d.f.*, $\Phi(x)$.

Thus, for the specific case when $c = 2$, we conclude:

$$\lim_{n\to\infty} \mathbb{P}\big\{G_{n,r(n)} \in \mathcal{P}_{\text{edge}}\big\} = \lim_{n\to\infty} \mathbb{P}\{M \leq 2n\} = \Phi\left(-x\right). \tag{A.64}$$

□

## A.13 Prop. 2.4 (Upper Bound for $\mathcal{P}_{\text{lop}}$ in $G_{n,r(n)}$)

*Proof.* Let $\Gamma_k$ be a feasible, connected, order $k$ graph. Let $G_e(\Gamma_k)$ and $G_v(\Gamma_k)$ be the edge-induced and vertex-induced subgraph counts of $\Gamma_k$ on graph $G_{n,r(n)}$, resp. Let $A_{\Gamma_k} = \{G_e(\Gamma_k) \geq 1\}$ and $B_{\Gamma_k} = \{G_v(\Gamma_k) \geq 1\}$ be the events that there are one or more edge-induced or vertex-induced copies of $\Gamma_k$ in $G_{n,r(n)}$, resp.

A necessary condition for $\mathcal{P}_{\text{lop}}$ is the absence of edge-induced cycles of length 6, which can be expressed as an intersection of a finite number of vertex-induced events, $\{\overline{B_{\Gamma_6}}\}$:

$$\mathbb{P}\{\mathcal{P}_{\text{lop}}\} \leq \mathbb{P}\big\{\overline{A_{C_6}}\big\} = \mathbb{P}\big\{\cap_{\Gamma_6 \in \mathcal{Y}} \overline{B_{\Gamma_6}}\big\}\,, \tag{A.65}$$

where $\mathcal{Y} \equiv \{\Gamma_6 : \Gamma_6 \subseteq K_6, C_6 \subseteq \Gamma_6, \Gamma_6 \text{ feasible}\}$.

By [26, Thm. 3.5], the finite collection of vertex-induced subgraph counts $\{G_v(\Gamma_6)\}$ converge to independent Poisson *r.v.*'s with rates $\{\lambda = c^5\mu_{\Gamma_6}\}$, for our choice of $r(n)^2$. The null probability of the subgraph counts becomes:

$$\lim_{n\to\infty} \mathbb{P}\left\{\bigcap_{\Gamma_6\in\mathcal{Y}} \overline{B_{\Gamma_6}}\right\} = \prod_{\Gamma_6\in\mathcal{Y}} \mathrm{e}^{-c^5\mu_{\Gamma_6}} = \exp\left(-c^5 \sum_{\Gamma_6\in\mathcal{Y}} \mu_{\Gamma_6}\right), \tag{A.66}$$

where $\mu_{\Gamma_6}$ is computed from [26, Eq. 3.2] for each vertex-induced subgraph. We may upper bound the exponential by considering a single term in the summation where $\Gamma_6 = K_6$ (the complete graph on 6 vertices) has $k = 6$ vertices and then expressing a lower bound for $\mu_{K_6,\mathbb{R}^2}$:

$$\mu_{K_6,\mathbb{R}^2} \overset{(a)}{=} \frac{1}{6!} \int_{\mathbb{R}^2} f(x)^2 \mathrm{d}x \int_{\mathbb{R}^2} h_{K_6}(\{0, x_1, ..., x_5\}) \mathrm{d}x_1, ..., \mathrm{d}x_5 \tag{A.67}$$

$$\overset{(b)}{=} \frac{1}{6!} \int_{\mathbb{R}^2} h_{K_6}(\{0, x_1, ..., x_5\}) \mathrm{d}x_1, ..., \mathrm{d}x_5 \overset{(c)}{\geq} \frac{(\pi/4)^5}{6!}, \tag{A.68}$$

where $(a)$ is simplified from [26, Eq. 3.2] for the subgraph type $K_6$, $(b)$ follows from $f(x)$ being the uniform distribution over the unit square $[-1/2, 1/2]^2$ used to generate *i.i.d.* vertex positions, and $(c)$ follows from $h_{K_6}(0, x_1, \ldots, x_5)$ being the indicator function on whether or not six vertices (one fixed at the origin) with unit edge distance form $K_6$. The lower bound results when limiting the placement of all five vertices to a disk of radius $1/2$ centered at the origin. Under this assumption, all six vertices are connected, form $K_6$, and yield $h_{K_6}(0, x_1, \ldots, x_5) = 1$. □

## A.14 Lem. 2.8 (Reg. Sharp Threshold for $\mathcal{P}_{\mathbf{conn}}$ in $G_{n,r(n)}$)

*Proof.* Let *r.v.* $T = T(G_{n,r(n)})$ be the minimum edge distance that yields a connected graph for $G_{n,r(n)}$. Thus, the graph $G_{n,r(n)}$ is connected iff $T \leq r(n)$. Using a specialization of [26, Cor. 13.21], we show that:

$$r(n)^2 \sim r^*(n)^2 + x\alpha(n) \Rightarrow \lim_{n\to\infty} \mathbb{P}\{T \leq r(n)\} = F(x), \tag{A.69}$$

where $F(x) = \mathrm{e}^{-\mathrm{e}^{-x}}$ for all continuous points of $F(x)$: $\mathbb{R}$.

For $r(n)^2 \in r^*(n)^2 + x\alpha(n) + o(\alpha(n))$:

$$\mathbb{P}\{T \leq r(n)\} \overset{(a)}{=} \lim_{n\to\infty} \mathbb{P}\big\{n\pi T^2 - \log(n) \leq x + o(1)\big\} \tag{A.70}$$

$$\overset{(b)}{=} \mathrm{e}^{-\mathrm{e}^{-x+\alpha(1)}} + o(1) \overset{(c)}{=} \mathrm{e}^{-\mathrm{e}^{-x}} + o(1) \tag{A.71}$$

where $(a)$ follows from squaring both sides of the inequality and expanding $r(n)^2$ in terms of the given $r^*(n)^2$ and $\alpha(n)$, $(b)$ results from a specialization of [26, Cor. 13.21] ($k = 0$, dimension $d = 2$, and $p$ = 2-norm distance function) which shows that the scaled minimum connectivity distance $n\pi T^2 - \log(n)$ converges in distribution to a Gumbel distribution, and $(c)$ follows from the continuity of the Gumbel *c.d.f.*.

Thus, for the given choice of $r(n)^2$:

$$\lim_{n\to\infty} \mathbb{P}\big\{G_{n,r(n)} \in \mathcal{P}_{\text{conn}}\big\} = \lim_{n\to\infty} \mathbb{P}\{T \leq r(n)\} = \mathrm{e}^{-\mathrm{e}^{-x}}.$$

□

## A.15 Lem. 2.9 (Reg. Threshold for $\mathcal{P}_{\text{giant}}$ in $G_{n,r(n)}$)

*Proof.* Given $\lambda_c \in (0, \infty)$, construct $r^*(n)^2 = \lambda_c/n$. We show that:

$$r(n)^2 \sim x r^*(n)^2 \Rightarrow \lim_{n\to\infty} \mathbb{P}\big\{G_{n,r(n)} \in \mathcal{P}_{\text{giant}}\big\} = F(x),$$

for all points of continuity of $F(x) \equiv \mathbf{1}\{x > 1\}$: $\mathbb{R} \setminus \{1\}$.

Suppose $r(n)^2 \sim x r^*(n)^2$ with $x \geq 0$. We have $r(n)^2 \sim \rho/n$ with $\rho = x\lambda_c$. With $h \in (0, 1/x)$, there exists a single, bounded population cluster at level $h$ equal to the unit square $R_1 = [-1/2, 1/2]^2 \subset \mathbb{R}^2$. Let $L_1$ be the normalized size of the largest component of $G_{n,r(n)}$. By [26, Thm. 11.9], we have that $L_1$ converges in probability to $I(R_1; \rho)$, since complete convergence implies convergence in probability:

$$\lim_{n\to\infty} \mathbb{P}\{|L_1/n - I(R_1;\rho)| > \epsilon\} = 0, \forall \epsilon > 0, \tag{A.72}$$

where $I(R_1;\rho) = p_\infty(x\lambda_c)$ is the percolation probability under communication radius function $r^*(n)^2 \sim x\lambda_c/n$.

Now, suppose that $x < 1$. By definition, the percolation probability is zero, and:

$$\lim_{n\to\infty} \mathbb{P}\{|L_1/n - I(R_1;\rho)| > \epsilon\} = 0, \forall \epsilon > 0 \tag{A.73}$$

$$\lim_{n\to\infty} \mathbb{P}\{|L_1/n| > \epsilon\} = 0, \forall \epsilon > 0 \tag{A.74}$$

$$\lim_{n\to\infty} \mathbb{P}\left\{G_{n,r(n)} \in \mathcal{P}_{\text{giant}}(\epsilon)\right\} = 0, \forall \epsilon > 0 \tag{A.75}$$

$$\lim_{n\to\infty} \mathbb{P}\left\{G_{n,r(n)} \in \mathcal{P}_{\text{giant}}\right\} = 0. \tag{A.76}$$

Alternately, suppose that $x > 1$. By definition, the percolation probability is positive, and:

$$1 = \lim_{n\to\infty} \mathbb{P}\{|L_1/n - I(R_1;\rho)| > \epsilon\}, \forall \epsilon > 0 \tag{A.77}$$

$$\leq \lim_{n\to\infty} \mathbb{P}\{L_1/n \geq I(R_1;\rho) - \epsilon\}, \forall \epsilon > 0 \tag{A.78}$$

$$= \lim_{n\to\infty} \mathbb{P}\{L_1/n \geq p_\infty(x\lambda_c) - \epsilon\}, \forall \epsilon \in (0, p_\infty(x\lambda_c)) \tag{A.79}$$

$$= \lim_{n\to\infty} \mathbb{P}\left\{G_{n,r(n)} \in \mathcal{P}_{\text{giant}}(\beta)\right\}, \forall \beta \in (0, p_\infty(x\lambda_c) - \epsilon) \tag{A.80}$$

$$= \lim_{n\to\infty} \mathbb{P}\left\{G_{n,r(n)} \in \mathcal{P}_{\text{giant}}\right\}. \tag{A.81}$$

By the squeeze theorem, we conclude that $\lim_{n\to\infty} \mathbb{P}\left\{G_{n,r(n)} \in \mathcal{P}_{\text{giant}}\right\} = 1$. □

## A.16 Thm. 2.6 (Mutual Excl. of $\mathcal{P}_{\text{lop}}$ and $\mathcal{P}_{\text{giant}}$ in $G_{n,r(n)}$)

*Proof.* By Lem. 2.9, $r(n)^2 \sim c/n, c < \lambda_c$ implies that $\mathcal{P}_{\text{giant}}$ holds *a.a.n.*. Therefore, $r(n)^2 \sim c/n, c \geq \lambda_c$ is a necessary condition for $\mathcal{P}_{\text{giant}}$ to hold *a.a.s.*. Under this necessary condition, we see that $r(n)^2 \in \omega(1/n^{6/5})$ and by Cor. 2.4, $\mathcal{P}_{\text{lop}}$ holds *a.a.n.*.

Thus, for $r(n)^2 \sim c/n, \forall c \leq \lambda_c$:

$$0 \leq \lim_{n\to\infty} \mathbb{P}\{\mathcal{P}_{\text{giant}} \cap \mathcal{P}_{\text{lop}}\} \leq \lim_{n\to\infty} \mathbb{P}\{\mathcal{P}_{\text{giant}}\} = 0 \tag{A.82}$$

Alternately, for $r(n)^2 \sim c/n, \forall c > \lambda_c$:

$$0 \leq \lim_{n\to\infty} \mathbb{P}\{\mathcal{P}_{\text{giant}} \cap \mathcal{P}_{\text{lop}}\} \leq \lim_{n\to\infty} \mathbb{P}\{\mathcal{P}_{\text{lop}}\} = 0 \tag{A.83}$$

In both cases, we can conclude that $\lim_{n\to\infty} \mathbb{P}\{\mathcal{P}_{\text{giant}} \cap \mathcal{P}_{\text{lop}}\} = 0$. □

## A.17 Prop. 2.5 ($\sigma$-LoP Bounds in $G_{n,r(n)}$)

*Proof.* Let $G = G_{n,r(n)}$.

$$\lim_{n\to\infty} \mathbb{P}\{1/2 \leq \sigma(G) \leq 2/3\} \overset{(a)}{=} \lim_{n\to\infty} \mathbb{P}\{\sigma(G) \leq 2/3\} \tag{A.84}$$

$$\overset{(b)}{\geq} \lim_{n\to\infty} \mathbb{P}\{C_6 \subseteq G\} \overset{(c)}{=} 1. \tag{A.85}$$

where $(a)$ the lower bound is always true by Lem. 2.5, $(b)$ the presence of $C_6$ is sufficient for $\sigma(G) \leq 2/3$ by Lem. 2.6, and $(c)$ $r(n)^2$ is above the threshold for the appearance of $C_6$, obtained from the argument of Prop. 2.4 in App. A.13. □

## A.18 Thm. 2.5 ($\mathbb{E}[\sigma]$ Bounds in $G_{n,r(n)}$)

*Proof.* Let $G = G_{n,r(n)}$. The lower bound follows immediately from the support bound $\sigma(G) \geq 1/2$ in Lem. 2.5. The upper bound can be derived:

$$\mathbb{E}[\sigma(G)] = \mathbb{E}[\sigma(G)|K_6 \subseteq G]\,\mathbb{P}\{K_6 \subseteq G\} + \mathbb{E}[\sigma(G)|K_6 \nsubseteq G]\,\mathbb{P}\{K_6 \nsubseteq G\} \tag{A.86}$$

$$\overset{(a)}{\leq} \frac{2}{3}(1 - \mathbb{P}\{K_6 \nsubseteq G\}) + \mathbb{P}\{K_6 \nsubseteq G\} \tag{A.87}$$

$$= \frac{1}{3}\left(2 + \mathbb{P}\{K_6 \nsubseteq G\}\right), \tag{A.88}$$

where $(a)$ $\sigma(G) \leq 2/3$ when $K_6 \subseteq G$ (*i.e.*, $C_6 \subset K_6$ and the presence of $C_6$ is sufficient for $\sigma(G) \leq 2/3$) and $\sigma(G) \leq 1$ is always true. Finally, we may upper bound $\lim_{n\to\infty} \mathbb{P}\{K_6 \nsubseteq G\}$ with $\exp\left(-(\pi c/4)^5/6!\right)$ by applying portions of the argument of Prop. 2.4 in App. A.13. □

# Appendix B: Proofs of Ch. 3

## B.1 Prop. 3.1 (Success of a Typical Transmission)

*Proof.* A transmission is successful when the SINR is greater than or equal to $\beta$:

$$p_s = \mathbb{P}\{\text{SINR}_o \geq \beta\} \overset{(a)}{=} \mathbb{P}\left\{H_{o,o} \geq \frac{\beta d^\alpha}{P_t G_{\text{T}}(\epsilon_{x_o}) G_{\text{R}}(\epsilon_{y_o})} I_o\right\} \mathbb{P}\left\{H_{o,o} \geq \frac{\beta d^\alpha \eta}{P_t G_{\text{T}}(\epsilon_{x_o}) G_{\text{R}}(\epsilon_{y_o})}\right\} \tag{B.1}$$

$$\overset{(b)}{=} \int_{0^+}^{\infty} \int_{0^+}^{\infty} \mathbb{E}\left[\mathrm{e}^{-sI_o}\right] \mathrm{e}^{-\frac{\beta d^\alpha \eta}{P_t g_{\text{T}} g_{\text{R}}}} f_{G_{\text{T}}}(g_{\text{T}})\, f_{G_{\text{R}}}(g_{\text{R}})\, \mathrm{d}g_{\text{T}} \mathrm{d}g_{\text{R}}, \tag{B.2}$$

where we $(a)$ expand $\text{SINR}_i \geq \beta$, isolate $H_{o,o}$, and apply the memoryless property of $H_{o,o}$, and $(b)$ marginalize the gains between the typical TX and RX; the first term is the Laplace transform of the interference evaluated at $s = \frac{\beta d^\alpha}{P_t g_{\text{T}} g_{\text{R}}}$; the second term is the *c.c.d.f.* of $H_{o,o}$.

Following along with Section 5.1.7 [52], we work with $\mathbb{E}\left[\mathrm{e}^{-sI_o}\right]$, an expectation over $\Phi$, the fading variables $H_{i,o}$, and the gains between interferers and the typical RX $\{G_{\text{T}_\text{I}}(\hat{\theta}_{x_i,y_o})\}$ and $\{G_{\text{R}_\text{I}}(\hat{\theta}_{y_o,x_i})\}$:

$$\mathcal{L}_I(s) = \mathbb{E}_{\hat{\Phi}}\left[\prod_{x_i \in \Phi} \mathrm{e}^{-sP_t G_{\text{T}_\text{I}}(\hat{\theta}_{x_i,y_o}) G_{\text{R}_\text{I}}(\hat{\theta}_{y_o,x_i}) H_{i,o} d_{i,o}^{-\alpha}}\right] \tag{B.3}$$

$$\overset{(a)}{=} \mathbb{E}_{\Phi}\left[\prod_{x_i \in \Phi} \mathbb{E}_{G_{\text{T}_\text{I}}, G_{\text{R}_\text{I}}, H}\left[\mathrm{e}^{-sP_t G_{\text{T}_\text{I}} G_{\text{R}_\text{I}} H d_{i,o}^{-\alpha}}\right]\right] \tag{B.4}$$

$$\overset{(b)}{=} \mathbb{E}_{\Phi}\left[\prod_{x_i \in \Phi} v(\|x_i\|)\right] \tag{B.5}$$

$$\overset{(c)}{=} \mathrm{e}^{-\int_0^\infty (1 - v(x))\lambda(x)\mathrm{d}x} \tag{B.6}$$

$$= \mathrm{e}^{-\int_0^\infty \mathbb{E}_{G_{\text{T}_\text{I}}, G_{\text{R}_\text{I}}, H}\left[1 - \mathrm{e}^{-sP_t G_{\text{T}_\text{I}} G_{\text{R}_\text{I}} H x^{-\alpha}}\right]\lambda(x)\mathrm{d}x}, \tag{B.7}$$

where we $(a)$ leverage the independence of $x$, $H$, $G_{\text{T}_\text{I}}$, and $G_{\text{R}_\text{I}}$ by bringing the latter three into the product and dropping the fading and gain indexing, $(b)$ collapse $\hat{\Phi}$ into a one-dimensional PPP on $\mathbb{R}^+$ with intensity $\lambda(x) = \lambda 2\pi x, \forall x \in \mathbb{R}^+$ and define $v(x) = \mathbb{E}_{G_{\text{T}_\text{I}}, G_{\text{R}_\text{I}}, H}\left[\mathrm{e}^{-sP_t G_{\text{T}_\text{I}} G_{\text{R}_\text{I}} H x^{-\alpha}}\right]$, and $(c)$ recognize that a mean of a product of $v(x)$ over the collapsed $\hat{\Phi}$ is a probability generating functional (pgfl) of the process; an explicit solution is given by Campbell's Theorem for PPPs.

Again mirroring the developments in [52], we work with the integral inside the exponential, $x$, $G_{\mathrm{T_I}}$, $G_{\mathrm{R_I}}$, and $H$ are independent, so their expectations can be evaluated separately:

$$\int_0^\infty \mathbb{E}_{G_{\mathrm{T_I}},G_{\mathrm{R_I}},H}\left[1-\mathrm{e}^{-sP_tG_{\mathrm{T_I}}G_{\mathrm{R_I}}Hx^{-\alpha}}\right]\lambda(x)\mathrm{d}x \tag{B.8}$$

$$\overset{(a)}{=}\mathbb{E}_{G_{\mathrm{T_I}},G_{\mathrm{R_I}},H}\left[\int_0^\infty(1-\mathrm{e}^{-sP_tG_{\mathrm{T_I}}G_{\mathrm{R_I}}Hx^{-\alpha}})\lambda(x)\mathrm{d}x\right] \tag{B.9}$$

$$=\mathbb{E}_{G_{\mathrm{T_I}},G_{\mathrm{R_I}},H}\left[\lambda\pi\int_0^\infty(1-\mathrm{e}^{-sP_tG_{\mathrm{T_I}}G_{\mathrm{R_I}}Hx^{-\alpha}})2x\mathrm{d}x\right] \tag{B.10}$$

$$\overset{(b)}{=}\mathbb{E}_{G_{\mathrm{T_I}},G_{\mathrm{R_I}}}\left[\lambda\pi\Gamma(1+2/\alpha)\Gamma(1-2/\alpha)(sP_tG_{\mathrm{T_I}}G_{\mathrm{R_I}})^{2/\alpha}\right] \tag{B.11}$$

$$\overset{(c)}{=}\lambda\pi\Gamma(1+2/\alpha)\Gamma(1-2/\alpha)(sP_t)^{2/\alpha}\mathbb{E}\left[G_{\mathrm{T_I}}^{2/\alpha}\right]\mathbb{E}\left[G_{\mathrm{R_I}}^{2/\alpha}\right]. \tag{B.12}$$

In $(a)$, we exchange the order of integration over $G_{\mathrm{T_I}}$, $G_{\mathrm{R_I}}$, and $H$ with that of $x$. Next, $(b)$ follows from Section 5.1.7 of [52] in the case of Rayleigh fading with omni-directional antennas. The substitution of the integration variables, integration by parts, evaluation of the resulting integral, and finally taking the expectation over $H$ produces:

$$\mathbb{E}_H\left[\lambda c_d\int_0^\infty(1-\mathrm{e}^{-\hat{s}Hx^{-\alpha}})dx^{d-1}\mathrm{d}x\right]=\lambda c_d\Gamma(1+\delta)\Gamma(1-\delta)\hat{s}^\delta, \tag{B.13}$$

where $d$ is the dimension of the space in which the points of $\Phi$ reside, $\delta=d/\alpha$ and $c_d$ is a constant depending on $d$. In our case, $d=2$ and it follows that $\delta=2/\alpha$ and $c_2=\pi$. By substituting $\hat{s}=sP_tG_{\mathrm{T_I}}G_{\mathrm{R_I}}$ and taking the expectation of both sides of (B.13) *w.r.t.* $G_{\mathrm{T_I}}$ and $G_{\mathrm{R_I}}$, we complete this step. Finally, in $(c)$, we find that the expectations over $G_{\mathrm{T_I}}$ and $G_{\mathrm{R_I}}$ reduce to taking moments of each *r.v.*, (as noted in [45]).

Now, the Laplace transform can be expressed:

$$\mathcal{L}_I(s)=\mathbb{E}\left[\mathrm{e}^{-sI_o}\right]=\mathrm{e}^{-\lambda\pi\Gamma(1+2/\alpha)\Gamma(1-2/\alpha)(sP_t)^{2/\alpha}\mathbb{E}\left[G_{\mathrm{T_I}}^{2/\alpha}\right]\mathbb{E}\left[G_{\mathrm{R_I}}^{2/\alpha}\right]}. \tag{B.14}$$

With $s = \frac{\beta d^\alpha}{P_t g_{\mathrm{T}} g_{\mathrm{R}}}$, we express success probability of a transmission between the typical pair $o$:

$$p_s = \int_{0^+}^{\infty} \int_{0^+}^{\infty} \mathbb{E}\left[\mathrm{e}^{-sI_o}\right] \mathrm{e}^{-\frac{\beta d^\alpha \eta}{P_t g_{\mathrm{T}} g_{\mathrm{R}}}} f_{G_{\mathrm{T}}}(g_{\mathrm{T}})\, f_{G_{\mathrm{R}}}(g_{\mathrm{R}})\, \mathrm{d}g_{\mathrm{T}} \mathrm{d}g_{\mathrm{R}} \tag{B.15}$$

$$= \int_{0^+}^{\infty} \int_{0^+}^{\infty} \mathrm{e}^{-\lambda \pi \Gamma(1+2/\alpha)\Gamma(1-2/\alpha)(sP_t)^{2/\alpha} \mathbb{E}\left[G_{\mathrm{T_I}}^{2/\alpha}\right] \mathbb{E}\left[G_{\mathrm{R_I}}^{2/\alpha}\right]} \mathrm{e}^{-\frac{\beta d^\alpha \eta}{P_t g_{\mathrm{T}} g_{\mathrm{R}}}} f_{G_{\mathrm{T}}}(g_{\mathrm{T}})\, f_{G_{\mathrm{R}}}(g_{\mathrm{R}})\, \mathrm{d}g_{\mathrm{T}} \mathrm{d}g_{\mathrm{R}}. \tag{B.16}$$

□

## B.2 Prop. 3.2 (TP using Sectors without Sidelobes)

*Proof.* The first and second derivatives of $\lambda p_s(\lambda)$ are:

$$\frac{\mathrm{d}}{\mathrm{d}\lambda} \lambda p_s(\lambda) = (1 - A\lambda) C \mathrm{e}^{-\lambda A - B} \tag{B.17}$$

$$\frac{\mathrm{d}^2}{\mathrm{d}\lambda^2} \lambda p_s(\lambda) = (A\lambda - 2) AC \mathrm{e}^{-\lambda A - B}, \tag{B.18}$$

where $A = \pi \kappa d^2 \beta^{2/\alpha} p^2$, $B = \frac{\beta d^\alpha \eta}{P_t g_1^2}$, and $C = u^2$. A single root of the first derivative exists at $\lambda^* = 1/A$, while the second derivative, when evaluated at $\lambda^*$, is negative:

$$\frac{\mathrm{d}^2}{\mathrm{d}\lambda^2} \lambda p_s(\lambda) \bigg|_{\lambda = \lambda^*} = -AC \mathrm{e}^{-1-B} \leq 0, \tag{B.19}$$

due to $A > 0$, $\mathrm{e}^{-1-B} > 0$, and $C = u^2 = F_{|\epsilon|}^2\left(\frac{\omega}{2}\right) > 0$ when $\omega > 0$. Thus, due to the first and second derivative tests, we have that $\lambda^*$ is the global maximizer of $\lambda p_s(\lambda)$. □

## B.3 Prop. 3.3 (Concave Error Distribution Implies Monotonicity of $\mathrm{TP_s}$ in Beamwidth)

*Proof.* We rewrite spatial throughput (3.15) by expanding $u$, $p$, $g_1$ in terms of $x = \omega/2$ and study $\mathrm{TP_s}(x)$ over $x \in [0, \pi]$. Specifically, we show that $\mathrm{TP_s}(x)$ is monotone decreasing over $(0, \pi]$. To do so, we will need $\mathrm{TP_s}$ and its derivative *w.r.t.* $x$:

$$\mathrm{TP_s}(x) = \frac{F_{|\epsilon|}^2(x)\, \mathrm{e}^{-Bx^2}}{Ax^2} \tag{B.20}$$

$$\mathrm{TP_s}'(x) = -\frac{2\mathrm{e}^{-Bx^2} F_{|\epsilon|}(x)}{Ax^3} \left((1 + Bx^2) F_{|\epsilon|}(x) - x f_{|\epsilon|}(x)\right), \tag{B.21}$$

with non-negative constants $A = \frac{1}{\pi} e\kappa d^2 \beta^{2/\alpha}$ and $B = \frac{\beta d^\alpha \eta}{\pi^2 P_t}$. Since $\frac{2\mathrm{e}^{-Bx^2} F_{|\epsilon|}(x)}{Ax^3} > 0$ for all $x \in (0, \pi]$, it suffices to show:

$$0 \leq \left((1 + Bx^2) F_{|\epsilon|}(x) - x f_{|\epsilon|}(x)\right) \tag{B.22}$$

$$\frac{f_{|\epsilon|}(x)}{F_{|\epsilon|}(x)} \leq \frac{1}{x} + Bx, \quad \forall x \in (0, \pi]. \tag{B.23}$$

in order to prove spatial throughput is monotone decreasing in $x$, $\mathrm{TP}_\mathrm{s}'(x) \leq 0$.

By the assumption of concavity over $[0, \pi]$, $F_{|\epsilon|}$ evaluated at $y \in [0, \pi]$ lies below its first order Taylor series approximation centered at $x \in [0, \pi]$:

$$F_{|\epsilon|}(y) \leq F_{|\epsilon|}(x) + f_{|\epsilon|}(x)\,(y - x), \quad \forall x, y \in [0, \pi]. \tag{B.24}$$

After setting $y = 0$, $F_{|\epsilon|}(0) = 0$, rearranging the result, and adding a positive quantity $Bx^2$ to the *r.h.s.*, we can conclude our proof:

$$\frac{f_{|\epsilon|}(x)}{F_{|\epsilon|}(x)} \leq \frac{1}{x} < \frac{1}{x} + Bx^2, \quad \forall x \in (0, \pi]. \tag{B.25}$$

□

## B.4 Cor. 3.5 (TP using Omni-directional Antennas)

*Proof.* The proof of Prop. 3.2 can be used with $A = \pi\kappa d^2 \beta^{2/\alpha}$, $B = \frac{\beta d^\alpha \eta}{P_t}$, and $C = 1$. Since $A$, $\mathrm{e}^{-B}$, and $C$ are all positive, $\lambda^* = 1/A$ is the global maximizer of $\lambda p_s(\lambda)$. □

## B.5 Prop. 3.4 (TC with Sectors without Sidelobes)

*Proof.* Rewrite (3.13) as $p_s = C\mathrm{e}^{-\lambda A - B}$, where $A = \pi\kappa d^2 \beta^{2/\alpha} p^2$, $B = \frac{\beta d^\alpha \eta}{P_t g_1^2}$, and $C = u^2$. Solving for $\lambda$ yields $\lambda(p_e) = \log\left(\frac{C\mathrm{e}^{-B}}{(1-p_e)}\right)/A$. Note that $\mathrm{e}^{-B} = 1 - (1 - \mathrm{e}^{-B})$, and let $p_\eta = 1 - \mathrm{e}^{-B}$, which represents fading outage due to background noise. Multiplying $\lambda(p_e)$ by the success rate $(1 - p_e)$ provides the maximum intensity of successful transmissions, subject to outage $p_e$. □

## B.6 Prop. 3.5 (Concavity of Error Distribution Implies Unimodality of $\mathrm{TC_s}$)

*Proof.* We rewrite transmission capacity (3.22) by expanding $u$, $p$, $g_1$ in terms of $x = \omega/2$ and study $\mathrm{TC_s}(x)$ over $x \in (0, \pi]$. Specifically, we show that $\mathrm{TC_s}(x)$ is *i)* monotone increasing over $(0, x_l]$, *ii)* quasiconcave over $[x_l, x_u]$, and *iii)* monotone decreasing over $(x_u, \pi]$, where $x_l = F_{|\epsilon|}^{-1}\big(\sqrt{1-p_e}\big)$ and $x_u = \epsilon_{\max}$. Once these three facts are established and combined with the continuity of $\mathrm{TC_s}$ over $(0, \pi]$, we can readily conclude that the unique maximizer of $\mathrm{TC_s}$ lies between $(x_l, x_u]$ and that $\mathrm{TC_s}$ is quasiconcave (unimodal) over this domain. To do so, we will need $\mathrm{TC_s}$ and its first two derivatives *w.r.t.* $x$:

$$\mathrm{TC_s}(x) = \frac{A}{x^2}\left(2\log(F(x)) + B\right) - AC \tag{B.26}$$

$$\mathrm{TC_s}'(x) = \frac{2A}{x^2}\left(\frac{f(x)}{F(x)} - \frac{2\log(F(x)) + B}{x}\right) \tag{B.27}$$

$$\mathrm{TC_s}''(x) = \frac{2A}{x^3}\left(3\frac{2\log(F(x)) + B}{x} - \frac{4f(x)}{F(x)} - \frac{xf(x)^2}{F(x)^2} + \frac{xf'(x)}{F(x)}\right), \tag{B.28}$$

with positive constants $A = \frac{\pi(1-p_e)}{\kappa d^2 \beta^{2/\alpha}}$, $B = \log\left(\frac{1}{1-p_e}\right)$, and $C = \frac{\beta d^\alpha \eta}{P_t \pi^2}$. Note: $\mathrm{TC_s}$ is smooth at $x_l$ and $\mathrm{TC_s}'(x_l) > 0$, but may not be differentiable (*i.e.*, have a sharp turn) at $x_u$.

For *i)*, note that $2\log(F(x)) + B$ is monotone increasing in $x$ due to the monotonicity of $F$ and log. It follows that when $x \le x_l$:

$$2\log(F(x)) + B \le 2\log(F(x_l)) + B \tag{B.29}$$

$$\le 2\log\left(F\left(F_{|\epsilon|}^{-1}\left(\sqrt{1-p_e}\right)\right)\right) + B \tag{B.30}$$

$$= \log(1-p_e) + \log(1/(1-p_e)) = 0. \tag{B.31}$$

Substituting this bound into (B.27), we obtain the desired monotonicity of $\mathrm{TC_s}$:

$$\mathrm{TC_s}'(x) \ge \frac{2A}{x^2}\frac{f(x)}{F(x)} > 0, \quad \forall x \in (0, x_l). \tag{B.32}$$

For *ii)*, we use a sufficient condition for quasiconcavity from Boyd and Vandenberghe [66]:

$$\mathrm{TC}_\mathrm{s}'(x) = 0 \Rightarrow \mathrm{TC}_\mathrm{s}''(x) < 0, \quad \forall x \in (x_l, x_u). \tag{B.33}$$

In words, if all stationary points are associated with local maxima, then only a single stationary point exists, which necessarily provides the global maximum. Let $x^* \in (x_l, x_u)$ be a stationary point of $\mathrm{TC}_\mathrm{s}$. From (B.27), $\mathrm{TC}_\mathrm{s}(x^*) = 0$ implies:

$$\frac{2\log(F(x^*)) + B}{x^*} = \frac{f(x^*)}{F(x^*)}. \tag{B.34}$$

Simplify (B.28) at this stationary point by substitution of the above equality:

$$\mathrm{TC}_\mathrm{s}''(x^*) = \frac{2A}{(x^*)^3}\left(-\frac{f(x^*)}{F(x^*)} - \frac{x^* f(x^*)^2}{F(x^*)^2} + \frac{x^* f'(x^*)}{F(x^*)}\right). \tag{B.35}$$

Over $(x_l, x_u)$, we have $F(x) > 0$, $f(x) > 0$, and $f'(x) \leq 0$, thus $\mathrm{TC}_\mathrm{s}''(x^*) < 0$ and $\mathrm{TC}_\mathrm{s}$ is unimodal over $(x_l, x_u)$ and thus $[x_l, x_u]$ by continuity of $\mathrm{TC}_\mathrm{s}$.

For *iii)*, note that $F(x) = 1$ and $f(x) = 0$ for all $x > x_u$. Thus, (B.27) can be simplified:

$$\mathrm{TC}_\mathrm{s}'(x) = \frac{-2AB}{x^3} < 0, \quad \forall x \in (x_u, \pi]. \tag{B.36}$$

Finally, since $\mathrm{TC}_\mathrm{s}$ is increasing on $(0, x_l]$ and decreasing on $(x_u, \pi]$, the maximization of $\mathrm{TC}_\mathrm{s}(x)$ can be reduced to searching over the remaining unimodal portion of $\mathrm{TC}_\mathrm{s}$: $(x_l, x_u]$. □

## B.7 Cor. 3.6 (Conditions on the Maximizing $\omega^*$ for $\mathrm{TC}_\mathrm{s}$)

*Proof.* First, by Prop. 3.5 and its proof in App. B.6, we know that $\mathrm{TC}_\mathrm{s}(x)$ with $x = \omega/2$ is unimodal and contains a unique maximizer within: $x^* \in \left(F_{|\epsilon|}^{-1}\left(\sqrt{1-p_e}\right), \epsilon_{\max}\right]$.

$\mathrm{TC}_\mathrm{s}(x)$ may have a sharp turn at $x = \epsilon_{\max}$, so we take the left derivative of $\mathrm{TC}_\mathrm{s}$ using (B.27).

Since $F(\epsilon_{\max}) = 1$, we have:

$$\mathrm{TC}_{\mathrm{s}}'(\epsilon_{\max}^{-}) = \lim_{x \to \epsilon_{\max}^{-}} \mathrm{TC}_{\mathrm{s}}'(x) = \frac{2A}{\epsilon_{\max}^2} \left( f(\epsilon_{\max}) - \frac{B}{\epsilon_{\max}} \right), \tag{B.37}$$

with positive constants $A = \frac{\pi(1-p_e)}{\kappa d^2 \beta^{2/\alpha}}$, $B = \log\left(\frac{1}{1-p_e}\right)$.

First, when $f(\epsilon_{\max}) < \frac{B}{\epsilon_{\max}}$, we have $\mathrm{TC}_{\mathrm{s}}'(\epsilon_{\max}^{-}) < 0$ and the maximizing $x^*$ must lie strictly less than $\epsilon_{\max}$. Second, when $f(\epsilon_{\max}) > \frac{B}{\epsilon_{\max}}$, we have $\mathrm{TC}_{\mathrm{s}}'(\epsilon_{\max}^{-}) > 0$ and the maximizing $x^*$ must be exactly $\epsilon_{\max}$ due to the unimodality of $\mathrm{TC}_{\mathrm{s}}$ over the rest of $\left(F_{|\epsilon|}^{-1}\left(\sqrt{1-p_e}\right), \epsilon_{\max}\right]$. Lastly, when $f(\epsilon_{\max}) = \frac{B}{\epsilon_{\max}}$, we have $\mathrm{TC}_{\mathrm{s}}'(\epsilon_{\max}^{-}) = 0$. We then take the left second derivative of $\mathrm{TC}_{\mathrm{s}}$ at $\epsilon_{\max}$ using (B.28), and since $\epsilon_{\max}$ is a stationary point of $\mathrm{TC}_{\mathrm{s}}$, we can apply (B.34):

$$\begin{aligned}
\mathrm{TC}_{\mathrm{s}}''(\epsilon_{\max}^{-}) &= \lim_{x \to \epsilon_{\max}^{-}} \mathrm{TC}_{\mathrm{s}}''(x) && \text{(B.38)} \\
&= \frac{2A}{\epsilon_{\max}^3} \left( 3\frac{2\log(F(\epsilon_{\max})) + B}{\epsilon_{\max}} - \frac{4f(\epsilon_{\max})}{F(\epsilon_{\max})} - \frac{\epsilon_{\max} f(\epsilon_{\max})^2}{F(\epsilon_{\max})^2} + \frac{\epsilon_{\max} f'(\epsilon_{\max}^{-})}{F(\epsilon_{\max})} \right) && \text{(B.39)} \\
&= \frac{2A}{\epsilon_{\max}^3} \left( -\frac{f(\epsilon_{\max})}{F(\epsilon_{\max})} - \frac{\epsilon_{\max} f(\epsilon_{\max})^2}{F(\epsilon_{\max})^2} + \frac{\epsilon_{\max} f'(\epsilon_{\max}^{-})}{F(\epsilon_{\max})} \right) && \text{(B.40)} \\
&= \frac{2A}{\epsilon_{\max}^3} \left( -f(\epsilon_{\max}) - \epsilon_{\max} f(\epsilon_{\max})^2 + \epsilon_{\max} f'(\epsilon_{\max}^{-}) \right), && \text{(B.41)}
\end{aligned}$$

where $F(\epsilon_{\max}) = 1$. Since $\epsilon_{\max} > 0$, $f(\epsilon_{\max}) > 0$, and $f'(\epsilon_{\max}^{-}) \leq 0$, we conclude that $\mathrm{TC}_{\mathrm{s}}''(\epsilon_{\max}^{-}) < 0$ and $\mathrm{TC}_{\mathrm{s}}$ is concave down at $\epsilon_{\max}^{-}$. Thus, the maximizing $x^*$ must be exactly $\epsilon_{\max}$ due to the unimodality of $\mathrm{TC}_{\mathrm{s}}$ over the rest of $\left(F_{|\epsilon|}^{-1}\left(\sqrt{1-p_e}\right), \epsilon_{\max}\right]$. □

## B.8 Cor. 3.7 (TC with Omni-directional Antennas)

*Proof.* The proof of Prop. 3.4 can be used with $A = \pi\kappa d^2 \beta^{2/\alpha}$, $B = \frac{\beta d^\alpha \eta}{P_t}$, and $C = 1$. □

# Appendix C: Proofs of Ch. 4

## C.1 Prop. 4.1 (Posterior Distribution)

*Proof.* We first address $\mathbb{P}\{\mathcal{H}_1|\mathcal{D}_1\}$ and then simply express all other probabilities in terms of $\mathbb{P}\{\mathcal{H}_1|\mathcal{D}_1\}$ it using standard probabilistic arguments.

Observe that the homogeneous PPP $\hat{\Phi}$ conditioned on the event $\mathcal{D}_1$ is stochastically equivalent to a PPP $\hat{\Phi}_{d_\mathrm{I}}$ with a radially isotropic intensity function that excludes TXs within distance $d_\mathrm{I}$ from the origin: $\lambda_{d_\mathrm{I}}(x) = \lambda \mathbf{1}\{\|x\| \geq d_\mathrm{I}\}$. We proceed to characterize the probability of success of the typical transmission under $\hat{\Phi}_{d_\mathrm{I}}$:

$$\mathbb{P}\{\mathcal{H}_1|\mathcal{D}_1\} = \mathbb{P}\{\mathrm{SINR}_o \geq \beta\} \tag{C.1}$$

$$\overset{(a)}{=} \mathbb{P}\{F_{o,o} \geq \beta d_\mathrm{T}^\alpha I_o\}\, \mathbb{P}\{F_{o,o} \geq \beta d_\mathrm{T}^\alpha \eta\} \tag{C.2}$$

$$\overset{(b)}{=} \mathcal{L}_{I_o}(s, d_\mathrm{I}) \exp(-s\eta)\,, \tag{C.3}$$

where we *(a)* expand $\mathrm{SINR}_o$, isolate $F_{o,o}$, and apply the memoryless property of $F_{o,o}$, and *(b)* recognize the first term is the Laplace transform of $I_o$ from PPP $\hat{\Phi}_{d_\mathrm{I}}$ with $s = \beta d_\mathrm{T}^\alpha$ and the second term is the *c.c.d.f.* of $F_{o,o}$.

Finally, we employ Prop. C.1 below to solve $\mathcal{L}_{I_o}(s, d_\mathrm{I})$ evaluated at $s$ with transmitter-free void zone radius $d_\mathrm{I}$. □

**Proposition C.1** (Laplace Transform for PPP with Void Ball)**.** *Let $\hat{\Phi}_{d_\mathrm{I}}$ be a marked PPP on $\mathbb{R}^d$ with isotropic intensity function $\lambda_{d_\mathrm{I}}(x)$:*

$$\lambda_{d_\mathrm{I}}(x) = \lambda \mathbf{1}\{\|x\| \geq d_\mathrm{I}\}\,, \quad \lambda > 0, \tag{C.4}$$

*which excludes points within a disk of radius $d_\mathrm{I}$ about the origin. The Laplace transform of the*

*resulting sum interference $I_o$ observed at the origin is:*

$$\mathcal{L}_{I_o}(s, d_{\mathrm{I}}) = \frac{\exp\big(-\lambda c_d \kappa s^{\delta}\big)\exp\big(-\lambda c_d s^{\delta} I_{\delta}(d_{\mathrm{I}}^{\alpha}/s)\big)}{\exp\big(-\lambda c_d d_{\mathrm{I}}^{d}\big)} \tag{C.5}$$

*where $I_{\delta}(x) = \int_0^x \delta t^{\delta}/(1+t)\mathrm{d}t$ is a convenience function for a specific form of the incomplete Beta function.*

*Proof.* We now follow the text of [52, p.103], adapting to the scenario at hand. The sum interference is:

$$I_o = \sum_{x \in \hat{\Phi}_{d_{\mathrm{I}}}} F_x l(x), \tag{C.6}$$

with $l(x) = x^{-\alpha}$ as the distance function and $F_x \sim \mathrm{Exp}(1)$ as the fading marks.

The Laplace transform can be manipulated as follows:

$$\mathcal{L}_{I_o}(s, d_{\mathrm{I}}) = \mathbb{E}_{\hat{\Phi}_{d_{\mathrm{I}}}}\left[\mathrm{e}^{-sI_o}\right] \overset{(a)}{=} \mathbb{E}_{\hat{\Phi}_{d_{\mathrm{I}}}}\left[\prod_{x \in \hat{\Phi}_{d_{\mathrm{I}}}} \mathrm{e}^{-sF_x l(x)}\right] \tag{C.7}$$

$$\overset{(b)}{=} \mathbb{E}_{\Phi_{d_{\mathrm{I}}}}\left[\prod_{x \in \Phi_{d_{\mathrm{I}}}} \mathbb{E}_F\left[\mathrm{e}^{-sFl(x)}\right]\right] \tag{C.8}$$

$$\overset{(c)}{=} \mathbb{E}_{\Phi_{d_{\mathrm{I}}}}\left[\prod_{x_i \in \Phi_{d_{\mathrm{I}}}} v(\|x_i\|)\right] \tag{C.9}$$

$$\overset{(d)}{=} \exp\left(-\int_0^{\infty} (1 - v(r))\, \tilde{\lambda}_{d_o}(r)\mathrm{d}r\right) \tag{C.10}$$

$$\overset{(e)}{=} \exp\left(-\mathbb{E}_F\left[\int_0^{\infty} \left(1 - \mathrm{e}^{-sF\tilde{l}(r)}\right) \tilde{\lambda}_{d_{\mathrm{I}}}(r)\mathrm{d}r\right]\right), \tag{C.11}$$

where *(a)* the sum $I_o$ results in a product of exponentials, *(b)* the expectation over $F$ is brought into the product, while the indexing on $F$ is dropped, *(c)* $\Phi_{d_{\mathrm{I}}}$ is mapped [52, Thm. 2.34] to one dimension with intensity $\tilde{\lambda}_{d_{\mathrm{I}}}(r) = \lambda_{d_{\mathrm{I}}}(r) c_d d r^{d-1}$ and distance function $\tilde{l}(\|x\|) \equiv l(x)$ with $v(r) = \mathbb{E}_F\left[\mathrm{e}^{-sF\tilde{l}(r)}\right]$, *(d)* the mean of a product $v(r)$ over the collapsed $\Phi_{d_{\mathrm{I}}}$ is a probability generating functional (pgfl) of the process [52, Thm. 4.9], *(e)* $v(r)$ is substituted back and the order of integration over $r$ and $F$ is exchanged.

Conditioned on $F = f$, the innermost integral of (C.11) becomes:

$$\int_0^\infty \left(1 - \mathrm{e}^{-sf\tilde{l}(r)}\right) \tilde{\lambda}_{d_\mathrm{I}}(r)\mathrm{d}r = \lambda c_d \int_{d_\mathrm{I}}^\infty \left(1 - \mathrm{e}^{-sfr^{-\alpha}}\right) dr^{d-1}\mathrm{d}r \tag{C.12}$$

$$\stackrel{(a)}{=} \lambda c_d \int_{d_\mathrm{I}^\alpha}^\infty \left(1 - \mathrm{e}^{-sf/y}\right) \delta y^{\delta-1}\mathrm{d}y \tag{C.13}$$

$$\stackrel{(b)}{=} \lambda c_d \int_0^{d_\mathrm{I}^{-\alpha}} \left(1 - \mathrm{e}^{-sfx}\right) \delta x^{-\delta-1}\mathrm{d}x \tag{C.14}$$

$$\stackrel{(c)}{=} \lambda c_d b^{-\delta} \left((bsf)^\delta \Gamma(1-\delta) + \delta E_{1+\delta}(bsf) - 1\right), \tag{C.15}$$

by *(a)* first substituting $y \leftarrow r^\alpha$, *(b)* substituting $x \leftarrow y^{-1}$, *(c)* substituting $b = d_\mathrm{I}^{-\alpha}$ for convenience and integrating by parts. Note, $\Gamma(s) = \int_0^\infty t^{s-1}\mathrm{e}^{-t}\mathrm{d}t$ is the gamma function and $E_s(x) = \int_1^\infty \mathrm{e}^{-xt}t^{-s}\mathrm{d}t$ is the generalized exponential function.

We make use of the following identities:

$$\Gamma(s,x) = (s-1)\Gamma(s-1,x) + x^{s-1}\mathrm{e}^{-x} \tag{C.16}$$

$$E_s(x) = x^{s-1}\Gamma(1-s,x), \tag{C.17}$$

where $\Gamma(s,x) = \int_x^\infty t^{s-1}\mathrm{e}^{-t}\mathrm{d}t$ is the upper incomplete gamma function.

Taking the expectation of (C.15) over $f$ (using Mathematica 10):

$$\lambda c_d b^{-\delta}\mathbb{E}_F\left[(bsf)^\delta\Gamma(1-\delta) + \delta E_{1+\delta}(bsf) - 1\right] \tag{C.18}$$

$$= \lambda c_d \left(s^\delta \pi\delta \csc(\pi\delta) + s^\delta(-1)^{1-\delta}\delta B_{\frac{-1}{bs}}(1+\delta,0) - b^{-\delta}\right) \tag{C.19}$$

$$= \lambda c_d \Gamma(1+\delta)\Gamma(1-\delta)s^\delta + \lambda c_d s^\delta I_\delta(\frac{1}{bs}) - \lambda c_d b^{-\delta}, \tag{C.20}$$

where $I_\delta(x)$ is a particular form of the incomplete Beta function, $B_x(a,b) = \int_0^x t^{a-1}(1-t)^{b-1}\mathrm{d}t$:

$$I_\delta(x) \equiv (-1)^{1-\delta}\delta B_{-x}(1+\delta,0) = \int_0^x \frac{\delta t^\delta}{1+t}\mathrm{d}t, \quad \forall x,\delta \geq 0. \tag{C.21}$$

Finally, substituting (C.20) into (C.11) and expanding $b = d_\mathrm{I}^{-\alpha}$ yields the desired Laplace trans-

form. □

## C.2 Thm. 4.1 (Minimum Bayes Risk)

*Proof.* Let $A = \lambda c_d \kappa s^\delta + s\eta$, $B(d_\mathrm{I}) = \lambda c_d d_\mathrm{I}^d$, and $C(d_\mathrm{I}) = \lambda c_d s^\delta I_\delta(d_\mathrm{I}^\alpha/s)$. For convenience, we will refer to $r(d_\mathrm{I})$, $B(d_\mathrm{I})$ and $C(d_\mathrm{I})$ without arguments, and all derivatives will be taken *w.r.t.* $d_\mathrm{I}$. The expression for Bayes risk and its first and second derivatives are (Mathematica 10):

$$r = c_{00} + (c_{01} - c_{00})\mathrm{e}^{-A} + (c_{10} - c_{00})\mathrm{e}^{-B} + (c_{11} + c_{00} - c_{10} - c_{01})\mathrm{e}^{-A-C} \tag{C.22}$$

$$r' = -(c_{10} - c_{00})B'\mathrm{e}^{-B} - (c_{11} + c_{00} - c_{10} - c_{01})C'\mathrm{e}^{-A-C} \tag{C.23}$$

$$r'' = (c_{10} - c_{00})\left((B')^2 - B''\right)\mathrm{e}^{-B} + (c_{11} + c_{00} - c_{10} - c_{01})\left((C')^2 - C''\right)\mathrm{e}^{-A-C}, \tag{C.24}$$

with:

$$B' = \delta\alpha\lambda c_d d_\mathrm{I}^{\delta\alpha-1} \qquad B'' = \frac{(\delta\alpha - 1)}{d_\mathrm{I}}B' \tag{C.25}$$

$$C' = \frac{d_\mathrm{I}^\alpha}{s + d_\mathrm{I}^\alpha}B' \qquad C'' = \frac{(\delta\alpha - 1)(s + d_\mathrm{I}^\alpha) + s\alpha}{d_\mathrm{I}(s + d_\mathrm{I}^\alpha)}C'. \tag{C.26}$$

The first order stationary points of $r$ are:

$$d_\mathrm{I}^* = 0 \tag{C.27}$$

$$d_\mathrm{I}^* : -(c_{10} - c_{00})\frac{B'}{C'}\mathrm{e}^{-B} = (c_{11} + c_{00} - c_{10} - c_{01})\mathrm{e}^{-A-C}. \tag{C.28}$$

When $c_{10} > c_{00}$, we show that there is a unique $d_\mathrm{I}^*$ that minimizes $r$. To do so, we employ a sufficient condition for quasi-convexity from Boyd and Vandenberghe [66, Eq. 3.22]:

$$r'(d_\mathrm{I}) = 0 \implies r''(d_\mathrm{I}) > 0, \quad \forall d_\mathrm{I} \in (0, \infty). \tag{C.29}$$

Thus, for all positive roots $d_{\mathrm{I}}^* > 0$, (C.28) must hold, and we substitute into (C.24):

$$r''|_{d_{\mathrm{I}}^*} = (c_{10} - c_{00})\left((B')^2 - B''\right)\mathrm{e}^{-B} + (c_{11} + c_{00} - c_{10} - c_{01})\left((C')^2 - C''\right)\mathrm{e}^{-A-C} \tag{C.30}$$

$$= (c_{10} - c_{00})\left((B')^2 - B''\right)\mathrm{e}^{-B} - (c_{10} - c_{00})\frac{B'}{C'}\left((C')^2 - C''\right)\mathrm{e}^{-B} \tag{C.31}$$

$$= (c_{10} - c_{00})B'\mathrm{e}^{-B}\left(\left(B' - \frac{B''}{B'}\right) - \left(C' - \frac{C''}{C'}\right)\right) \tag{C.32}$$

$$= (c_{10} - c_{00})B'\mathrm{e}^{-B}\left((B' - C') + \left(\frac{C''}{C'} - \frac{B''}{B'}\right)\right) \tag{C.33}$$

$$> 0, \tag{C.34}$$

where $c_{10} - c_{00} > 0$, $B' > 0$, $\mathrm{e}^{-B} > 0$, and:

$$B' - C' = \frac{sB'}{s + d_{\mathrm{I}}^{\alpha}} > 0 \qquad\qquad \frac{C''}{C'} - \frac{B''}{B'} = \frac{s\alpha}{d_{\mathrm{I}}(s + d_{\mathrm{I}}^{\alpha})} > 0. \tag{C.35}$$

Thus, we may conclude that $r$ is quasi-convex over $d_{\mathrm{I}} \in (0, \infty)$. Due to the strict inequality in (C.29), we further conclude that (C.28) yields a unique solution corresponding to the global minimizer $d_{\mathrm{I}}^*$ to the Bayes risk $r$. □

## C.3 Prop. 4.6 (Protocol Model Error Bounds)

*Proof.* The lower bound immediately follows from the optimality of $d_{\mathrm{I}}^*$. We now address the upper bound:

$$p_{\mathrm{E}}(d_{\mathrm{I}}) = \mathrm{e}^{-A} + \mathrm{e}^{-B(d_{\mathrm{I}})} - 2\mathrm{e}^{-A-C(d_{\mathrm{I}})} \tag{C.36}$$

$$\overset{(a)}{\leq} \mathrm{e}^{-A} + \mathrm{e}^{-B(d_{\mathrm{I}})} - 2\mathrm{e}^{-2A}\mathrm{e}^{-2C(d_{\mathrm{I}})} \tag{C.37}$$

$$\overset{(b)}{\leq} \mathrm{e}^{-A} + \mathrm{e}^{-B(d_{\mathrm{I}})} - 2\mathrm{e}^{-2A}\mathrm{e}^{-2B(d_{\mathrm{I}})} \tag{C.38}$$

$$= \left(\mathrm{e}^{-A} - \mathrm{e}^{-B(d_{\mathrm{I}})}\right)^2 \tag{C.39}$$

$$= \left(\mathrm{e}^{-B(d_{\mathrm{I}})}\left(1 - \mathrm{e}^{-(A - B(d_{\mathrm{I}}))}\right)\right)^2, \tag{C.40}$$

where we obtain $(a)$ from $A \geq 0$ and $C(d_{\mathrm{I}}) > 0$, and $(b)$ from $C(d_{\mathrm{I}}) \leq B(d_{\mathrm{I}})$ due to the fact that the integrand of $I_\delta(d_{\mathrm{I}}^\alpha/s)$ may be upper bounded by $\delta t^{\delta-1}$.

We now show that under the choice $d_{\mathrm{I,DI}}$, $A - B(d_{\mathrm{I,DI}}) \geq 0$. Note that the guard zone may be rewritten from (4.23) as:

$$d_{\mathrm{I,DI}} = \frac{s^\delta}{(1+s\eta)^\delta}. \tag{C.41}$$

Next, we substitute the above into the expression $A - B(d_{\mathrm{I,DI}})$:

$$A - B(d_{\mathrm{I,DI}}) = \lambda c_d \kappa s^\delta + s\eta - \lambda c_d d_{\mathrm{I,DI}}^d \tag{C.42}$$

$$= \lambda c_d s^\delta \left(\kappa - \frac{1}{(1+s\eta)^\delta}\right) + s\eta \geq 0, \tag{C.43}$$

due to the fact that $\kappa \geq 1$ and $1/(1+s\eta)^\delta \leq 1$ for relevant parameter regimes, and the remaining terms are all positive. We now continue to bound the total error rate:

$$p_{\mathrm{E}}(d_{\mathrm{I,DI}}) \leq \left(\mathrm{e}^{-B(d_{\mathrm{I}})}\left(1 - \mathrm{e}^{-(A-B(d_{\mathrm{I}}))}\right)\right)^2 \tag{C.44}$$

$$\overset{(a)}{\leq} \left(1 - \mathrm{e}^{-(A-B(d_{\mathrm{I}}))}\right)^2 \tag{C.45}$$

$$\overset{(b)}{\leq} 1 - \mathrm{e}^{-(A-B(d_{\mathrm{I,DI}}))} \tag{C.46}$$

$$\leq 1 - \mathrm{e}^{-A} = \mathbb{P}\{\mathcal{H}_0\}, \tag{C.47}$$

where $(a)$ follows from $B(d_{\mathrm{I}}) \geq 0$, and $(b)$ follows from the fact that $A - B(d_{\mathrm{I,DI}}) \geq 0$ and thus $1 - \mathrm{e}^{-(A-B(d_{\mathrm{I,DI}}))} \in [0,1]$. □

## C.4 Prop. 4.7 (Posterior Distribution w/ Directional Antennas)

*Proof.* We first address $\mathbb{P}\{\mathcal{H}_1|\mathcal{D}_1\}$ and then simply express all other probabilities in terms of $\mathbb{P}\{\mathcal{H}_1|\mathcal{D}_1\}$ using standard probabilistic arguments.

Let the homogeneous PPP $\hat{\Phi}$ conditioned on the event $\mathcal{D}_1$ be denoted $\hat{\Phi}_{\mathcal{D}_1}$. We proceed to

characterize the probability of success of the typical transmission under $\hat{\Phi}_{\mathcal{D}_1}$:

$$\mathbb{P}\{\mathcal{H}_1|\mathcal{D}_1\} = \mathbb{P}\{\text{SINR}_o \geq \beta\} \tag{C.48}$$

$$\stackrel{(a)}{=} \mathbb{P}\left\{F_{o,o} \geq \frac{\beta d_{\text{T}}^{\alpha}}{g_{\max}^2} I_o\right\} \mathbb{P}\left\{F_{o,o} \geq \frac{\beta d_{\text{T}}^{\alpha}}{g_{\max}^2}\eta\right\} \tag{C.49}$$

$$\stackrel{(b)}{=} \mathcal{L}_{I_o}(\tilde{s}, \Delta)\exp(-\tilde{s}\eta)\,, \tag{C.50}$$

where we *(a)* expand $\text{SINR}_o$, isolate $F_{o,o}$, and apply the memoryless property of $F_{o,o}$, and *(b)* recognize the first term is the Laplace transform of $I_o$ from PPP $\hat{\Phi}_{\mathcal{D}_1}$ with $\tilde{s} = s/g_{\max}^2 = \beta d_{\text{T}}^{\alpha}/g_{\max}^2$ and the second term is the *c.c.d.f.* of $F_{o,o}$.

Finally, we employ Prop. C.2 below to solve $\mathcal{L}_{I_o}(\tilde{s}, \Delta)$ evaluated at $\tilde{s}$ with guard zone factor $\Delta$ associated with the conditioned event $\mathcal{D}_1$. □

**Proposition C.2** (Laplace Transform for PPP under $\mathcal{D}_1$ w/ Directional Antennas)**.** *Let the homogeneous PPP $\hat{\Phi}$ conditioned on the event $\mathcal{D}_1$ with guard zone factor $\Delta$ be denoted $\hat{\Phi}_{\mathcal{D}_1}$. The Laplace transform of the resulting sum interference $I_o$ observed at the origin is:*

$$\mathcal{L}_{I_o}(\tilde{s}, \Delta) = \frac{\exp\left(-\lambda c_d \kappa s^{\delta}\tilde{G}^2\right)\exp\left(-\lambda c_d s^{\delta}\tilde{G}^2 I_{\delta}(\Delta^{\alpha})\right)}{\exp\left(-\lambda c_d s^{\delta}\tilde{G}^2\Delta^{d}\right)} \tag{C.51}$$

*where $I_{\delta}(x) = \int_0^x \delta t^{\delta}/(1+t)\mathrm{d}t$ is a convenience function for a specific form of the incomplete Beta function.*

*Proof.* First, observe that the points retained by $\hat{\Phi}_{\mathcal{D}_1}$ must satisfy the guard factor constraint in (4.35), *i.e.*, given the independent gains between each point and the typical receiver, $g_T$ and $g_R$ resp., the point must be outside the following guard zone distance:

$$d_{\text{I}}(g_T, g_R) = \Delta\left(\frac{g_T g_R}{g_{\max}^2}\right)^{1/\alpha}\beta^{1/\alpha}. \tag{C.52}$$

We now follow the text of [52, p.103], adapting to the scenario at hand. The sum interference is:

$$I_o = \sum_{x \in \hat{\Phi}_{d_\mathrm{I}}} F_x G_{T,x} G_{R,x} l(x), \tag{C.53}$$

with $l(x) = x^{-\alpha}$ as the distance function, $F_x \sim \mathrm{Exp}(1)$ as the fading marks, and $G_{T,x} \sim f_{G_T}$ and $G_{R,x} \sim f_{G_R}$ as the gain marks.

The Laplace transform can be manipulated as follows:

$$\mathcal{L}_{I_o}(\tilde{s}, \Delta) = \mathbb{E}_{\hat{\Phi}_{\mathcal{D}_1}}\left[\mathrm{e}^{-\tilde{s} I_o}\right] \overset{(a)}{=} \mathbb{E}_{\hat{\Phi}_\Delta}\left[\prod_{x \in \hat{\Phi}_{\mathcal{D}_1}} \mathrm{e}^{-\tilde{s} F_x G_{T,x} G_{R,x} l(x)}\right] \tag{C.54}$$

$$\overset{(b)}{=} \mathbb{E}_{\Phi_{\mathcal{D}_1}}\left[\prod_{x \in \Phi_{\mathcal{D}_1}} \mathbb{E}_{F,G_T,G_R}\left[\mathrm{e}^{-\tilde{s} F G_T G_R l(x)}\right]\right] \tag{C.55}$$

$$\overset{(c)}{=} \mathbb{E}_{\Phi_{\mathcal{D}_1}}\left[\prod_{x_i \in \Phi_{\mathcal{D}_1}} v(\|x_i\|)\right] \tag{C.56}$$

$$\overset{(d)}{=} \exp\left(-\int_0^\infty (1 - v(r))\, \tilde{\lambda}_\Delta(r) \mathrm{d}r\right) \tag{C.57}$$

$$\overset{(e)}{=} \exp\left(-\mathbb{E}_{F,G_T,G_R}\left[\int_0^\infty \left(1 - \mathrm{e}^{-\tilde{s} F G_T G_R \tilde{l}(r)}\right) \tilde{\lambda}_\Delta(r) \mathrm{d}r\right]\right), \tag{C.58}$$

where *(a)* the sum $I_o$ results in a product of exponentials, *(b)* the expectation over $F$ is brought into the product, while the indexing on $F$ is dropped, *(c)* $\Phi_{\mathcal{D}_1}$ is mapped [52, Thm. 2.34] to one dimension with intensity $\tilde{\lambda}_\Delta(r) = \lambda_\Delta(r) c_d d r^{d-1}$ and distance function $\tilde{l}(\|x\|) \equiv l(x)$ with $v(r) = \mathbb{E}_{F,G_T,G_R}\left[\mathrm{e}^{-\tilde{s} F G_T G_R \tilde{l}(r)}\right]$, *(d)* the mean of a product $v(r)$ over the collapsed $\Phi_{\mathcal{D}_1}$ is a probability generating functional (pgfl) of the process [52, Thm. 4.9], *(e)* $v(r)$ is substituted back and the order of integration over $r$ and $F, G_T, G_R$ are exchanged.

Conditioned on $F = f$, $G_T = g_T$, and $G_R = g_R$ the innermost integral of (C.58) becomes:

$$\int_0^\infty \left(1 - \mathrm{e}^{-\tilde{s} f g_T g_R \tilde{l}(r)}\right) \tilde{\lambda}_\Delta(r) \mathrm{d}r$$

$$= \lambda c_d \int_{d_\mathrm{I}(g_T, g_R)}^\infty \left(1 - \mathrm{e}^{-\tilde{s} f g_T g_R r^{-\alpha}}\right) dr^{d-1} \mathrm{d}r \tag{C.59}$$

$$\stackrel{(a)}{=} \lambda c_d \int_{d_\mathrm{I}(g_T, g_R)^\alpha}^\infty \left(1 - \mathrm{e}^{-\tilde{s} f / y}\right) \delta y^{\delta - 1} \mathrm{d}y \tag{C.60}$$

$$\stackrel{(b)}{=} \lambda c_d \int_0^{d_\mathrm{I}(g_T, g_R)^{-\alpha}} \left(1 - \mathrm{e}^{-\tilde{s} f x}\right) \delta x^{-\delta - 1} \mathrm{d}x \tag{C.61}$$

$$\stackrel{(c)}{=} \lambda c_d b^{-\delta} \left( (b \tilde{s} f g_T g_R)^\delta \Gamma(1 - \delta) + \delta E_{1+\delta}(b \tilde{s} f g_T g_R) - 1 \right), \tag{C.62}$$

by *(a)* first substituting $y \leftarrow r^\alpha$, *(b)* substituting $x \leftarrow y^{-1}$, *(c)* substituting $b = d_\mathrm{I}(g_T, g_R)^{-\alpha}$ for convenience and integrating by parts. Note, $\Gamma(s) = \int_0^\infty t^{s-1} \mathrm{e}^{-t} \mathrm{d}t$ is the gamma function and $E_s(x) = \int_1^\infty \mathrm{e}^{-xt} t^{-s} \mathrm{d}t$ is the generalized exponential function.

We make use of the following identities:

$$\Gamma(s, x) = (s - 1)\Gamma(s - 1, x) + x^{s-1} \mathrm{e}^{-x} \tag{C.63}$$

$$E_s(x) = x^{s-1} \Gamma(1 - s, x), \tag{C.64}$$

where $\Gamma(s, x) = \int_x^\infty t^{s-1} \mathrm{e}^{-t} \mathrm{d}t$ is the upper incomplete gamma function.

Taking the expectation of (C.15) over $f$ (using Mathematica 10):

$$\lambda c_d b^{-\delta} \mathbb{E}_F \left[ (b \tilde{s} f g_T g_R)^\delta \Gamma(1 - \delta) + \delta E_{1+\delta}(b \tilde{s} f g_T g_R) - 1 \right] \tag{C.65}$$

$$= \lambda c_d \left( (\tilde{s} g_T g_R)^\delta \pi \delta \csc(\pi \delta) + (\tilde{s} g_T g_R)^\delta (-1)^{1-\delta} \delta B_{\frac{-1}{b \tilde{s} g_T g_R}}(1 + \delta, 0) - b^{-\delta} \right) \tag{C.66}$$

$$= \lambda c_d \Gamma(1 + \delta) \Gamma(1 - \delta) (\tilde{s} g_T g_R)^\delta + \lambda c_d (\tilde{s} g_T g_R)^\delta I_\delta(\frac{1}{b \tilde{s} g_T g_R}) - \lambda c_d b^{-\delta} \tag{C.67}$$

$$= \lambda c_d \Gamma(1 + \delta) \Gamma(1 - \delta) (\tilde{s} g_T g_R)^\delta + \lambda c_d (\tilde{s} g_T g_R)^\delta I_\delta(\Delta^\alpha) - \lambda c_d b^{-\delta}, \tag{C.68}$$

where $I_\delta(x)$ is a particular form of the incomplete Beta function, $B_x(a,b) = \int_0^x t^{a-1}(1-t)^{b-1}\mathrm{d}t$:

$$I_\delta(x) \equiv (-1)^{1-\delta}\delta B_{-x}(1+\delta,0) = \int_0^x \frac{\delta t^\delta}{1+t}\mathrm{d}t, \quad \forall x,\delta \geq 0. \tag{C.69}$$

and $1/(b\tilde{s}g_T g_R) = \Delta^\alpha$.

Taking the expectation of (C.68) over $g_T$ and $g_R$ followed by expansion of $\tilde{s} = s/g_{max}^2$ yields:

$$\lambda c_d \Gamma(1+\delta)\Gamma(1-\delta)\tilde{s}^\delta \mathbb{E}\big[G_T^\delta\big]\,\mathbb{E}\big[G_R^\delta\big] + \lambda c_d \tilde{s}^\delta \mathbb{E}\big[G_T^\delta\big]\,\mathbb{E}\big[G_R^\delta\big]\, I_\delta(\Delta^\alpha) - \lambda c_d \mathbb{E}_{G_T,G_R}\big[b^{-\delta}\big] \tag{C.70}$$

$$= \lambda c_d \lambda c_d \kappa s^\delta \tilde{G}^2 + \lambda c_d \lambda c_d s^\delta \tilde{G}^2 I_\delta(\Delta^\alpha) - \lambda c_d \lambda c_d s^\delta \tilde{G}^2 \Delta^d. \tag{C.71}$$

Finally, substituting (C.71) into (C.58) yields the desired Laplace transform. □

## C.5 Thm. 4.2 (Minimum Bayes Risk w/ Directional Antennas)

*Proof.* Let $A = \lambda c_d \kappa s^\delta \tilde{G}^2 + \frac{s\eta}{g_{\max}^2}$, $B(\Delta) = \lambda c_d s^\delta \tilde{G}^2 \Delta^d$, and $C(\Delta) = \lambda c_d s^\delta \tilde{G}^2 I_\delta(\Delta^\alpha)$. For convenience, we will refer to $r(\Delta)$, $B(\Delta)$ and $C(\Delta)$ without arguments, and all derivatives will be taken *w.r.t.* $\Delta$. The expression for Bayes risk and its first and second derivatives are (Mathematica 10):

$$r = c_{00} + (c_{01}-c_{00})\mathrm{e}^{-A} + (c_{10}-c_{00})\mathrm{e}^{-B} + (c_{11}+c_{00}-c_{10}-c_{01})\mathrm{e}^{-A-C} \tag{C.72}$$

$$r' = -(c_{10}-c_{00})B'\mathrm{e}^{-B} - (c_{11}+c_{00}-c_{10}-c_{01})C'\mathrm{e}^{-A-C} \tag{C.73}$$

$$r'' = (c_{10}-c_{00})\left((B')^2 - B''\right)\mathrm{e}^{-B} + (c_{11}+c_{00}-c_{10}-c_{01})\left((C')^2 - C''\right)\mathrm{e}^{-A-C}, \tag{C.74}$$

with:

$$B' = \delta\alpha\lambda c_d s^\delta \tilde{G}^2 \Delta^{\delta\alpha-1} \qquad B'' = \frac{\delta\alpha-1}{\Delta}B' \tag{C.75}$$

$$C' = \frac{\Delta^\alpha}{1+\Delta^\alpha}B' \qquad C'' = \frac{(\delta\alpha-1)(1+\Delta^\alpha)+\alpha}{\Delta(1+\Delta^\alpha)}C'. \tag{C.76}$$

The first order stationary points of $r$ are:

$$\Delta^* = 0 \tag{C.77}$$

$$\Delta^* : -(c_{10} - c_{00})\frac{B'}{C'}\mathrm{e}^{-B} = (c_{11} + c_{00} - c_{10} - c_{01})\mathrm{e}^{-A-C}. \tag{C.78}$$

When $c_{10} > c_{00}$, we show that there is a unique $\Delta^*$ that minimizes $r$. To do so, we employ a sufficient condition for quasi-convexity from Boyd and Vandenberghe [66, Eq. 3.22]:

$$r'(\Delta) = 0 \implies r''(\Delta) > 0, \quad \forall \Delta \in (0, \infty). \tag{C.79}$$

Thus, for all positive roots $\Delta^* > 0$, (C.78) must hold, and we substitute into (C.74):

$$r''|_{d_{\mathrm{I}}^*} = (c_{10} - c_{00})\left((B')^2 - B''\right)\mathrm{e}^{-B} + (c_{11} + c_{00} - c_{10} - c_{01})\left((C')^2 - C''\right)\mathrm{e}^{-A-C} \tag{C.80}$$

$$= (c_{10} - c_{00})\left((B')^2 - B''\right)\mathrm{e}^{-B} - (c_{10} - c_{00})\frac{B'}{C'}\left((C')^2 - C''\right)\mathrm{e}^{-B} \tag{C.81}$$

$$= (c_{10} - c_{00})B'\mathrm{e}^{-B}\left(\left(B' - \frac{B''}{B'}\right) - \left(C' - \frac{C''}{C'}\right)\right) \tag{C.82}$$

$$= (c_{10} - c_{00})B'\mathrm{e}^{-B}\left((B' - C') + \left(\frac{C''}{C'} - \frac{B''}{B'}\right)\right) \tag{C.83}$$

$$> 0, \tag{C.84}$$

where $c_{10} - c_{00} > 0$, $B' > 0$, $\mathrm{e}^{-B} > 0$, and:

$$B' - C' = \frac{B'}{1 + \Delta^\alpha} > 0 \qquad\qquad \frac{C''}{C'} - \frac{B''}{B'} = \frac{\alpha}{\Delta(1 + \Delta^\alpha)} > 0. \tag{C.85}$$

Thus, we may conclude that $r$ is quasi-convex over $\Delta \in (0, \infty)$. Due to the strict inequality in (C.79), we further conclude that (C.78) yields a unique solution corresponding to the global minimizer $\Delta^*$ to the Bayes risk $r$. □

## C.6 Prop. 4.10 (Protocol Model Error Bounds w/ Directional Antennas)

*Proof.* The lower bound immediately follows from the optimality of $\Delta^*$. We now address the upper bound following the same strategy as in App. C.3:

$$p_{\mathrm{E}}(\Delta) \leq \left(\mathrm{e}^{-B(\Delta)}\left(1-\mathrm{e}^{-(A-B(\Delta))}\right)\right)^2, \tag{C.86}$$

where in this case we also have $C(\Delta) \leq B(\Delta)$, again due to the fact that the integrand of $I_\delta(\Delta^\alpha)$ may be upper bounded by $\delta t^{\delta-1}$.

We now show that under the choice $\Delta_{\mathrm{DI}} = 1$, $A - B(\Delta_{\mathrm{DI}}) \geq 0$.

$$A - B(\Delta_{\mathrm{DI}}) = \lambda c_d \kappa s^\delta \tilde{G}^2 + \frac{s\eta}{g_{\max}^2} - \lambda c_d s^\delta \tilde{G}^2 \Delta_{\mathrm{DI}}^d \tag{C.87}$$

$$= \lambda c_d s^\delta \tilde{G}^2 (\kappa - 1) + s\eta \geq 0, \tag{C.88}$$

due to the fact that $\kappa \geq 1$. We now continue to bound the total error rate:

$$p_{\mathrm{E}}(\Delta_{\mathrm{DI}}) \leq \left(\mathrm{e}^{-B(\Delta_{\mathrm{DI}})}\left(1-\mathrm{e}^{-(A-B(\Delta_{\mathrm{DI}}))}\right)\right)^2 \tag{C.89}$$

$$\overset{(a)}{\leq} \left(1-\mathrm{e}^{-(A-B(\Delta))}\right)^2 \tag{C.90}$$

$$\overset{(b)}{\leq} 1-\mathrm{e}^{-(A-B(\Delta_{\mathrm{DI}}))} \tag{C.91}$$

$$\leq 1-\mathrm{e}^{-A} = \mathbb{P}\{\mathcal{H}_0\}, \tag{C.92}$$

where $(a)$ follows from $B(\Delta) \geq 0$, and $(b)$ follows from the fact that $A - B(\Delta_{\mathrm{DI}}) \geq 0$ and thus $1-\mathrm{e}^{-(A-B(\Delta_{\mathrm{DI}}))} \in [0,1]$. □

# Vita

Jeffrey William Wildman II was born in Willingboro, New Jersey. After graduating from Cherokee High School, Marlton, New Jersey in 2003, he moved to Philadelphia, Pennsylvania to attend Drexel University. He received the dual M.S./B.S. degree and the Ph.D. degree, both in electrical engineering, from Drexel University in 2009 and 2015, respectively. During this time, he has also interned and visited with the Wideband Tactical Networking Group, MIT Lincoln Laboratory (2007, 2009); with the Network Operating Systems Technology Group, Cisco Systems, Inc. (2012); and most recently with the Center for Wireless Communications at the University of Oulu, Finland (2013).